Volume 65C
Number 2
Apr.–June 1961

THE UNIVERSITY OF MICHIGAN
JUN 23 1961
ENGINEERING LIBRARY

Engineering and Instrumentation

SECTION C

JOURNAL OF RESEARCH

NATIONAL BUREAU OF STANDARDS

Journal of Research
of the
National Bureau of Standards

C. Engineering and Instrumentation

APR.–JUNE • 1961

VOLUME • 65C

NUMBER • 2

Editor: W. A. Wildhack

Associate Editors: G. F. Montgomery, R. B. Jacobs

Publication dates:
Feb. 15, May 15, Aug. 15, Nov. 15, 19[illegible]

JOURNAL OF RESEARCH

The National Bureau of Standards Journal of Research reports research and development in the fields of activity shown at right. Also included from time to time are survey articles on topics closely related to the Bureau's scientific and technical program.

The Journal is published in four separate sections as follows:

A. Physics and Chemistry

Contains papers of interest primarily to scientists working in these fields. Issued six times a year. Annual subscription: domestic, $4.00; foreign, $4.75

B. Mathematics and Mathematical Physics

Presents studies and compilations designed mainly for the mathematician and the theoretical physicist. Issued quarterly. Annual subscription: domestic, $2.25; foreign, $2.75.

C. Engineering and Instrumentation

Reports research and development results of interest chiefly to the engineer and the applied scientist. Issued quarterly. Annual subscription: domestic, $2.25; foreign, $2.75.

D. Radio Propagation

Reports work in radio propagation physics and upper atmospheric research. Issued six times a year. Annual subscription: domestic, $4.00; foreign, $4.75.

U.S. DEPARTMENT OF COMMERCE
Luther H. Hodges, Secretary

NATIONAL BUREAU OF STANDARDS
A. V. Astin, Director

Functions and Activities

The functions of the National Bureau of Standards are set forth in the Act of Congress, March 3, 1901, as amended. These include the development and maintenance of the national standards of measurement and the provision of means and methods for making measurements consistent with these standards; the determination of physical constants and properties of materials; the development of methods and instruments for testing materials, devices, and structures; advisory services to Government agencies on scientific and technical problems; invention and development of devices to serve special needs of the Government; and the development of standard practices, codes, and specifications. The work includes basic and applied research, development, engineering, instrumentation, testing, evaluation, calibration services, and various consultation and information services. The Bureau also serves as the Federal technical research center in a number of specialized fields. The scope of activities of the National Bureau of Standards is suggested in the following listing of the divisions and sections engaged in technical work.

Washington, D.C.

Electricity. Resistance and Reactance, Electrochemistry. Electrical Instruments. Magnetic Measurements. Dielectrics.

Metrology. Photometry and Colorimetry. Refractometry. Photographic Research. Length. Engineering Metrology. Mass and Scale. Volumetry and Densimetry.

Heat. Temperature Physics. Heat Measurements. Cryogenic Physics. Equation of State. Statistical Physics.

Radiation Physics. X-Ray. Radioactivity. Radiation Theory. High Energy Radiation. Radiological Equipment. Nucleonic Instrumentation. Neutron Physics.

Analytical and Inorganic Chemistry. Pure Substances. Spectrochemistry. Solution Chemistry. Standards Reference Materials. Applied Analytical Research.

Mechanics. Sound. Pressure and Vacuum. Fluid Mechanics. Engineering Mechanics. Rheology. Combustion Controls.

Organic and Fibrous Materials. Rubber. Textiles. Paper. Leather. Testing and Specifications. Polymer Structure. Plastics. Dental Research.

Metallurgy. Thermal Metallurgy. Chemical Metallurgy. Mechanical Metallurgy. Corrosion. Metal Physics. Electrodeposition.

Mineral Products. Engineering Ceramics. Glass. Refractories. Enameled Metals. Crystal Growth. Physical Properties. Constitution and Microstructure.

Building Research. Structural Engineering. Fire Research. Mechanical Systems. Organic Building Materials. Codes and Safety Standards. Heat Transfer. Inorganic Building Materials.

Applied Mathematics. Numerical Analysis. Computation. Statistical Engineering. Mathematical Physics.

Data Processing Systems. Components and Techniques. Digital Circuitry. Digital Systems. Analog Systems. Applications Engineering.

Atomic Physics. Spectroscopy. Radiometry. Solid State Physics. Electron Physics. Atomic Physics.

Instrumentation. Engineering Electronics. Electron Devices. Electronic Instrumentation. Mechanical Instruments. Basic Instrumentation.

Physical Chemistry. Thermochemistry. Surface Chemistry. Organic Chemistry. Molecular Spectroscopy. Molecular Kinetics. Mass Spectrometry. Molecular Structure and Radiation Chemistry.

• Office of Weights and Measures.

Boulder, Colo.

Cryogenic Engineering. Cryogenic Equipment. Cryogenic Processes. Properties of Materials. Gas Liquefaction.

Ionosphere Research and Propagation. Low Frequency and Very Low Frequency Research. Ionosphere Research. Prediction Services. Sun-Earth Relationships. Field Engineering. Radio Warning Service.

Radio Propagation Engineering. Data Reduction Instrumentation. Radio Noise. Tropospheric Measurements. Tropospheric Analysis. Propagation-Terrain Effects. Radio-Meteorology. Lower Atmosphere Physics.

Radio Standards. High Frequency Electrical Standards. Radio Broadcast Service. Radio and Microwave Materials. Atomic Frequency and Time Interval Standards. Electronic Calibration Center. Millimeter-Wave Research. Microwave Circuit Standards.

Radio Systems. High Frequency and Very High Frequency Research. Modulation Research. Antenna Research. Navigation Systems. Space Telecommunications.

Upper Atmosphere and Space Physics. Upper Atmosphere and Plasma Physics. Ionosphere and Exosphere Scatter. Airglow and Aurora. Ionospheric Radio Astronomy.

Order all publications from the Superintendent of Documents
U.S. Government Printing Office, Washington 25, D.C.

Use of funds for printing this publication approved by the Director of the Bureau of the Budget (June 24, 1958).

JOURNAL OF RESEARCH of the National Bureau of Standards—C. Engineering and Instrumentation
Vol. 65C, No. 2, April–June 1961

An Experimental Study Concerning the Pressurization and Stratification of Liquid Hydrogen[1, 2]

A. F. Schmidt, J. R. Purcell, W. A. Wilson, and R. V. Smith[3]

(December 19, 1960)

A 625 gallon powder-insulated Dewar has been built and appropriately instrumented to provide information concerning pressurization gas consumption, ullage pressure, liquid level (ullage volume, indirectly), horizontal and vertical temperature surveys throughout the test fluid, and lapsed time. Pressurization levels of 25, 75, 125, and 180 psig have been examined individually. Two techniques—one based on the case of one-dimensional heat flow in a semi-infinite solid and the other founded on an electrical network analog of the thermal system—are given for making reasonable predictions concerning liquid-phase hydrogen temperature distribution in well-insulated, rapidly-pressurized storage vessels. A thermal analysis is presented which indicates the mechanics of heat transmission and adsorption in the fluid.

1. Introduction

The so-called temperature stratification phenomenon, which has been observed in containers of cryogenic fluids under certain conditions, is of sufficient interest in the field of cryogenic engineering to warrant special investigation. Areas in which the results of such research may be applied profitably include those concerning the transfer of liquefied gases by pressurization, the transfer of liquefied gases by pumping, and the sealed storage of liquefied gases. In the first case, the stratification of contents in a vessel used to supply transfer fluid permits the utilization of subcooled liquid, the properties of which are desirable from the aspect of single-phase flow characteristics. In the second case, stratification provides a means to attain, and sustain, Net Positive Suction Head for transfer by pumping, the absolute magnitude of NPSH required here depending upon both fluid and pump characteristics and the geometry of the pumping situation. For the final case, the effect of stratification is undesirable, generally, due to the accompanying promotion of an excessive rate of pressure rise in the storage vessel ullage space; the undesirability is pronounced for sealed "no-loss" transport containers in which the maximum time permissible in transit is a direct function of the container design pressure.

2. Experimental Equipment

An elevation assembly drawing of the 625 gallon Dewar used in this study is presented in figure 1. The inner vessel is supported within the outer shell by means of a 15 in. diam stainless steel cylinder which is fastened between central portions of the two top dished heads as shown in the drawing. The diameter of this cylinder was chosen to provide a manway into the test container for relatively easy access to the internal instrumentation. Evacuated perlite is the insulating medium, and filtered vacuum pump connections are located on both the top and the bottom dished heads; flanges attached directly to the base of each evacuation port permit filling and draining of the insulation space. A static Dewar vacuum of 10 to 15 μ is achieved in the cold, hydrogen-filled Dewar.

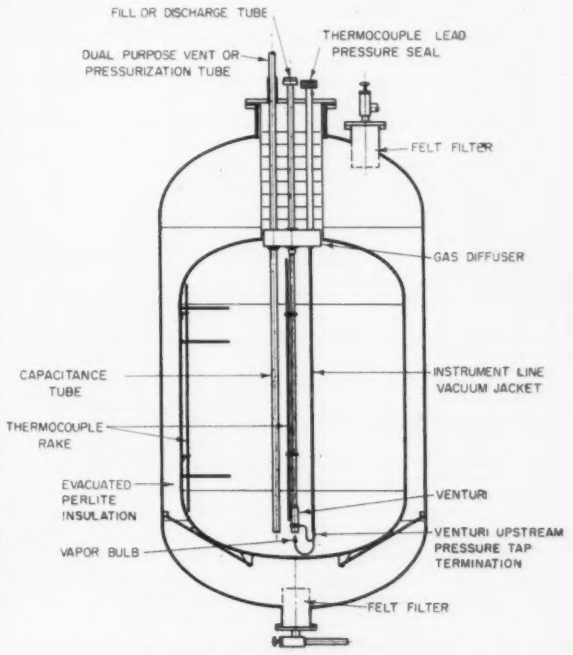

FIGURE 1. *625 gallon test Dewar.*

[1] This work was supported by the U.S. Atomic Energy Commission.
[2] This paper is an expanded version of a paper presented at the 1959 Cryogenic Engineering Conference, Berkeley, Calif., September 4, 1959.
[3] Associate Professor of Mechanical Engineering, Colorado State University.

583172—61——1

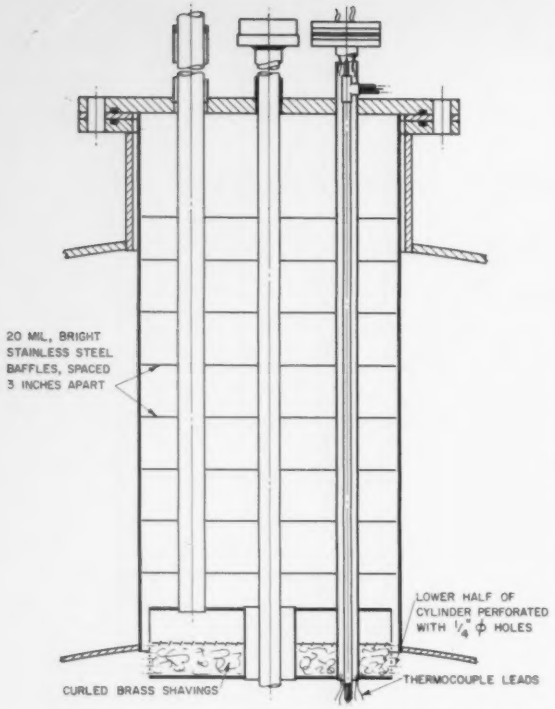

FIGURE 2. *625 gallon test Dewar-manway section*

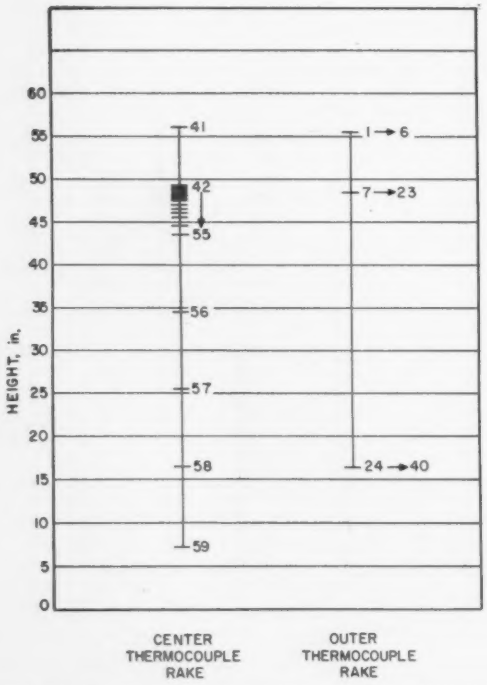

FIGURE 3. *Position of thermocouples in vertical direction 625 gallon Dewar*

Essentially all critical test components are attached to the manway cover, thereby providing an orderly means for placing, removing, and examining internal equipment, when necessary, with a minimum of difficulty (fig. 2). Horizontal, bright stainless steel baffles are soldered to the fill, vent, and instrument lead tubes at regular intervals within the access cylinder to minimize hydrogen gas circulation and thermal radiation in this region. One common method of insulating a zone such as this, which may be exposed to temperatures approximating 300 °K on one side and something less than 100 °K on the other, is to build an evacuated-powder or high-vacuum insulated plug with a cylindrical stainless steel wall. However, in the case of a moderate or high-pressure rated container, the plug must be built to withstand vessel design pressure—implying relatively heavy plug walls. As a consequence of the thermal conduction characteristics of various materials involved, the hydrogen gas-baffle arrangement provides a better heat barrier across the manway than would a plug of adequate pressure rating. For this reason, and for the sake of simplicity and economy, the baffle construction was used. It may be of interest to note that the thermal conductivity of hydrogen gas is approximately one hundred times that of evacuated powder and one-hundredth that of stainless steel.

Located immediately beneath the bottom opening of the access cylinder is a gas diffuser which diverts the incoming pressurization gas 90° through curled brass shavings and introduces the stream tangentially to the underside of the inner shell top dished head. The diffuser is fed by a 1½ in. tube which also serves as a gas vent when the test vessel is being filled or depressurized.

A capacitance probe, hanging from the bottom of the diffuser, is used to provide the liquid contents (level) determination—the signal of the probe being furnished to a direct-reading recorder. Auxiliary level information may be obtained by observing the Dewar ullage pressure, by then noting the saturation temperature corresponding to this pressure on a hydrogen vapor pressure-temperature diagram, and finally by locating this temperature in data provided by the vertical thermocouple rake. Knowledge of the liquid surface location derived by the latter method has proved to be quite precise in the zone of closely-grouped thermocouples; in other regions, the precision is understandably lacking.

Further examination of figure 1 reveals a Venturi tube which is attached to the inlet of the fluid discharge tube to permit evaluation of such a device in cryogenic media. Results of this work are presented in another paper.[4]

In the experimental program, two thermocouple rakes are utilized—one installed vertically in the center of the vessel, and the other fastened to the side wall, capable of sensing horizontal temperature profiles from zero to 11 in. from the wall at three distinct levels (approximately 17, 49, and 56 in. from

[4] J. R. Purcell, A. F. Schmidt, R. B. Jacobs, The Venturi tube as a liquefied gas flow measuring device, Advances in Cryogenic Engineering, **5**, pp. 282 to 288 (Plenum Press, New York, N.Y., 1960).

the tank bottom, respectively). Figure 3 illustrates the placement of each thermocouple in the vertical direction.

The system of differential thermocouples—59 in all—is composed of one 36 gage gold-cobalt lead and an appropriate number of 36 gage copper leads, each of which passes through a rubber compression-type seal at the top of the tank. A reference junction for the entire series of 'couples is attached to a small parahydrogen-filled vapor-pressure bulb located below the inlet of the Venturi; reference temperature information, therefore, is derived from bulb pressure data and a parahydrogen vapor pressure-temperature curve. Temperatures, corresponding to the vapor bulb pressure readings, are accurate to ± 0.05 °K.

Hydrogen pressurization gas is stored at high pressure in a standard tube trailer of 260 ft^3 free volume, from which it passes through a preset pressure-recorder-actuated solenoid valve and on into the Dewar during pressurization.

3. Test Procedure and Results

In an effort to present the data accumulated from each pressurization run most descriptively, tests A–2, A–3, A–4, and B–1 have been analyzed graphically through temperature-time and temperature-height curves (fig. 4 to 9). Test identification symbols listed above refer to the conditions of table 1.

Tests A–1 through A–4 were conducted in the following manner: The test vessel liquid inlet connection was sealed off, and the container was maintained at ¾ psig for a minimum of 16 hr by venting into a hydrogen gasholder. At the end of this period (actually the start of the test day), during which time the fluid contents had reached an equilibrium state, a complete set of thermocouple readings was taken and recorded as the initial condition. The vent-to-gasholder valve was then closed, a pressure-recorder-actuated solenoid valve between the hydrogen gas tube trailer and the test container gas diffuser was opened and pressurization of the Dewar to a preselected level was effected within 30 sec. Additional small quantities of gas were generally required for 15 min after the initial pressurization in order to maintain the desired pressure level, after which time the liquid evaporation rate became more than sufficient to furnish the needed gas. Rather than disturb the temperature gradients being established in the test space by continuously releasing

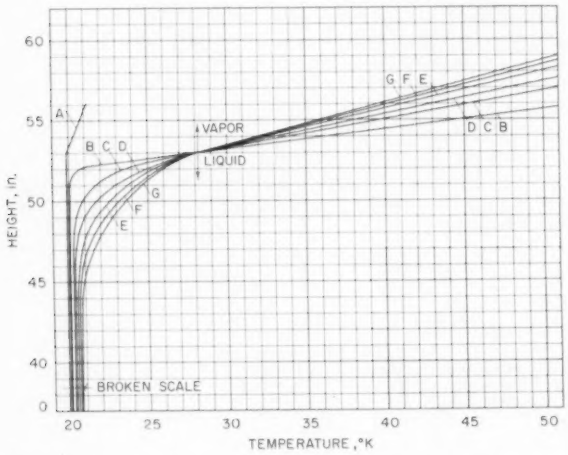

FIGURE 4. *Temperature versus height, hydrogen test A-2, 75 psig.*

A, O+ time
B, O+¼ hr
C, O+1¾ hr
D, O+3¼ hr
E, O+4¾ hr
F, O+6¼ hr
G, O+7¾ hr

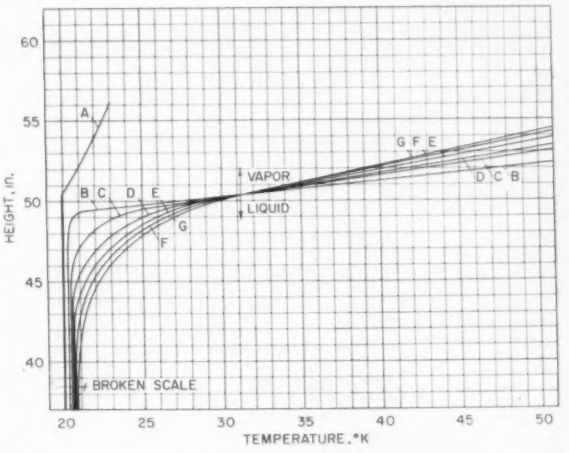

FIGURE 5. *Temperature versus height, hydrogen test A–3, 125 psig.*

A, O+ time
B, O+¼ hr
C, O+1¾ hr
D, O+3¼ hr
E, O+4¾ hr
F, O+6¼ hr
G, O+7¾ hr

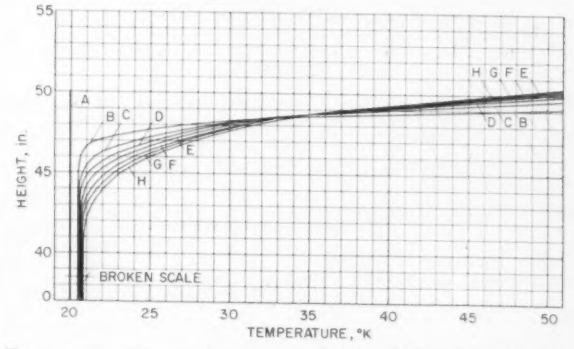

FIGURE 6. *Temperature versus height, hydrogen test A–4, 180 psig.*

A, O+ time
B, O+¼ hr
C, O+¾ hr
D, O+1¼ hr
E, O+1¾ hr
F, O+2¼ hr
G, O+2¾ hr
H, O+3¼ hr

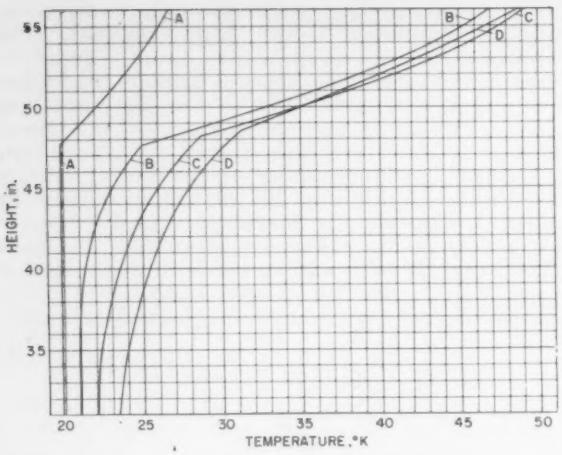

FIGURE 7. *Temperature versus height, hydrogen test B–1, pressure build-up due to normal heat leak.*

A, O+ time
B, O+24 hr
C, O+48 hr
D, O+72 hr

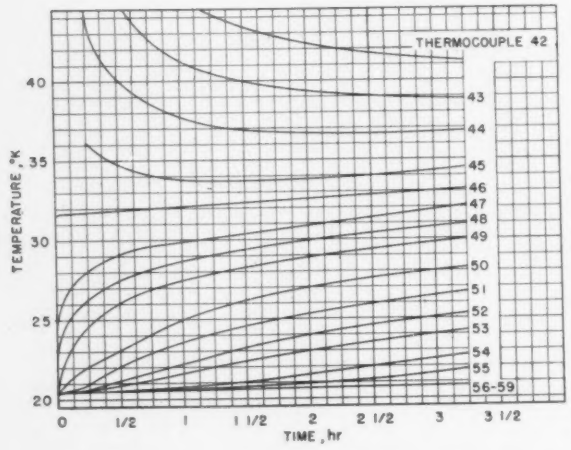

FIGURE 8. *Temperature versus time, hydrogen test A–4, 180 psig.*

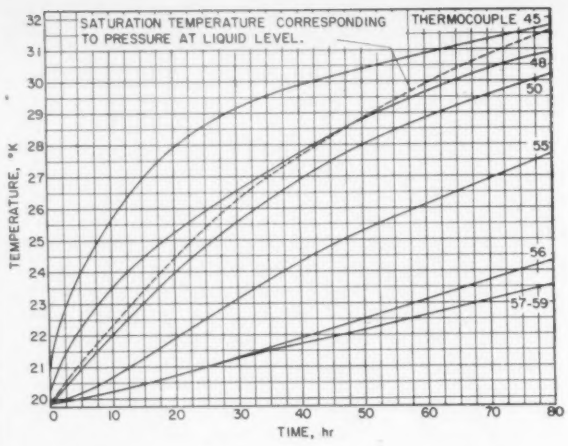

FIGURE 9. *Temperature versus time, hydrogen test B–1, pressure build-up due to normal heat leak.*

the gas overpressure, the vent was kept closed and the pressure was permitted to rise naturally throughout the test period. Thermocouple and vapor pressure data were recorded every ½ hr for 8 hr. Termination of the test after 8 hr was accomplished simply by deactivating the recorder-actuated solenoid valve and depressurizing the tank to gasholder conditions for overnight standby. Gas consumed in each of the tests listed above was measured by opening enough tubes in the gas trailer manifold to exceed, by a small margin, a precalculated demand; the temperature and pressure of this gas were then recorded, pressurization of the test Dewar occurred, and the final trailer manifold temperature and pressure were noted. Knowledge of the fluid capacity of each tube in the trailer, coupled with the pressure-temperature data recorded above, then provided information concerning the amount of pressurizing gas required in each test.

Pressure build-up test B–1 was effected by completely sealing off the experimental chamber and recording the necessary data three times a day over an 80 hr test run.

TABLE 1.

Test No.	Initial pressure (zero time)	Test pressure [a] (zero time plus ½ min)	Final pressure [b] (zero time plus 7¾ hr)	Pressurization gas consumption	Liquid volume	Ullage volume (including manway volume)
	psig	*psig*	*psig*	*scf*	*cf*	*cf*
A–1	¾	25	46	110	67.2	20.3
A–2	¾	75	102	310	63.2	24.3
A–3	¾	125	160	465	59.7	27.8
A–4	¾	180	(195)[c]	700	57.3	30.2
B–1	¾	¾	10	----	56.3	31.2

[a] Test pressure refers to level achieved with tube trailer pressurization gas.
[b] Final pressure refers to level achieved at completion of test (pressure resulting from combination of tube trailer gas and gas evolved during test period).
[c] Final pressure after 3¼ hr.

4. Discussion

Data obtained from the program described here were studied and used in several different ways:

(1) Pressurization gas consumption data were recorded and several attempts were made to correlate this information; an insufficient number of vapor-phase thermocouples plus the additional complication of irregular vessel geometry due to the manway volume discouraged extensive work in this area;

(2) Considering system geometry and certain properties of the test fluid, metal containing wall and evacuated-powder insulation, a thermal analysis was made to determine the mechanics of heat transmission and absorption in the fluid;

(3) A method useful in predicting the change of temperature with time at any given point in a solid was applied to the experimental quantity of liquid hydrogen—the theoretical results were compared with experimental information;

(4) An electrical network analog of the thermal system was constructed and a comparison with the theoretical method (3) was made.

4.1. Pressurization Gas Consumption

Information pertaining to the consumption of pressurization gas, pressure level and ullage volume in this series of tests is presented in table 1. One interesting observation can be made from these data. For a perfect gas—using Boyle's Law ($pV=p'V'$)—the amount of gas required to elevate the pressure p in a known volume V' to a specified level p' may be calculated (assuming no condensation, evaporation, etc.). Results of the four tests reported here indicate that the pressurization gas consumed in any test can be predicted to an accuracy of 10 percent by first using the perfect gas relationship to compute a required volume V of gas at standard conditions, then doubling the answer. To restate, the amount of gas needed to pressurize a vessel of this particular geometry is approximately twice that computed from Boyle's Law. Gas temperature, pressurization time and diffuser configuration should also be considered in the final analysis. Although the correlation is crude, it may be of some value in estimating the requirements of subsequent work of this nature.

4.2. Thermal Analysis

Heat transmission into the liquid hydrogen was considered to occur in the following manner:

(1) The uniform (bulk) temperature portion of the liquid is warmed by heat transferred from the containing surface and thence by convection;

(2) The stratified liquid layer is warmed by heat conducted from vapor above the interface and by condensation at the interface;

(3) Vaporization occurs at the outer periphery of the interface where liquid contacts the warmer metal.

Validity of these assumptions may be tested by heat balances using internal energy and apparent heat transfer information. Taking experimental data from the last hour and a half of test A–3 (fig. 5) as an example, calculations indicate a total internal energy change rate of 53.8 w:

Internal Energy Change Rate

In uniform temperature portion of liquid (below 38″)	17. 5 w
In stratified portion of liquid (above 38″ to 50.3″)	24. 0 w
To raise mass of liquid to be vaporized to saturation temperature	6. 5 w
To raise mass of liquid to be vaporized from saturated liquid to final vapor state	22. 3 w
	70. 3 w
To cool initial mass of vapor to final state	−16. 5 w
	53. 8 w

In determining apparent heat transfer through the evacuated-powder tank insulation and down the manway, a value of insulation conductivity ($k=40$ μw/cm °K) was chosen such that the heat transmission computed from Dewar geometry (below) equalled the computed rate of change in internal energy (above). The reason for choosing a value of k in the manner described relates back to some uncertainty existing in the absolute value of this property, even with a fair knowledge of material substance, size and interstitial pressure. The value computed is within the range of values considered reasonable for the material.

Heat Transfer Rate

Through bottom head of test vessel	10.7 w
Through cylindrical wall of uniform temperature portion of liquid (below 38″)	14.2 w
Through cylindrical wall of stratified portion of liquid (above 38″ to 50.3″)	7.3 w
Through vessel wall surrounding vapor phase (above 50.3″)	8.1 w
Through manway (hydrogen gas and metal neck)	13.5 w
	53.8 w

Checking premise (1), *The uniform (bulk) temperature portion of the liquid is warmed by heat transferred from the containing surface, and thence by convection:*

Internal energy change rate ≈ Heat transfer rate

17.5 w ≈ 24.9 w

Then with respect to the stratified layer, an assumption is made that heat transferred through the wall surrounding this portion of fluid provides the energy required to raise the temperature of the liquid, which is to be vaporized, from the bulk temperature to a saturated condition.

Internal energy change rate ≈ Heat transfer rate

6.5 w ≈ 7.3 w

An apparent surplus of transferred heat (7.4+0.8=8.2 w), from the two zones (or regions) considered, may be assumed to contribute to vaporization at the periphery interface.

From premise (2), *The stratified liquid layer is warmed by heat conducted from vapor above the interface and by condensation at the interface:*

Condensation rate (interface)	≈ Internal energy change rate (stratified layer)	− Heat conduction rate (vapor to liquid)
	≈24.0 w	−5.5 w
	≈18.5 w	

where the heat conduction rate is computed from the gas phase portion of curves F and G (test A–3) near the interface.

To complete the account of heat distribution in the Dewar, from interface up, gas phase temperature and pressure information over the chosen hour and one-half test interval is used to calculate a system mass (gas) increase. This Δm is then multiplied by the latent heat of vaporization of hydrogen, resulting in a net vaporization energy value of 8.5 w. Total vaporization rate, therefore, is equal to the condensation rate computed previously plus the net vaporization rate computed above, or

$$\text{Total vaporization rate} = 18.5 + 8.5 = 27.0 \text{ w}$$

This rate, plus the 5.5 w conducted through the vapor to the interface, must be supplied from above the interface and from the apparent surplus beneath the interface.

4.3. Semi-Infinite Solid

The experimental volume of liquid hydrogen has been treated as a semi-infinite solid with the liquid-vapor interface representing a constant temperature bounding face. Since equilibrium temperatures are observed throughout the test fluid prior to pressurization, and since the plane surface temperature immediately after pressurization is also known (saturation temperature corresponding to interfacial pressure), the uniform temperature of the liquid and the suddenly-changed surface temperature are known. With this information, and certain physical fluid properties, the case of one-dimensional heat flow in a semi-infinite solid may be calculated.

A solution for the temperature history $T(x, \theta)$ must satisfy the partial-differential equation of Fourier,

$$\frac{\partial T}{\partial \theta} = \alpha \frac{\partial^2 T}{\partial x^2}.$$

By imposing appropriate initial and boundary conditions and proceeding through the necessary mathematical sequence, the desired relationship is found to be

$$\frac{t - t_1}{t_i - t_1} = \frac{2}{\sqrt{\pi}} \int_0^{x/2\sqrt{\alpha\theta}} e^{-\lambda^2} d\lambda$$

where

t = temperature at distance x below liquid-vapor interface,
t_1 = saturation temperature corresponding to pressure at interface,
t_i = initial fluid equilibrium temperature,
x = distance below interface at temperature t,
θ = time,
α = thermal diffusivity, $= k/\rho C_p$
k = thermal conductivity,
ρ = density,
C_p = specific heat at constant pressure,

$\frac{2}{\sqrt{\pi}} \int_0^{x/2\sqrt{\alpha\theta}} e^{-\lambda^2} d\lambda$ = error function, or probability integral.

A primary decision one faces in working out the mechanics of this problem concerns a somewhat arbitrary choice in the value of thermal diffusivity. Clearly, it must be evaluated at some temperature between t_i and t_1. For the case of liquid hydrogen, the variation in α is not considerable—the value at 20 °K being approximately one-third higher than that at 31 °K; further, it is $\sqrt{\alpha}$ that is used in this computation. With this knowledge then, and the additional stipulation that C_p be used as heat capacity in the diffusivity determination, one may choose essentially any value of α between t_i and t_1, run through the simple mathematics of the problem and arrive at an excellent approximation of fluid temperature distribution. In most cases, the accuracy associated with such a method of choosing α is more than sufficient. If, however, it is desired to refine the calculation, the initial approximation (above) may be used to provide basic temperature versus distance curves, from which any value, or values, of α can be selected for the final computation.

This method of theoretically simulating the actual physical conditions described previously is not without limitation when applied to liquefied gases of small latent heat of vaporization and low temperature. An efficient thermal insulation was used to envelop the test container in this work, thereby permitting relatively little heat to flow into the fluid. Should the liquid be submitted to a progressively higher heat flux, degradation of the established temperature gradients would be noted at some increased value of this flux due to greater boiling, and hence agitation, of the liquid. A poorly insulated volume of liquid, fluid containers utilizing high-thermal conductivity materials of construction in shell walls, liners, baffles, etc., and Dewars in transit, may not be adapted to this type of analysis.

As implied in preceding paragraphs, the representation of a quantity of liquefied gas by a semi-infinite solid is interesting and apparently feasible. The method has been applied to the reported experimental data with excellent results. Test data were not completely analogous in that the bulk fluid temperature shifted slightly with time, due to the combined effects of heat transmitted into the liquid from the containing wall and compression of the liquid, and also because of the fact that the interface temperature shifted somewhat during the test period as a result of the pressure increase in the nonvented Dewar.

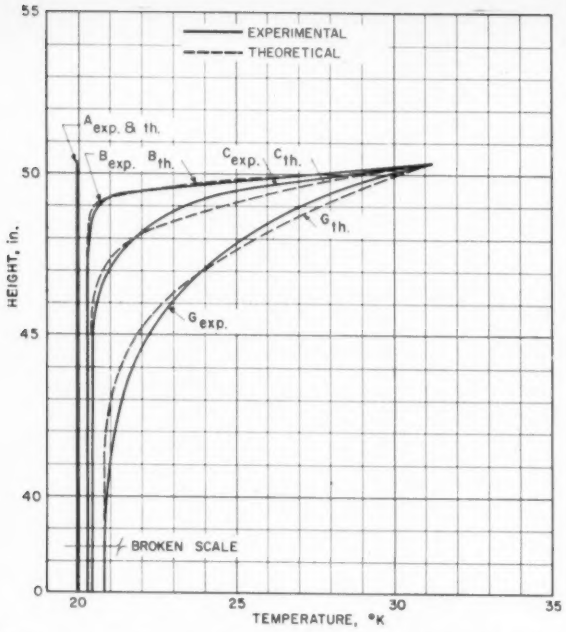

FIGURE 10. *Temperature versus height, hydrogen test A–3, 125 psig.*

A, O+ time
B, O+¾ hr
C, O+1¾ hr
G, O+7¾ hr

However, these deviations had only a secondary effect on the problem. A comparison of theoretical and experimental values for the 125 psig test (A–3) reveals the following information (see fig. 10): Using an interface temperature of 30.8 °K and a liquid bulk temperature of 20.3 °K, a temperature difference of 10.5 °K has been established. For distances greater than 3 in. below the surface of the liquid, and for any time between zero and 8 hr, the *maximum* deviation between theoretical and experimental work is 0.3 °K, or 3 percent of the temperature span, while the average deviation is less than 0.1 °K. The first 3 in. beneath the surface are affected more by an increase in interface (saturation) temperature with time and by the slight increase in volume of the liquid, so that a direct comparison here is likely to show the greatest error. Even so, the maximum error is seen to be less than 1.5 °K.

4.4. Electrical Network Analog

In order to evaluate more directly the effect of bulk and surface temperature shift previously mentioned, some time was devoted to the use of an electrical analog as a means of most conveniently examining this shift. Also, the ability to physically observe experimental phenomena requiring 8 hr being simulated electrically in a few seconds is of considerable interest.

The electrical analog is based on the equation $\frac{\partial V}{\partial \theta}=\frac{1}{RC}\frac{\partial^2 V}{\partial x^2}$ (compare with the Fourier equation $\frac{\partial T}{\partial \theta}=a\frac{\partial^2 T}{\partial x^2}$ previously mentioned), if distributed constants are used in the circuitry. Using lumped constants—that is, conventional resistors and capacitors—the error is slight if reasonable consideration is given to circuit construction. It is seen from the above equations that voltage is analogous to temperature in the thermal circuit and that the electrical diffusivity 1/RC corresponds to the thermal diffusivity a. In the overall circuit, it is not necessary to define resistance and capacitance individually—only the product which determines the time constant and thus the ratio a/1/RC, or aRC. This ratio is generally quite large (approximately 20,000 in the present case) due to practical limitations of the circuit. However, the advantage of such a circuit is understandable in that the curves are plotted very rapidly.

Results obtained by this technique were exactly comparable with those achieved by the method of the semi-infinite solid. Unfortunately, circumstances did not permit further refinement of the circuit to provide for the gradual shift of bulk and surface temperatures with time; it is hoped that this may be accomplished in the near future.

5. Conclusions

It is evident from the preceding paragraphs that reasonable predictions can be made concerning liquid-phase hydrogen temperature distribution in well-insulated, rapidly-pressurized storage vessels.

By treating the liquid as a semi-infinite solid, one may foretell the temperature history, temperature gradient and heating rate of the stratified fluid portion beneath the liquid-vapor interface; where numerous succeeding initial and boundary conditions are to be imposed in the manner of trial and error, where these conditions are to vary with time for any one given situation, or where a variation of thermal properties must be taken into account, the electrical analog method may be modified to permit more rapid solutions.

Additionally, if heat flux through the containing vessel wall is known, bulk liquid temperature rise may be predicted in a very rough manner.

Finally, it will be noted by the curves presented here, and by theory, that an increase in ullage pressure—hence an increase of interfacial temperature—results in the transfer of more heat to the stratified layer, the quantity of which is calculable using the method of the semi-infinite solid. Knowledge of this may serve as one criterion in the optimization of pressure level within a liquefied gas storage or transfer system.

(Paper 65C2–58)

JOURNAL OF RESEARCH of the National Bureau of Standards—C. Engineering and Instrumentation
Vol. 65, No. 2, April–June 1961

Temperature Dependence of Elastic Constants of Some Cermet Specimens[1]

Sam Spinner

(June 16, 1960)

The temperature dependence of both Young's and shear modulus of four types of cermet specimens, known as "nickel-bonded titanium carbide," as well as Ni and TiC have been determined by a dynamic resonance method.

The Young's modulus temperature curves of the cermets are characterized by a linear decrease from room temperature until about 700 to 1,000 °C. In this upper temperature region, an inflection in the relation develops, accompanied by an increase in internal friction. Both these effects are attributed to viscous grain boundary slip.

For shear modulus, only the linear portion of the modulus temperature relation was obtained. In this linear region, the relative decrease in shear modulus for the cermet specimens is greater than the relative decrease in Young's modulus for the same type of specimen. This means that Poisson's ratio rises with temperature for the cermets.

1. Introduction

Among the more noteworthy properties of cermets in general are their high values of elastic moduli. Although the literature dealing with the properties of cermets devotes considerable attention to their elastic constants [1,2,3],[2] comparatively little attention has been paid to the values of these constants at elevated temperatures.[3]

Inasmuch as these cermets are intended to be used as structural members at elevated temperatures, and inasmuch as these studies [4, 5] have shown that their elastic moduli may decrease by as much as 15 percent at around 1,000 °C from their room temperature values, and may decrease by another 20 percent in the next 200 °C or so, it would appear that further data concerning the variation of these elastic constants with temperature would be most useful. The main purpose of this paper is to present such data. Furthermore, since the four types of cermets selected for obtaining these data are composed basically of the same constituents, varying from each other mainly in the relative proportions of metal and ceramic, comparison of the results among these types presents interesting possibilities for analysis.

2. Experimental Procedures

2.1. Specimens

The cermet specimens used in this investigation are known as "nickel-bonded titanium carbide". They were taken from among those used by Lang [1] for his room temperature measurements. These specimens were all in the shape of rectangular bars about 6 in. by $\frac{1}{2}$ in. by $\frac{1}{4}$ in. Table 1, which gives the number of sets of determinations for both Young's and shear modulus performed on all of the specimens, retains Lang's scheme for identifying the cermet specimens as well as the manufacturer's designation. The table also includes the nominal metal content by weight of each type of cermet; the remainder (of each type) consisting of a solid solution composed of TiC and 8 percent of specimen weight of (TiC+NbC+TaC). A description of the composition and microstructure of many types of cermets including some used in this investigation is contained in a report by Shevlin et al. [6]. The TiC and nickel specimens, which are included for comparison, are polycrystalline materials of commercial purity. The TiC specimen was cylindrical in shape, about 6 in. long and $\frac{1}{2}$ in. in diameter. The nickel specimen was about 7 in. long and $\frac{1}{2}$ in. square in cross section.

TABLE 1. *Designation and number of determinations made on all specimens*

Specimens		Nominal metal content	Number of sets of Young's modulus determinations	Number of sets of shear modulus determinations
M'frs. designation	Lang's designation			
K–150 B	[a] 31–1	10% Ni	6	2
	31–4		3	3
K–151 B	32–1	20% Ni	1	
	32–2		2	2
K–152 B	33–1	30% Ni	1	
	33–10		2	2
K–162 B	34–1	25% Ni, 5% Mo	3	1
Titanium Carbide			5	
Nickel			3	

[a] The number preceding the dash indicates the type of cermet and corresponds to the manufacturer's designation. The number following the dash indicates the particular specimen.

[1] This investigation was carried on under the sponsorship of the Division of Research, U.S. Atomic Energy Commission.

[2] Figures in brackets indicate the literature references at the end of this paper.

[3] A paper by Watchman and Lam [4] containing one curve of Young's modulus as a function of temperature for one of the types of cermets used in this study, and a WADC report [5] showing Young's modulus temperature curves on several cermet materials are the only data along these lines known to the author.

2.2. Method and Calculations

The elastic moduli measurements at elevated temperatures were performed by a dynamic resonance method as described by Wachtman and Lam [4]. Essentially, the method consists of suspending the specimen in a furnace from two fibers, one fiber being attached to an electromagnetic driver and the other to a crystal pickup. The driver and pickup are outside the furnace and connected to appropriate electronic equipment for arousing and detecting the mechanical resonance frequencies of the specimen. The evidence of resonance is indicated by a Lissajou pattern on a cathode ray oscilloscope. The most satisfactory suspension elements were found to be molybdenum wires coated with nickel and chromium to prevent oxidation [7].

If the suspension wires are tied at opposite sides of the specimen, as shown in the sketch (fig. 1) from a previous paper [8], then, in addition to the usual flatwise flexural resonance vibrations, the edgewise flexural resonance vibrations and, even more important, the torsional resonance vibrations of the specimens can be detected. The response of one of the flexural resonance frequencies, usually the edgewise, usually died out at a lower temperature than the other. Also, because of the geometry of the specimens (the fairly low ratio of width to depth of the cross section) the response of the torsional resonance frequency was weaker than the flexural ones and died out at the lowest temperature.

Occasionally, the torsional response would disappear at one temperature and reappear at a higher one before dying out completely. The larger number of sets of Young's modulus-temperature determinations in table 1, as compared with the number of sets of shear modulus-temperature determinations, is mainly due to the fact that the experimental phase of the investigation of the cermet specimens had been about half completed before it was noticed that the torsional resonance vibrations could be detected at all. Nevertheless, at least one set of torsional resonance vibrations was obtained for each type of cermet. The flexural vibrations are related to Young's modulus while the torsional vibrations are related to the shear modulus. Because of the square and circular cross section of the Ni and TiC specimens, a satisfactory torsional mode could not be obtained at elevated temperatures, so that for these specimens only Young's modulus as a function of temperature could be determined.

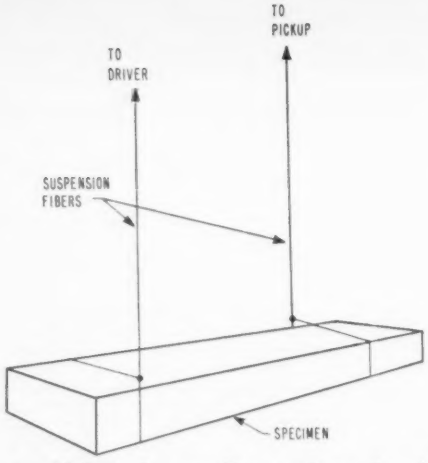

FIGURE 1. *Method of suspending specimens for obtaining torsional as well as flexural vibrations.*

The ratio of a particular elastic modulus at elevated temperature to the same modulus at room temperature, E_t/E_0, was calculated from the well-known equation,

$$\frac{E_t}{E_0}=\left(\frac{f_t}{f_0}\right)^2\Big/\left(1+\frac{\Delta l}{l}\right) \tag{1}$$

where f_t/f_0 is the ratio of the corresponding resonance frequencies.

The factor, $[1+(\Delta l/l)]$ is the correction for thermal expansion of the specimen from room temperature to the temperature of measurement. Values of $\Delta l/l$, the linear thermal expansion over the required temperature range, were obtained for the cermet specimens from dilatometer measurements. These data are shown in figure 2. Corresponding data for TiC

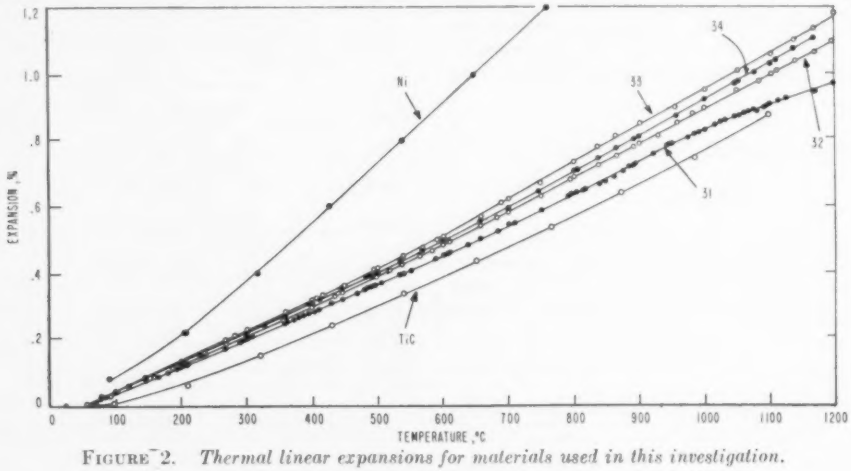

FIGURE 2. *Thermal linear expansions for materials used in this investigation.*

and nickel were taken from the literature [9, 10, 11]. They are also included in figure 2 for comparison with the cermets.

Equation (1) makes no restriction as to the type of vibration frequencies involved in obtaining E_t/E_0 [12]. The conditions that must be fulfilled are that the specimens do not change in shape on heating and that f_t and f_0, in a particular ratio, both represent the same type of vibration frequency, whether torsional, flexural flatwise or flexural edgewise. Thus, if f_t/f_0 are flatwise or edgewise flexural resonance frequencies, then E_t/E_0 becomes the ratio of Young's moduli, Y_t/Y_0, and if f_t/f_0 are torsional resonance frequencies, then E_t/E_0 becomes the ratio of the shear moduli, G_t/G_0. Equation (1) also holds if f_t/f_0 represent overtones of the fundamental of any type of vibration. However, in this study, the fundamental resonance frequencies were used almost entirely.

If more than one resonance frequency for calculating a particular elastic modulus is used, then the agreement in E_t/E_0 from these resonance frequencies provides an internal check on the consistency of the data. The agreement in Y_t/Y_0 from the two resonance flexural frequencies at any particular temperature at which both could be detected was on the order of 0.1 percent justifying the use of the average of these two values for that temperature. For the G_t/G_0 determinations, usually only one ratio of resonance frequencies was available for a particular point (under some unusually favorable conditions, the first overtone of torsion could be obtained and similarly averaged with the fumndamental), so that the agreement of repeated sets of determinations served as a measure of the precision of the data. Repeated sets of determinations were available in all but one case (table 1) for G_t/G_0. For Y_t/Y_0, a larger number of determinations was available in all cases. From these repeated measurements, it is estimated that the precision over the linear range of Y_t is on the order of 0.3 percent and that of G_t is about 0.4 percent. These repeated measurements, and consequently the above figures of precision, include the data for both specimens of each type (when two specimens were used), and no distinction is indicated in the notation in figures 3 and 4 between the two specimens of each type.

If G_t as well as Y_t are determined, then the speci-

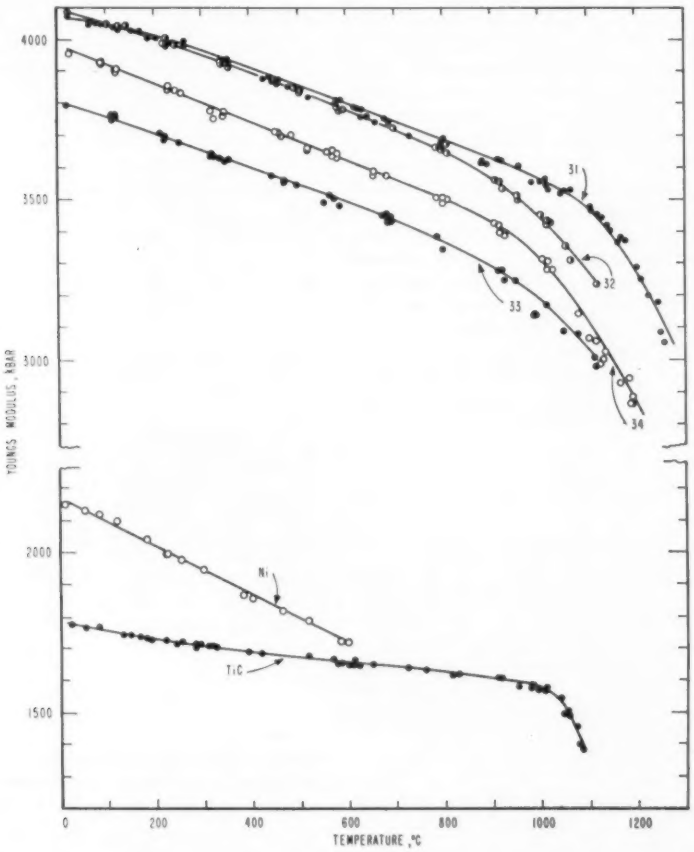

FIGURE 3. *Young's modulus—temperature relations for the materials of this investigation.*

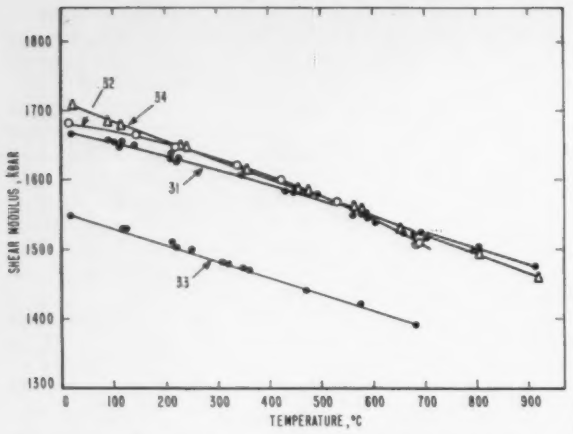

FIGURE 4. *Shear modulus—temperature relations for the four types of cermets used in this study.*

mens are completely specified elastically over the temperature range over which these two moduli can be measured, since, for isotropic materials [4] all elastic constants are related by well-known equations in such a way that if any two are known the others can be determined. In this study Poisson's ratio, μ, was computed from these two moduli.

In order to plot Y_t and G_t directly as a function of temperature, a room temperature or base value of both Young's and shear modulus, Y_0 and G_0 must be obtained. For the cermets, these values (of Y_0 and G_0) were obtained by averaging the values obtained by Lang[1] for the particular specimens of each type used. For TiC, Y_0 and G_0 were determined from the flexural and torsional resonance frequencies, respectively, the mass and the dimensions based on Pickett's relations [13]. The value for nickel was taken from the literature [14]. The values so obtained for all the types of specimens used are given in table 2. Since Y_0 and G_0 are available for each type of specimen, Poisson's ratio, μ, may also be calculated from the familiar relation,

$$\mu=\frac{Y}{2G}-1. \tag{2}$$

This is given in the final column of the table.

It should be noted that the choice of the base values, Y_0 and G_0, is not critical. Had different values of these moduli been chosen on the basis of some other reasonable selection, it would not have significantly changed the shape of the temperature modulus curves shown in figures 3 and 4, but would only have caused a slight upward or downward displacement of these curves.

[4] The materials are considered to be isotropic because, although the individual grains of which they are composed are antisotropic, nevertheless their orientation and distribution are random, so that macroscopically this condition of isotropy is substantially fulfilled. Actually, some of Lang's[1] results indicated that some preferred crystal orientation or inhomogeneity might exist in the specimens. However, these departures from isotropy, if they exist at all, are small and do not significantly affect the relations based on the assumption of isotropy.

TABLE 2. *Room temperature base values of specimens used in this investigation*

Specimen type	Young's modulus Y_0	Shear modulus G_0	Poisson's ratio μ
	kilobars	*kilobars*	
31	4074	1669	0.220
32	4077	1681	.213
33	3791	1550	.223
34	3952	1701	.162
TiC	1774	748.9	.184
Ni	2147	----------	----------

2.3. Oxidation

The specimens oxidized slightly at elevated temperatures. This oxidation was noted by a decrease in the resonance frequencies, as well as the usual change in surface appearance and increase in mass, after the specimens had been returned to room temperature, as compared with the original values. This irreversible decrease in resonance frequencies is superimposed on the reversible decrease associated with increased temperature in the course of a modulus-temperature determination. Table 3 gives typical data of such changes in mass and one of the resonance frequencies for some specimens before and after heating.

TABLE 3. *Typical changes in mass and a resonance frequency before and after heating*

Specimen	Mass		$\frac{m_b}{m_a}$ [1]	Resonance frequency		$\left(\frac{f_a}{f_b}\right)^2$ [2]
	Before m_b	After m_a		Before f_b	After f_a	
	g	*g*		*c/s*	*c/s*	
31-1	71.296	71.561	0.9963	2534	2515	0.9851
32-1	77.205	77.370	.9979	2410	2404	.9950
33-1	75.489	75.726	.9969	2312	2302	.9914
34-1	73.960	74.015	.9993	2445	2444	.9992

[1] Ratio of mass before to mass after heating.
[2] Square of ratios of fundamental flatwise flexural resonance frequencies before and after heating.

No significance can be given to the different changes for the different specimens inasmuch as they were not subjected to the same time-temperature schedules. It is seen that the largest increases in mass are associated with the largest decreases in resonance frequency. However, the decrease in resonance frequency cannot be accounted for completely by the increase in mass. In order for this condition to obtain the following relation would have to hold:

$$\frac{m_b}{m_a}=\left(\frac{f_a}{f_b}\right)^2 \tag{3}$$

where m is the mass; f is a particular resonance frequency, and the subscripts b and a stand for "before" and "after" heating. Comparison of columns 4 and 7 of table 3 shows that the change in mass accounts for only a part of the change in resonance frequency. If the oxide only forms a

coating over the main body of the specimen, as seems likely, this would account for the fact that $(f_a/f_b)^2 \neq m_b/m_a$.[5]

It was first hoped that if a specimen was heated once or, if necessary, several times, an oxide coating would eventually form which would inhibit further oxidation, so that subsequent determinations on such specimens would require no correction for this phenomenon. Unfortunately, this did not occur. Successive heatings, especially if the times involved were not short, always resulted in some further oxidation.

Clearly, the most effective way to avoid oxidation would be to have the specimen in a vacuum or inert atmosphere during the measurements at elevated temperatures. An apparatus for making such measurements in vacuo is available and was used to obtain the data for the TiC specimen, in which the oxidation was more extensive than in the cermets. Wachtman and Lam [4] also used this same apparatus for their determination on the K–150B cermet (No. 31). However, it was found more convenient to use the larger furnace in open atmosphere for the rest of the specimens, mainly because this larger furnace had smaller thermal gradients, and also because the torsional response could be obtained much more readily in the larger (air) furnace.

After a number of sets of determinations were made in this furnace in an air environment, the amount of further oxidation was considerably reduced by having the furnace flushed with nitrogen gas during a determination. The sets of determinations for the cermet specimens listed in table 1 include those made in ordinary and nitrogen flushed atmosphere.

The temperature-frequency relations were adjusted for the decrease due to oxidation by raising the recorded frequency at the highest temperature reached by multiplying by the factor, f_b/f_a, and linearly interpolating this increase from the highest temperature down to 800 °C. Below this temperature, it was established experimentally that no significant oxidation took place in the times ordinarily involved.

Also, since the oxide coating which a specimen took on on heating did not apparently affect its intrinsic elastic modulus nor its temperature dependence, the new lower values of f_0 after a particular heating could be used with the original values of Y_0 and G_0 in subsequent sets of determinations. This procedure appeared justified by the reproducibility of successive sets of determinations when it was adopted.

The nickel specimen did not oxidize sufficiently to require correction.

3. Results

3.1. Grain Boundary Slip

We consider first the Young's modulus temperature curves in figure 3. The general pattern is seen to be an approximately linear decrease until a temperature around 800 to 1,000 °C in which region a sharper decrease takes place. This inflection in the modulus-temperature characteristic is attributed to grain boundary slip (henceforth designated by the initials g.b.s.). This phenomenon has been discussed by Zener [15] using data from polycrystalline metals and extended by Wachtman and Lam [4] to polycrystalline ceramics.

A qualitative explanation of what is believed to occur may be presented in the following way:

Until the temperature region of g.b.s. is reached, the grain boundaries do not contribute significantly to the elastic modulus, the main contribution arising from the elastic properties of the grains themselves. The "normal" linear decrease in modulus with temperature is due to the odd and even powered terms of the anhormonic expansion as described by Stern [16[. (The thermal expansion is due only to the odd powered terms of the same expansion.)

At some elevated temperature (which marks the onset of g.b.s.), viscous flow between grains adds a nonrecoverable, relaxed component to the purely elastic (unrelaxed) strains which were predominant up to this region. Consequently, there is a rapid decrease in the measured modulus, which is superimposed on the linear decrease that has taken place up to this temperature region. This process continues at a faster rate as the temperature rises and the effective viscosity decreases. Since this viscous movement between grains involves energy losses, the region of g.b.s. is characterized not only by a more rapid decrease in the measured modulus but also by an increase in internal friction (Q^{-1}). The decrease in amplitude and sharpness of the resonance responses, indicative of this rise in Q^{-1}, did indeed take place and was chiefly responsible for the loss in precision in this region. In fact, this increase in Q^{-1} is as much a feature of the region of g.b.s. as the inflection in the temperature-modulus characteristic. Had these inflections taken place without the concomitant increase in Q^{-1}, then some other mechanism would be required to explain them.

As the temperature continues to rise, the effective intergranular viscosity also continues to decrease so that the energy losses associated with g.b.s. should also decrease. This should eventually result in a decrease in Q^{-1}, though not to the level existing before the region of g.b.s. This should be evidenced by a partial restoration of the amplitude and sharpness of the resonance responses and also by a second inflection in the modulus temperature curve. This marks the end of the region of g.b.s. Zener [15] cites experimental evidence of this second inflection with metals.

However, no reliable evidence of having traversed the region of g.b.s. was found for any of the materials of this investigation, nor, for that matter, with any ceramic materials measured by the author, even when the temperature was raised more than 200 °C higher than that for which a final reliable resonance response could be detected. Wachtman and Lam's data also gives no evidence of having traversed the region of g.b.s. Two possible explanations which suggest themselves for this are that the region of g.b.s. covers a much wider temperature region than antic-

[5] The changes in the resonance frequencies of the specimens on oxidation suggest the possibility of their utilization as a means of studying oxidation as a function of time and temperature in addition to the conventional methods (of changes in mass or gas pressure).

ipated, or that, if the region is traversed, the improved response is not sufficient to be detected above the higher general noise level associated with the various mechanisms which are more likely at elevated temperatures.

The upper temperature limit of recorded elastic moduli was reached, then, when the responses became so diffuse and weak that they could not be distinguished from the general background noise and spurious responses which inevitably develop when it becomes necessary to drive the specimens harder and harder as the true responses become progressively weaker. For the nickel specimen this limit occurred when the modulus temperature relationship was still linear, as it did mainly for the torsional responses of the cermet specimens, shown in figure 4.

The general characteristics of the modulus temperature curves as well as the recovery of sharpness and amplitude of the resonance responses are found to be reversible on cooling. Also, in the absence of oxidation, the specimens generally return to the same room temperature values of resonance frequency that they had originally, indicating no permanent average structural change due to g.b.s.

It is also noted from figure 2 that no noticeable corresponding inflection occurs in the thermal expansion curves around the temperature region in which the inflection associated with g.b.s. occurs in figure 3.

We now compare the types of specimens with respect to g.b.s. It is noted that for TiC the inflection indicating the start of this region comes at a higher temperature than for the cermets; and, once started, the modulus drops more sharply for TiC than for the cermets. The presence of the metal in the cermet has the effect of hastening the start of, and broadening the measurable region of g.b.s. The contribution of the nickel on this region in the cermets is difficult to evaluate since the responses for the nickel itself died out before g.b.s. developed. However, it seems reasonable that the presence of more than one type of grain boundary should result in a broadening of the g.b.s. region. The presence of two types of grains such as are present in the cermets results in three types of grain boundaries, Ni-Ni, carbide-carbide, and Ni-carbide.

In general, if there are n types of grains, and it is assumed that each grain forms a boundary either with another grain of the same type or with a different type of grain, then the number of types of grain boundaries will be given by $n(n+1)/2$.

3.2. Temperature Coefficient of Elastic Moduli

The relative decrease with temperature in Young's and shear modulus in the linear region, $-1/Y_0(\Delta Y/\Delta t)$ and $-1/G_0(\Delta G/\Delta t)$, and their standard deviations are given in table 4. These values were computed from a least square solution of the numerical data on which figures 3 and 4 are based. The range of Δt selected (and also given in the table) was as wide as possible to give representative values without entering into the inflection region marking the onset of g.b.s.

TABLE 4. *Relative decrease in Young's and shear moduli over the linear range*

Specimen	$-\frac{1}{Y_0}\left(\frac{\Delta Y}{\Delta t}\right)$ [a] $\times 10^{-5}$ per °C	Δt [b] in °C	$-\frac{1}{G_0}\left(\frac{\Delta G}{\Delta t}\right)$ [c] $\times 10^{-5}$ per °C	Δt [b] in °C
TiC	10.4±0.3 [d]	950		
31	12.4± .1	900	13.2±0.3	900
32	13.3± .2	800	14.9± .8	690
33	14.4± .2	700	15.9± .3	675
34	14.5± .1	800	15.6± .1	800
Ni	35.7± .6	600		

[a] Relative decrease in Young's modulus.
[b] Temperature range from room temperature to value given.
[c] Relative decrease in shear modulus.
[d] Standard deviation.

It is seen from table 4 that both $-1/Y_0(\Delta Y/\Delta t)$ and $-1/G_0(\Delta G/\Delta t)$ increase in absolute value with increasing metal content. TiC and Ni (for which only $-1/Y_0(\Delta Y/\Delta t)$ are available) have the lowest and highest values of relative slope respectively, forming the "end members" in the foregoing pattern.

Cermets No. 33 and 34, which have the same percent of metal content and vary from each other only in that one (No. 33) contains only nickel as the metal while the other (No. 34) contains 25 percent nickel and 5 percent molybdenum, show very little difference in $-1/Y_0(\Delta Y/\Delta t)$ and $-1/G_0(\Delta G/\Delta t)$. From figure 2, it may also be seen that the specimens arrange themselves in the same order with respect to positive coefficients of thermal expansion, $1/l_0(\Delta l/\Delta t)$ as they do for the negative temperature coefficients of elastic moduli; i.e., the steepest slopes for both these coefficients regardless of sign are associated with nickel and decrease in the same order for the remainder of the specimens.

3.3. Titanium Carbide and Nickel

The value of Y_0 obtained for the TiC specimen (given in table 3) is not definitive for TiC in general. First, the specimen is of commercial purity and small impurities present probably affect the measured value of Y_0 to some extent. Second, in the process of manufacture, TiC is often not produced in the proper stochiometric ratio [17]. This can also affect the value of Y_0. The third and most important factor affecting the value of Y_0 of the TiC specimen was that it was quite porous. Its density, as derived from the mass and volume, computed from its dimensions was 3.558 gm/cm^3. Using the theoretical density of 4.938 gm/cm^3 of Schwartzkopf [17] one calculates the porosity of the specimen to be 28 percent.

Mackenzie [18] has developed a theoretical relation showing how the elastic modulus increases as the porosity decreases. Coble and Kingery [19] have obtained experimental results in good agreement with Mackenzie's relation using Al_2O_3 specimens of different porosites. Using Mackenzie's relation, the Y_0 of the TiC specimen was estimated to be 3411 kilobars at theoretical density. One should also be cautioned here that the ceramic phase of the cermets is not "pure" TiC but a solid solution consisting of TiC and other carbides (sec. 2, 2.1, a).

Coble and Kingery also showed in the paper just referred to that the relative slopes of the Young's modulus temperature curves, $-1/Y_0(\Delta Y/\Delta t)$, in the linear region were essentially independent of the porosity of the specimens. If it is assumed that this also holds for TiC, then the value of $-1/Y_0(\Delta Y/\Delta t)$ given in table 4 will not be affected. Incidentally, the relative changes in the elastic moduli may be computed directly from the primary data, Y_t/Y_0 or G_t/G_0, and are independent of the particular values selected for Y_0 or G_0.

The value of $-1/Y_0(\Delta Y/\Delta t)$ obtained here for nickel (3.6×10^{-4} per °C) was in fairly good agreement, as far as could be determined from the graphs, with that obtained by Koster [19] for a cold worked unmagnetized specimen (3.8×10^{-4} per °C). Koster's range of Δt was from -180 to 400 °C, but Δt selected for the value just given was from 20 to 400 °C. Further data taken with this specimen were also in general agreement with those obtained by Koster for annealed specimens.

3.4. Comparison of Relative Slopes of Young's and Shear Modulus

Inspection of table 4 also shows for each type of specimen (where both values exist) that

$$\left|\frac{1}{G_0}\left(\frac{\Delta G}{\Delta t}\right)\right| > \left|\frac{1}{Y_0}\left(\frac{\Delta Y}{\Delta t}\right)\right|. \tag{5}$$

This means that Poisson's ratio, μ, increases with increasing temperature.

Individual values of μ calculated, from the numerical values of Y_t and G_t in all cases where both values existed, from eqn (2) confirmed this small but significant increase in μ with increasing temperature.

Coble and Kingery [19] also found Poisson's ratio to increase with temperature for Al_2O_3 as did Lang and Knudsen [20] using ThO_2+0.5 percent CaO by weight.

Zener [15] has deduced from theoretical considerations that the relaxation associated with g.b.s. should cause the relative decrease in the measured value of G to be three times that of Y. Unfortunately this result cannot be checked experimentally, not only because this region could not be observed for G, but also because the upper temperature region of g.b.s could not be determined for Y.

4. Summary

1. The temperature dependence of Young's modulus and shear modulus on four types of nickel-bonded TiC specimens have been determined by a dynamic resonance method. Similar measurements have also been made on nickel and TiC for comparison.

2. The relative decrease in both Young's and shear modulus with temperature was in the following order with the material having the smallest relative decrease listed first: TiC, 10 percent nickel content cermet, 20 percent nickel, 30 percent nickel, and 25 percent nickel +5 percent molybdenum, and nickel.

3. The inflection in the Young's modulus temperature curves was attributed to grain boundary slip.

4. The relative decrease in shear modulus with temperature was greater than that for Young's modulus, where both values were known, for the same type of specimen. Therefore Poisson's ratio rises slightly with temperature.

The author is indebted to J. Pastine for performing a portion of the calculations on which figures 3 and 4 were based, and to H. S. Parker and S. M. Lang for making the thermal expansion measurements on the cermet specimens.

5. References

[1] S. M. Lang, Properties of high temperature ceramics and cermets elasticity and density at room temperature, NBS Mono. 6 (Mar. 1, 1960).

[2] M. J. Kerper, L. E. Mong, M. B. Stiefel, and S. F. Holley, Evaluation of tensile, compressive, torsional, transverse, and impact tests and correlation of results for brittle cermets, J. Research NBS **61** 149 (1958) RP 2895.

[3] J. W. Graham and J. C. Redmond, Cermets, in High Temperature Technology (I. E. Campbell, ed.) chap. 10, p208 (John Wiley & Sons, Inc., New York, N.Y., 1956).

[4] J. B. Wachtman Jr. and D. G. Lam Jr., Young's modulus of various refractory materials as a function of temperature, J. Am. Ceram. Soc. **42,** [5] 254 (1959).

[5] E. J. Soxman, M. T. Curran, J. R. Tinklepaugh (from N.Y. State College of Ceramics, Alfred Univ.), Impact testing of cermets, progress Rept. No. 2, July 1 to Oct. 1954, Contract No. AF33 (616) 2380 expenditure order No. R–506–67C SR 7Z to power plant laboratory (WCLPG–5), Wright Air Development Center, Wright-Patterson Air Force Base, Ohio, Chap. VII—Modulus of elasticity P. 52.

[6] T. S. Shevlin, H. W. Newkirk, E. G. Stevens and H. M. Greenhouse, Preliminary microscopic studies of cermets at high temperatures, WADC Technical Rept 54–33 Part 2, The Ohio State University Research Foundation WADC (Feb. 1956).

[7] D. E. Couch, H. Shapiro, J. K. Taylor, and A. Brenner, Protection of molybdenum from oxidation at elevated temperatures J. Elec. Soc. **105,** [8] 450 (1958).

[8] S. Spinner and R. C. Valore Jr., Comparison of theoretical and empirical relations between the shear modulus and torsional resonance frequencies for bars of rectangular cross section, J. Research NBS **60,** (5) 459 (1958) RP2861.

[9] H. W. Newkirk, Jr. and H. H. Sisler, Determination of residual stresses in titanium carbide base cermets by high temperature X-ray diffraction, J. Am. Ceram. Soc. **41,** (3) 93 (1958).

[10] F. A. Mauer and L. H. Bolz, Measurement of thermal expansion of cermet components by high-temperature X-ray diffraction WADC Tech. Rept. 55–473 (Dec. 1955).

[11] F. C. Nix and D. MacNair, Thermal expansion of pure metals: copper, gold, aluminum, nickel, and iron, Phys. Rev. **60,** 597 (1941).

[12] S. Spinner, Elastic moduli of glasses at elevated temperatures by a dynamic method, J. Am. Ceram. Soc. **39** [3] 113 (1956).

[13] G. Pickett, Equations for computing elastic constants from flexural and torsional resonant frequencies of vibration of prisms and cylinders, Am. Soc. Testing Materials **45,** 846 (1945).

[14] W. Koster, Citation from Richard M. Bozorth, Ferromagnetism, P. 693 (D. Van Nostrand Co., Inc., New York, N.Y., 1951).
[15] C. Zener, Elasticity and anelasticity of metals, The University of Chicago Press, Chicago, Ill. (1948).
[16] E. A. Stern, Theory of the anharmonic properties of solids, Phys. Rev. **111** 786 (1958).
[17] P. Schwartzkopf and R. Kiefer, W. Leszynski, and F. Benesovsky, Refractory hard metals, ch. V, p. 67 The MacMillan Co., New York, N.Y. (1953).
[18] J. K. Mackenzie, The elastic constants of a solid containing spherical holes, Proc. Phys. Soc. (London) **63B** (1) p. 2 (1950).
[19] R. L. Coble and W. D. Kingery, Effect of porosity on physical properties of sintered alumina, J. Am. Ceram. Soc. **39** [11] p. 377 (1956).
[20] S. M. Lang and F. P. Knudsen, Some physical properties of high-density thorium dioxide, J. Am. Ceram. Soc. **39** (12) p. 415 (1956).

(Paper 65C2–59)

JOURNAL OF RESEARCH of the National Bureau of Standards—C. Engineering and Instrumentation
Vol. 65C, No. 2, April–June 1961

Analog Simulation of Zone Melting

H. L. Mason

(January 13, 1961)

An analog computer was used to simulate zone melting in small-diameter tungsten rods of 0.2 to 1 centimeter. Heat balance equations take account of electron bombardment, heat capacity, radial conduction, axial conduction, and surface radiation. Diagrams are given for the chosen spatial subdivision and for the computer mechanization. Predicted temperature-time curves are shown for a rod of 0.4-centimeter diameter with optimum power input of 650 watts. Unsatisfactory operation is predicted for zone melting of a 1-centimeter rod.

As part of the NBS program for attempting to supply metal samples so pure that no spurious lines can be detected by spectroscopy, G. A. Moore of the Chemical Metallurgy Section has developed an apparatus for zone melting of small-diameter tungsten rods. Because of the high cost of the semi-purified material used in the process, it became desirable to simulate the heat transfer operation as a means of determining optimum relations between rod diameter, heating rate, and progress of the molten zone.

The technique is applicable to other materials, and the problem is interesting from the simulation viewpoint for several reasons. The conventional diffusion equation frequently used for analog computation is not suitable because it requires precise knowledge of the temperature distribution at the surface. A model must be set up in terms of heat flows; these too are unknown, but can more readily be estimated from the physical situation. The model must include radiation losses, which at these high temperatures require fourth-power nonlinear terms. The change of state at the melting point results in a local interruption of the temperature rise in the melting zone. Conductivity, thermal capacity, and emissivity will change with temperature and with state. Time rates of temperature change will be treated as infinitesimals, spatial rates as discrete increments. The incremental dimensions for radial and axial subdivision must be carefully chosen if optimum use is to be made of the limited number of integrating amplifiers available.

The radii r_s of the 5 rods to be simulated range from 0.1 to 0.5 cm; lengths (actually 3 or 4 ft) are assumed infinite. Heating is by continuous electron bombardment in a vacuum from a heated wire of 1.2 mm diameter, shaped to an annulus of 4.0-cm diameter surrounding the rod as shown in figure 1. The heater is initially fixed near one end, but after melting begins it is moved very slowly up (or down) the rod. The impurities are retained in the molten zone and are carried to one end, leaving the purer metal to solidify again to rod form. This motion is neglected in the simulation. Circumferential symmetry and an isomorphic rod are assumed, and the heat input from the wire is taken to be a step function of time.

Because of symmetry on either side of the heater midplane, it is enough to consider only half the length of the rod. Preliminary estimates indicated that temperatures would rise only slightly at points 20 mm distant from that plane, so that heat flow beyond this was neglected. Steep temperature gradients may be expected near the heater, and it is necessary to assure that metal will not drip off the outer surface before the core is melted. One purpose of the simulation, therefore, was to find whether the molten zone advanced radially at least as fast as it advanced axially. Subdivisions into annuli or cylinders with lengths Δy, outer radii r_o, and inner radii r_i were decided upon. Their generalized proportions relative to surface radii r_s are given in table 1.

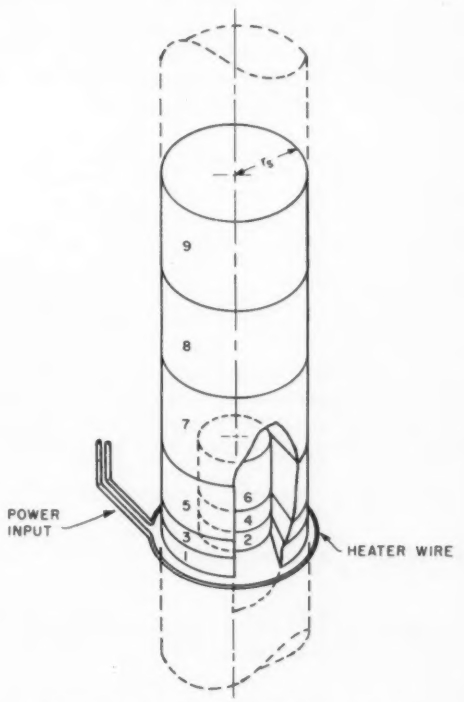

FIGURE 1. *Assumed subdivision of rod.*

The heat stored per unit time in zone 1, which is assumed to have a uniform temperature of T_1 degrees Kelvin, at time θ seconds after heating begins, is the thermal capacity of the zone volume multiplied by the rate of temperature rise. With density γg/cm^3 and temperature-dependent specific heat $c=c(T_1)$ cal/g-deg K, this storage rate is $\gamma c\pi(r_s^2-r_i^2)\Delta y\, dT_1/d\theta$. Similar expressions hold for the other zones, with r_o replacing r_s and $r_i=0$ for the inner ones.

TABLE 1.

Zone	r_o/r_s	r_i/r_s	Δy
			Mm
1	1	0.5	1
2	0.5	0	1
3	1	0.5	1
4	0.5	0	1
5	1	0.5	3
6	0.5	0	3
7	1	0	5
8	1	0	5
9	1	0	5

Heat inflow to zone 1 will be 239 P cal/sec, where P is the steady kilowatt power input to the half-rod. Heat outflow by reason of conductivity $k=k(T_1)$ cal/(sec) (cm)^2 (deg K/cm) will be radially inward to zone 2 across the area $2\pi r_i\Delta y$ with the gradient $(T_1-T_2)/(r_1-r_2)$, where r_1 and r_2 are mean radii. Also, there will be conduction axially to zone 3, at the rate $\pi k(r_s^2-r_i^2)\,(T_1-T_3)/(y_1-y_3)$ where y_1 and y_3 are mean lengths. No heat is transferred beyond the heater midplane, since there is no gradient across that boundary. However, zone 1 loses heat by radiation to ambient temperature T_a at the rate $1.37\epsilon\,(2\pi r_s\Delta y)$ $[(T_1/1000)^4-(T_a/1000)^4]$ where $\epsilon=\epsilon(T_1)$ is the temperature-dependent emissivity. The heat flow balance equation for zone 1, at any time up to the instant of local melting, is then

$$\gamma c\pi(r_s^2-r_i^2)\Delta y\,\frac{dT_1}{d\theta}=239P-2\pi r_i k\Delta y\left[\frac{T_1-T_2}{r_1-r_2}\right]$$
$$-\pi k(r_0^2-r_i^2)\left[\frac{T_1-T_3}{y_1-y_3}\right]$$
$$-1.37\epsilon(2\pi r_s\Delta y)\left[\left(\frac{T_1}{1000}\right)^4-\left(\frac{T_a}{1000}\right)^4\right].$$

Similar heat flow balance equations can be written for the other zones except that $239P$ is replaced by radial or axial conductive inputs, and there is no radiation for the interior zones where r_0 replaces r_s and $r_i=0$.

For zone 3, for example, the equation is

$$\gamma c\pi(r_s^2-r_i^2)\Delta y\,\frac{dT_3}{d\theta}=-2\pi r_i k\Delta y\left[\frac{T_3-T_4}{r_3-r_4}\right]$$
$$+\pi k(r_s^2-r_i^2)\left[\frac{T_1-T_3}{y_1-y_3}\right]-\pi k(r_s^2-r_i^2)\left[\frac{T_3-T_4}{y_3-y_4}\right]$$
$$-1.37\epsilon(2\pi r_s\Delta y)\left[\left(\frac{T_3}{1000}\right)^4-\left(\frac{T_a}{1000}\right)^4\right]$$

Numerical values of the properties γ, c, k, and ϵ were known only imprecisely for tungsten, but it appeared that they change only slowly in the range from $T_a=300$ to $T_m=3700$, the melting point. Accordingly, the values of table 2 were used in the computation, based on preliminary estimates of temperatures with zone 1 melted and zones 2 and 3 just beginning to melt. The heat of fusion in zone 1, about 44 cal/g, was neglected in this approximation. For each zone, the initial temperature was assumed to be 300 °K, and regions beyond zone 9 were assumed to remain at this temperature.

Substitution of numerical values in the 9 expressions for heat flow gave for the rod of 1-cm diameter the following set of simultaneous first-order difference-differential equations for solution by the analog computer:

$$+0.2\dot{T}_1=.015\mathrm{P}-.0394(T_1-T_2)-.369(T_1-T_3)$$
$$-.0498\mathrm{T}_1^4/10^6$$
$$-2\dot{T}_2=-.118(T_1-T_2)+.363(T_2-T_4)$$
$$-0.2\dot{T}_3=-.369(T_1-T_3)+.0388(T_3-T_4)+.173(T_3-T_5)$$
$$+.0498T_3^4/10^6$$
$$+0.2\dot{T}_4=+.406(T_2-T_4)+.1302(T_3-T_4)-.23(T_4-T_6)$$
$$+0.2\dot{T}_5=+.439(T_3-T_5)-.3195(T_5-T_6)-.261(T_5-T_7)$$
$$-.134T_5^4/10^6$$
$$-2\dot{T}_6=-.115(T_4-T_6)-.2116(T_5-T_6)+.067(T_6-T_7)$$
$$-\dot{T}_7=-.129(T_5-T_7)-.0504(T_6-T_7)+.167(T_7-T_8)$$
$$-\dot{T}=-.167(T_7-T_8)+.167(T_8-T_9)$$
$$+\dot{T}_9=+.167(T_8-T_9)-.167T_9+.502$$

TABLE 2

Zone	T	γc	k	ϵ
1	3700	0.84	0.31	0.36
2	3700	.84	.31	----
3	3700	.84	.31	.36
4	3000	.75	.30	----
5	1100	.55	.27	.13
6	700	.50	.39	----
7,8,9	500	.50	.42	.05

Figure 2 shows the computer patchboard diagram for the first two and last two of these equations. The time scale was slowed in the ratio of 1:20, and 1 machine volt represented 100° Kelvin. Heater input P was adjusted by trial with the aim of establishing an optimum value which would use a minimum of energy without causing zone 3 to melt ahead of zone 2. For the 1-cm rod, such a value could not be found, since zone 3 always reached 3,700° before zone 2, while the temperature of zone 1 went up to about 4,600°. This represents an undesirable physical situation which in practice may prevent satisfactory processing of a rod of this large diameter. In view of the uncertainty as to actual values of γ, c, k, and ϵ, it was considered unnecessary to carry through the computation for a more refined approximation.

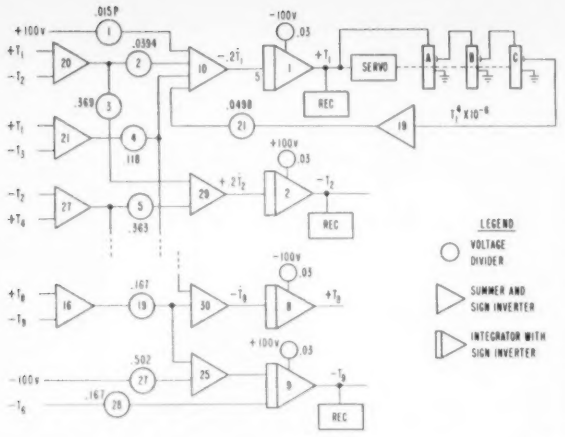

FIGURE 2. *Initial and final stages of computer patching.*

A set of temperature-time curves for one of the smaller rods with a 650-watt input is shown in figure 3. It will be noted that the melting of zone 3 lags that of zones 1 and 2, and hence that the power can be adjusted so that zone 3 just fails to melt. This assures formation of a thin liquid layer which is physically stable. The rod is nearly melted through in about 3 sec. This finding required modification of the power control circuits of the experimental apparatus by addition of rapid-response components to supplement the original servomechanism, which had required about 30 sec to establish an equilibrium setting.

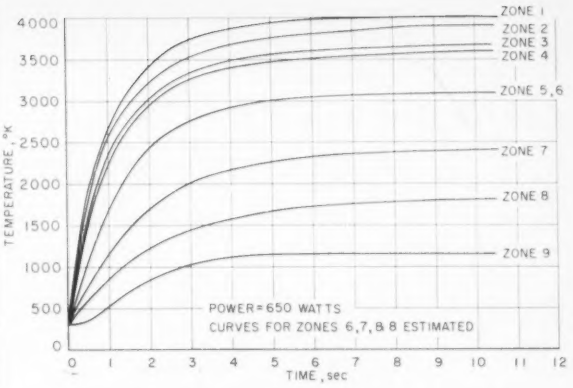

FIGURE 3. *Zone melting 2-mm-radius tungsten rod.*

Assistance on this problem came from NBS colleagues G. A. Moore, who supplied the physical constants and offered much constructive advice; P. K. Wong, who operated the computer; and R. Shives, who plotted the curves.

(Paper 65C2–60)

JOURNAL OF RESEARCH of the National Bureau of Standards—C. Engineering and Instrumentation
Vol. 65C, No. 2, April–June 1961

Residual Losses in a Guard-Ring Micrometer-Electrode Holder for Solid-Disk Dielectric Specimens

Arnold H. Scott and William P. Harris

(January 19, 1961)

A guard-ring micrometer-electrode holder especially designed for use in making dielectric measurements on solid-disk specimens of low-loss materials has been constructed. A method of determining the separation of the electrodes to ± 1 micron, using ball reference gages, is described. Residual losses in the guard-ring holder, and also in the bridge standard capacitor used in the Schering bridge employed for the measurements, caused by losses in surface films on the electrodes and by series resistance in the leads, were accurately measured. It is shown that at frequencies from 100 cycles per second to 100 kilocycles per second these residual losses are not more than a few microradians. Using corrections thus obtained, the holder-bridge combination can be used to measure the losses of low-loss materials with greater accuracy than heretofore.

1. Introduction

This paper describes a guard-ring micrometer-electrode holder and methods by which the separation of the electrodes, the capacitance, and the residual losses of the holder can be precisely determined. The holder is one which was designed and constructed to meet the need for a very accurate method of measuring the dielectric properties of some standard reference specimens of dielectrics.

Such standard reference specimens [1] [1] are useful in checking the various techniques and equipment used for measurements of the dielectric constant and dissipation factor of insulating materials. Two general classes of dielectric measurements are used: two terminal and three terminal. The three terminal method is usually more accurate, but may require more time, especially if a three-terminal bridge with an earthing circuit is used. For routine measurements in quantity, the two terminal method is often used. This method generally requires corrections for the edge capacitance and ground capacitance of the specimen under test. Standard dielectric reference materials permit a check on the accuracy of such measurements.

Recently there have come into general use two-terminal holders which eliminate most of the edge capacitance and all of the ground capacitance from the measurement, and permit relatively rapid measurements to be made. However, the loss measurements include the loss over the edge of the specimen and the loss through the insulation of the high-potential electrode of the holder. Accurate determination of the electrode spacing is also required. Here again, standard dielectric reference specimens are useful in checking the techniques and measurements involved.

In order for standard reference specimens to be useful, it is necessary that their properties be known accurately, apart from the methods and equipment used to measure these properties. This requires that residual losses and capacitances in the specimen holder be reduced to negligible proportions, or if this is not feasible, that they be accurately determined and separated from the measurements made on the specimens. A further complication arises from the fact that most materials that might be used for standard reference specimens exhibit properties that are affected by the ambient humidity, and must therefore be studied under different conditions of humidity in order that this effect might be evaluated, and that the dielectric properties under a given set of conditions might be known. This involves the determination of the variation of the residuals as a function of humidity. Of course, temperature dependence must also be considered.

The foregoing considerations prompted the construction of the specimen holder to be described, and led to the measurements made to determine the residual losses under various conditions. Methods are described which permit the determination of the losses in the holder, arising from series resistance in the connecting leads, from losses inherent in any film that may exist on the surfaces of the electrodes, or from any other source. From this, corrections can be applied to measurements made on specimens placed in the holder.

A useful bonus of the method used was that the losses in the standard bridge capacitor used were also determined, and a correction for this source of error was obtained.

2. Description of the Specimen Holder

The holder consists of a heavy cylindrical case with the electrodes mounted coaxially inside. The central guide rod of the movable electrode extends through the top of the case and its position is controlled by a thin nut located just above the top of the case. The position of the movable electrode is

[1] Figures in brackets indicate the literature references at the end of this paper.

sensed by a micrometer which comes in contact with the top of the guide rod. Figure 1 is a cross sectional diagram of the holder, and figure 2 shows the holder installed in a controlled-humidity chamber.

The guarded electrode and guard-ring are mounted on a ceramic disk. This disk was ground to nearly optical flatness and fits into a machined recess in the base of the case structure. A hole was ground in the center of this ceramic disk so that the centering rod of the guarded electrode would fit snugly into this hole thus holding the guarded electrode accurately centered on the ceramic disk. The guarded electrode is held snugly against the ceramic disk by means of screws in recessed holes in the ceramic disk. The guard-ring was recessed to fit snugly over the outside edge of the ceramic disk so that the guard-ring is also accurately centered on the ceramic disk. This permits the maintenance of a uniform gap between the guarded electrode and the guard-ring. Screws through the base plate and the ceramic disk into the guard-ring hold this electrode assembly rigidly against the base plate and make the necessary electrical connection between the guard-ring and the surrounding case assembly. The surface of this electrode assembly was ground optically flat.

The upper movable electrode is also mounted on a ceramic disk whose surfaces have been accurately ground. This ceramic disk is in turn mounted on the carefully machined surface of a metal disk attached to a guide rod which extends through the top of the barrel assembly. This guide rod passes through two guide bearings about 7 cm apart. A metal bellows is attached to the mounting disk and to a collar which fits over the guide bearing assembly.

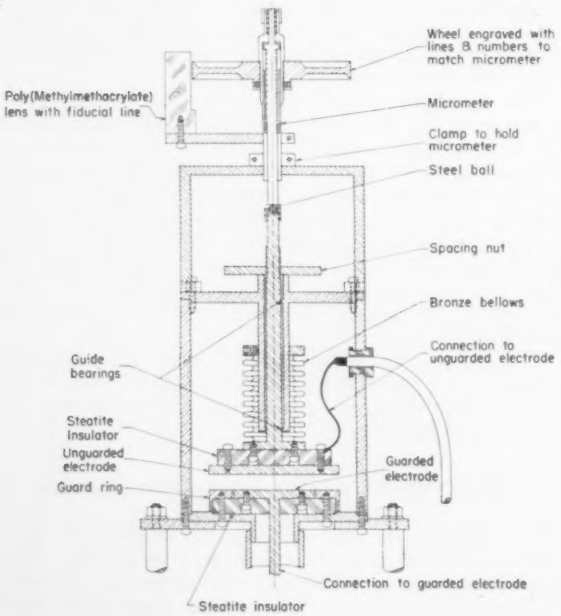

FIGURE 1. *Schematic diagram of the guard-ring micrometer-electrode holder for solid-disk dielectric specimens.*

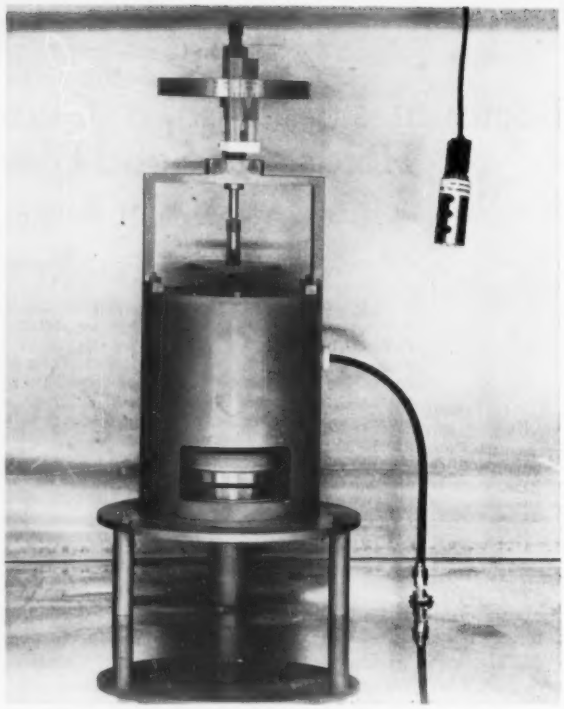

FIGURE 2. *Photograph of the new holder in place in controlled-atmosphere chamber.*

A set screw in the collar permits the location of the collar so that the bellows can be made to apply a force tending to move the movable electrode toward the guard-ring assembly. The collar and bellows also prevent the rotation of the movable electrode assembly.

The upper end of the guide rod is threaded, and a large diameter knurled nut is used on this to set the spacing between the electrodes. This nut works against the top of the guide bearing assembly. Fine threads (32 threads per inch) are used so that with care the spacing between the electrodes can be set within 1 μ.

The spacing between the electrodes is determined by means of a micrometer which is mounted on a frame so that it is held directly above the end of the guide rod. A steel ball is mounted on the end of the guide rod and the position of the guide rod is determined by screwing the micrometer down until it just touches this ball.

Contact with the ball can be accurately determined by a very light touch. The micrometer is equipped with a large graduated wheel so that the smallest divisions are equivalent to 2 μ. With a little practice and skill the micrometer measurements can be made repeatedly within a micron, by different observers.

The top and bottom of the cylindrical case can be removed to expose the electrode surfaces. The ends of the cylindrical case are carefully machined to be accurately perpendicular to the axis of the cylinder.

The end plates and electrode assemblies are carefully ground and machined so that when they are placed on the end of the cylindrical case the electrode surfaces are also perpendicular to the axis of the cylinder. Only slight adjustments are necessary to make the electrode surfaces parallel to the accuracy which is required in this work.

The electrodes were made of A.I.S.I. Type 304 stainless steel. No plating or coating was applied. The surfaces were ground and lapped smooth.

Connection is made to the guarded electrode by means of a coaxial connector whose outer case is attached to the base plate of the holder. Connection is made to the upper electrode by a flexible wire which is clamped under one of the mounting screws which hold the electrode to the ceramic disk. The other end is connected to the core of the coaxial cable which passes through the wall of the cylindrical case.

Two windows about 7-cm wide and 3-cm high are cut in opposite sides of the cylindrical case at the electrode level to permit the introduction and removal of samples from between the electrodes. A sliding band around the cylindrical case can be used to cover these openings if complete shielding is required.

3. Determination of the Area of the Guarded Electrode

To determine the area of the guarded electrode the base plate and guarded electrode assembly were removed from the cylindrical case. The diameter of the guarded electrode, and the gap between the guarded electrode and the guard-ring were measured by means of a traveling microscope. The effective area of the guarded electrode was then computed using the gap corrections published in ASTM D–150 [2]. The effective area was found to be 20.366 cm².

4. Determination of the True Spacing of the Electrodes

In order to adjust the upper and lower electrodes to be parallel and to measure the actual separation of the electrodes, a set of ball reference gages was prepared and accurately measured. Steel balls with nominal diameters of $\frac{3}{32}$, $\frac{1}{8}$, $\frac{5}{32}$, $\frac{3}{16}$, $\frac{7}{32}$, and $\frac{1}{4}$ in. were rigidly mounted in strips of plastic. These strips served as handles for placing the gages at the desired points between the electrodes, and the rigid mounting insured that a definite diameter was always presented. These reference gages were measured by the Engineering Metrology Section of NBS, and their diameters determined under no-load condition with an accuracy of ± 0.00005 cm.

Parallelism of the electrodes was established by using a ball mounted similarly to those described, but not necessarily accurately measured, to complete the electrical circuit of an ohmmeter connected to the two electrodes. The electrodes were brought together by the thumb nut to such a distance that the ball just made contact between the electrode surfaces, but yet was free enough to move about. If there was any lack of parallelism, this was made readily apparent by the existence of areas on one side of the electrodes where contact was not made while at the opposite side contact was made, or possibly the ball would not slide easily between the electrodes. Adjustments were made by tightening or loosening the appropriate screws located around the circumference of the case.

It was found that after such adjustments had been made, their full effect was not immediately seen. It took several hours for the dimensions to stabilize. This is attributed to two effects. First, the act of making the adjustment requires some handling of the cell, with some disturbance of the temperatures of the various parts of the cell case. The other factor, and perhaps the major contributor to the long time required for dimensional stability to be reestablished, is that the metal probably creeps for a time after the stresses are altered. The result of these effects is that the final adjustments must be made by making very small changes and then waiting several hours or overnight for the ensuing changes in the metal to take place.

This same ball-gage technique can be used to determine whether the guard ring and the guarded electrode are in the same plane, using the other electrode as a reference surface.

After the electrodes had been made parallel, a comparison was made between the measured capacitance and that computed for the separation of the electrodes as determined by ball reference gages of different diameters. Typical results are shown in table 1. It was concluded, from the fact that excellent agreement was obtained, that the reference gages could now be used for occasional check measurements, the measured capacitance used to determine the electrode separation with the holder empty, and these measurements used to find the zero correction to be applied to the micrometer readings. It is desirable to have a rapid means of determining this micrometer zero correction, because any adjustments of the micrometer mount, or of the electrodes, such as resetting them to be parallel, changes the micrometer zero correction.[2] It was found that the zero correction can be determined readily and repeatably from capacitance measurements. Some results of such measurements are shown in table 2.

TABLE 1. *Comparison of measured capacitance with the capacitance computed from the electrode separation*

Spacing by ball gage	Computed C	Measured C	ΔC
cm	*pf*	*pf*	*pf*
0.31773	5.6754	5.6755	0.0001
.47638	3.7853	3.7856	.0003
.55558	3.2457	3.2456	.0001

The agreement of the micrometer zero correction determined for the various spacings is acceptable,

[2] A significant change of temperature could also change the correction. For this work, temperature is held constant to ±1 degree C. The effect of this small temperature change was found to be negligible.

TABLE 2. *Determination of micrometer zero correction from measured capacitance*

Micrometer reading	Capacitance	Computed spacing	Difference
cm	*pf*	*cm*	*cm*
0.2499	7.177	0.2513	0.0014
.1194	14.926	.1208	.0014
.0793	22.324	.0808	.0015
.0590	29.847	.0604	.0014
.0471	37.159	.0485	.0014
.0390	44.566	.0405	.0015
.0332	52.077	.0346	.0014

and following these measurements a zero correction of 14 μ was used until further adjustments were made to the electrodes.

It is estimated that the separation of the electrodes can be determined to about ± 1 μ, using the micrometer in this fashion.

5. Losses in the Specimen Holder and Standard Bridge Capacitor

5.1. General Considerations

It was intended that this holder should be used during accurate measurements of the losses in materials that have rather small losses. Therefore it was necessary to evaluate the holder for the effects of inherent losses. It is evident that any series resistance in the leads connecting the holder into the measuring circuit will appear in the measurements as a loss. Also, losses in any surface films on the electrodes must be evaluated. It is known that some electrode materials form oxide films which might be expected to exhibit losses [3, 4, 5, 6, 7, 8, 9, 10, 13].

5.2. The Bridge

A low-voltage Conjugate Schering Bridge was used to make the measurements. The substitution method was employed. A diagram of the bridge circuit is shown in figure 3. Because the residual losses in the variable bridge standard capacitor C_2 are involved in the measurements, it is necessary to evaluate these losses. This requirement was no appreciable handicap, because the method employed yielded simultaneously the losses in both the specimen holder and the standard bridge capacitor.

Measurements by the substitution method are made by setting C_H to some value of capacitance by adjusting the separation of the electrodes, and setting C_2, the standard bridge capacitor, to some initial value, usually 20.000 pf. The capacitor C_3 is also set to some convenient initial value. After setting Sw 1 to position A, the bridge is balanced by varying C_1, C_4, C_5, and R_5, while alternately setting switch 2 to the A and B positions, until the detector shows a null in both A and B positions. The values of C_2 and C_3 are noted, and will be designated C_2' and C_3', respectively. Sw 1 is now moved to position B. Leaving C_1 and C_4 unchanged, the bridge is rebalanced by varying C_2, C_3, C_5, and R_5. The new values of C_2 and C_3 are noted, and will be designated as C_2'' and C_3''. The difference between the second and first values of C_2, ΔC_2, is the capacitance of the holder,[3] C_H. The difference between the second and first values of C_3, ΔC_3 is used to compute the value of the dissipation factor of the holder, D_H, according to the equation [4]

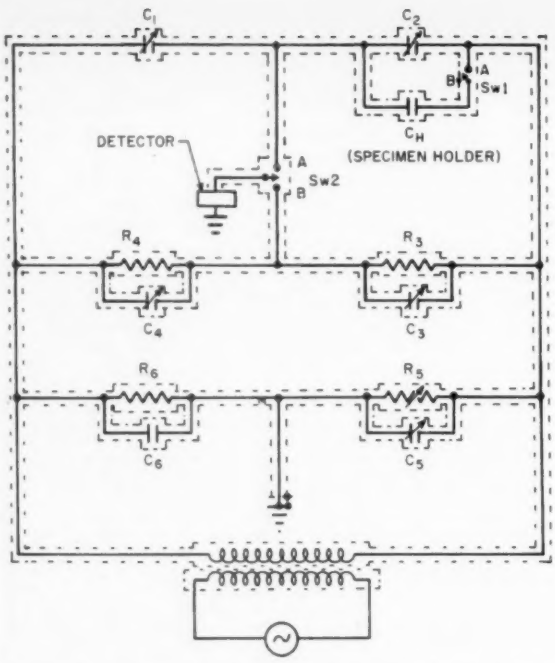

FIGURE 3. *Schematic diagram of the conjugate Schering bridge used for this investigation.*

$$D_H = \frac{\omega R_3 C_2'' \Delta C_3}{\Delta C_2} + \frac{G_2'' - G_2'}{\omega \Delta C_2}, \qquad (5.1)$$

where

D_H = dissipation factor (tan δ) of the specimen holder;
R_3 = value of R_3, figure 3, in ohms;
C_2'' = capacitance of C_2 with Sw 1 in position B, which is the total capacitance in the measuring arm of the bridge;
$\Delta C_3 = C_3'' - C_3'$ = difference between final and initial values of C_3;
$\Delta C_2 = C_2'' - C_2'$ = difference between final and initial values of C_2;
G_2' = equivalent parallel conductance of C_2 corresponding to the initial value C_2'; and
G_2'' = equivalent parallel conductance of C_2 corresponding to C_2''.

The first term on the right in eq (5.1), $\omega R_3 C_2'' \Delta C_3 / \Delta C_2$ is the dissipation factor computed without re-

[3] This statement is true for the case at hand, where the correction terms in the exact expression are negligible. The exact form is given in the appendix, section 7.
[4] This equation is derived in the appendix, section 7, and appears there as eq (7.7).

gard to the second term, which is a correction term taking into account the effect of non-zero and non-constant dissipation factor, D_2, in the bridge standard capacitor, C_2. Let us then write

$$D_H = D_M + D_2, \tag{5.2}$$

where

$D_M = \omega R_3 C_2'' \Delta C_3 / \Delta C_2$ = the measured or apparent dissipation factor as given by the uncorrected bridge measurement.

and

$D_2 = (G_2'' - G_2')/\omega \Delta C_2$ = the correction term to be applied to the apparent dissipation factor to take into account the dissipation factor of the bridge standard capacitor, C_2.

In order to consider the effect of elements that behave as series resistances, it will be more convenient to have eq (5.2) written in its series equivalent form, neglecting for the moment elements that behave as parallel conductances. If we separate the series resistance associated with the bridge standard capacitor, C_2, into two parts, one part corresponding to the series ohmic resistance of the leads to C_2, the other part corresponding to the losses caused by a surface film on the electrodes of C_2, eq (5.2) becomes [5]

$$D_H = D_M + 2\omega R_{2SL} C_2' + \omega R_{2SL} \Delta C_2 + \omega C_2' R_{2SF}' \tag{5.3}$$

where

R_{2SL} = the equivalent series resistance of the ohmic resistance of the leads, connections, etc., of C_2,

and

R_{2SF} = the equivalent series resistance of the film on the surfaces of the electrodes of C_2.

5.3. Consequences of Equation 5.3

Examination of eq (5.3) reveals that there are two correction terms involving R_{2SL}, one dependent on C_2', the initial value of the bridge standard capacitor, the other dependent on ΔC_2. There is one term involving R_{2SF}.

Let us now consider the behavior of these correction terms as a function of the capacitance of C_2, and examine their effect on the value of D_M, the uncorrected or measured value of D_H. In the following arguments, it will be assumed that all measurements are made at a fixed frequency, except as stated. Also, for any single set of curves, it will be assumed that C_2' has a single value, usually, in the actual measurements to be presented later, 20.000 pf.

[5] This relation is derived in full in the appendix, section 7.

Taking first the simplest case, involving only the term due to losses in a surface film, assuming for the moment that R_{2SL} is negligible, we see that the correction term is

$$\omega R_{2SF}' C_2' = D_{2F} \tag{5.4}$$

This term is a constant, even for different values of C_2', because R_{2SF}' is inversely proportional to the capacitance, [6] in this case C_2'. Therefore we may plot this term versus capacitance as a straight line of zero slope, as shown in figure 4.

If we now consider the effect of a lossy surface film on the holder electrodes, where the area is constant and the capacitance is a function of the separation of the electrodes, we see that a dissipation factor proportional to the capacitance results. [7] Let us designate this component of dissipation factor, due to a lossy surface film in the holder, as

$$D_{HF} = \omega R_{HSF} C_H = \omega R_{HSF} \Delta C_2, \tag{5.5}$$

where R_{HSF} is the equivalent series resistance corresponding to the surface film losses in the holder. A plot of D_{HF} versus capacitance would be a straight line with positive slope, passing through $D=0$, $\Delta C_2 = 0$ (or nearly so, depending on the ground capacitances [11, 12]). This is shown in figure 4.

From eq (5.2), we see than $D_M = D_H - D_2$, or in this case $D_M = D_{HF} - D_{2F}$. D_M is plotted in figure 4, where it is seen that it is a straight line with the same slope as the plot of D_{HF}, and with a negative intercept equal in magnitude to the constant value of D_{2F}, if the previously assumed conditions exist.

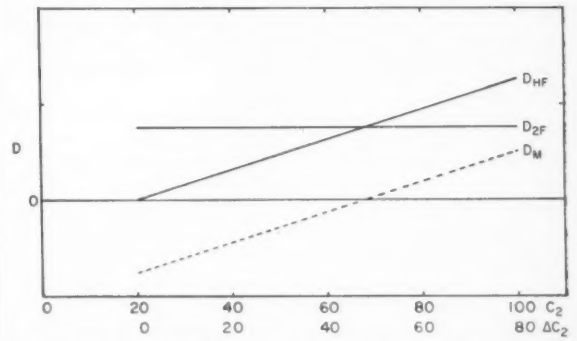

FIGURE 4. *A plot of assumed, arbitrary values of dissipation factor due to a lossy surface film on the electrodes of the specimen holder,* D_{HF}, *and those of the bridge standard capacitor,* D_{2F}.

The dissipation factor that would be indicated by the bridge under these conditions, $D_M = D_{HF} - D_{2F}$, is also plotted. These are plotted against ΔC_2 (see text), assuming an initial value of C_2 of 20.000 pf.

[6] It seems reasonable to assume that a surface film would be uniformly distributed over the surface. Thus, the conductance of the film would be proportional to the active electrode area. The capacitance is also proportional to the active electrode area. Therefore the resistance R_{2SF} is inversely proportional to the capacitance.

Near the edges of the capacitor places, where fringing occurs, this proportionality would not hold exactly. However, results show that the nonlinearity is negligible in the present case, as might be expected from the geometry of the capacitor used.

[7] This assumes that the equivalent series resistance corresponding to the surface film losses is independent of the electric field. Tests at various voltages applied to the bridge yielded the same results, thus making this assumption appear reasonable for this case.

Let us now consider the effect of the series resistance of the leads, switches, or other circuit components used to connect the specimen holder into the measuring circuit. A component of dissipation factor, which we shall designate D_{HL}, would result. This dissipation factor would behave in the same manner as D_{HF}, because it is of the same form:

$$D_{HL}=\omega R_{HSL}\Delta C_2. \tag{5.6}$$

Figure 5 shows a plot of D_{HL}, D_{HF}, and the total dissipation factor of the holder D_{HT}.

$$D_{HT}=D_{HL}+D_{HF}. \tag{5.7}$$

Assuming the same dissipation factor for the bridge standard capacitor as in the previous case, D_{2F}, and plotting $D_M=D_{HT}-D_{2F}$, we have the results plotted in figure 5. We see that the slope of the D_M plot is the same as that of D_{HT}, with negative intercept equal in magnitude to D_{2F}.

Let us now consider the effect of series resistance in the leads connecting the bridge standard capacitor C_2 to the measuring circuit. From eq (5.3), we see that there are two terms involving this resistance: $2\omega R_{2SL}C_2'$ and $\omega R_{2SL}\Delta C_2$. Let these be designated D_{2La} and D_{2Lb} respectively. These terms plot as shown in figure 6. Also plotted is D_{2T}, the total dissipation factor of C_2.

$$D_{2T}=D_{2F}+D_{2La}+D_{2Lb}. \tag{5.8}$$

If we plot also the dissipation factor of the specimen holder, D_{HT}, and D_M, the results are as shown in figure 6. Once again we see that D_M plots as a straight line, with a negative intercept equal to the value of D_{2T} at $\Delta C=0$. The slope of the plot of D_M is now different from that of the plot of D_H, because of the fact that D_{2Lb} is not constant.

Because the purpose of all these hypotheses is to provide a means of evaluating the various components of dissipation factor and to separate the dissipation factor of the specimen holder from that of the bridge standard capacitor, let us suppose that we

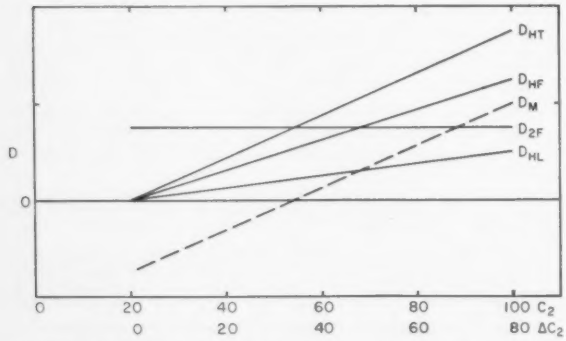

FIGURE 5. *A plot similar to figure 4, but including now a component of dissipation factor due to series resistance in the leads to the specimen holder,* D_{HL}.

The total dissipation factor of the holder, $D_{HT}=D_{HF}+D_{HL}$, is plotted, and now $D_M=D_{HT}-D_{2F}$.

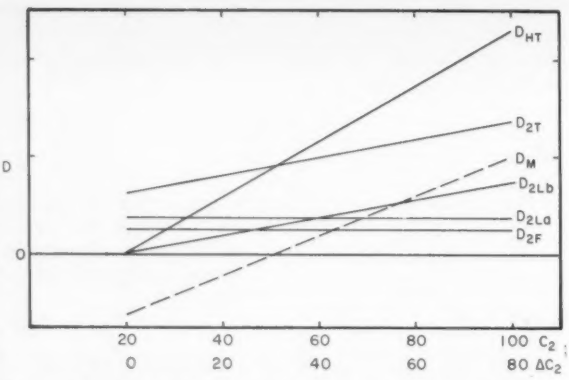

FIGURE 6. *A plot similar to figure 5, including components of dissipation factor due to series resistance in the leads to* C_2, *the bridge capacitor.*

As discussed in the text, there are two such components, one constant with capacitance, the other proportional to ΔC. D_{2T} is the sum of all components of the dissipation factor of C_2.

have just made a set of measurements that yielded the plot [8] of D_M seen in figure 6. The slope of this curve will be the same as that of the plot of D_H only if the slope of D_{2T} is zero. To determine the slope of D_{2T}, we can make another set of measurements starting from a different C_2'. This would change the value of D_{2La}, and would permit an evaluation of this component of dissipation factor. Another revealing test would be a set of measurements at different frequencies. It can be seen that such measurements would permit the separation of dissipation factor components due to series resistance, in either the bridge standard capacitor leads or the holder leads. The behavior of the slope and intercept of the plot of D_M would indicate the presence or absence of appreciable resistance in the leads of the bridge standard capacitor.

We have now dealt with losses in a surface film, and losses due to series resistance. Let us turn our attention to losses due to a fixed parallel conductance.

If a fixed parallel conductance occurs in the branch containing the bridge standard capacitor, it is readily apparent from eq (5.1) that it will not make any contribution to the apparent dissipation factor of the unknown being measured, for if $G_2'=G_2''$, the correction term is zero.

If, however, there is a fixed conductance in parallel with the specimen holder, it will contribute a component of dissipation factor that varies with capacitance in the manner shown by the plot labelled D_{HP} in figure 7. When this is added to the other components of dissipation factor of the holder, the sum is D_{HT}, plotted in figure 7. Subtracting from this D_{2T}, the total dissipation factor of C_2, we have D_M, also plotted in figure 7. It is evident that this plot behaves in a manner quite different from those previously considered, and a plot of measured values

[8] Combining equations 5.2, 5.3, 5.4, 5.5, 5.6 and 5.7, we can write the collected expression for D_m:

$$D_M=\underbrace{\omega R_{HSL}\Delta C_2+\omega R_{HSF}\Delta C_2}_{D_H}-\underbrace{\omega R_{2SF}'C_2'-2\omega R_{2SL}C_2'-\omega R_{2SL}\Delta C_2}_{D_2}.$$

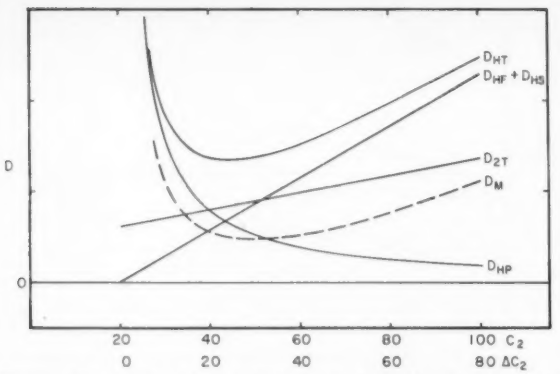

FIGURE 7. *A plot similar to figure 6, including a dissipation factor component due to a fixed parallel conductance in the holder,* D_{HP}.

A similar conductance in C_2 would produce no effect in the measurements (see text).

of D_M would readily reveal such a parallel conductance. In practice, such a conductance is not to be expected in the present set of circumstances, and actual measurements confirmed the absence of parallel conductance.

5.4. Results of Measurements

From the foregoing discussion, it is evident that we have available a means of evaluating the dissipation factor of the empty specimen holder, and also that of the bridge standard capacitor, C_2. It is only necessary to use the Schering bridge to measure the apparent dissipation factor, D_M, at several values of C_H, the capacitance of the specimen holder, recalling that (footnote 3) $C_H \cong \Delta C_2$.

Measurements were made of the losses of the new specimen holder, known as Holder No. 4, using General Radio Co. Type 722–DS29, Serial 7128 as the standard capacitor.

The measurements were made during the winter months, with room relative humidity ranging between 10 percent and 40 percent, mostly at about 20 percent.

The bridge standard capacitor, C_2, was maintained in an enclosure dried by a stream of dry nitrogen. This nitrogen stream was dried by bubbling it through concentrated sulfuric acid, thence passing it through a drying column containing calcium chloride or calcium sulfate, and finally through a dry cotton filter.

The effect of relative humidity on the dissipation factor of the holder was of considerable importance, because the holder was constructed to measure the losses in low-loss materials under different conditions of humidity, principally very dry and 52 percent relative humidity, in order to compare the results. Therefore, measurements were made on the empty holder under two conditions of relative humidity. The holder was enclosed in a chamber which was very thoroughly dried by exposing therein a generous quantity of P_2O_5, which held the relative humidity well below 1½ percent, which was the lower limit of the relative humidity measuring apparatus used. By exposing within this chamber a saturated solution of $Mg(NO_3)_2$, the relative humidity could be maintained very close to 52 percent.

Note that the controlled atmosphere applies to the specimen holder only, and not to the bridge standard capacitor, which for all measurements was dried by a stream of dry nitrogen.

Two typical sets of measurements are presented in figure 8, for the purpose of showing that a straight line provides a reasonable fit for all the data. There is no pronounced tendency to exhibit a curve, such as the plot of D_M in figure 7, thus indicating that there is no appreciable parallel conductance in the holder. Note that the dissipation factors are all very small, and the slope is also small. It is not profitable to try to place any interpretation on the small digressions from the straight line, because the resolution of the apparatus is not great enough to permit more accurate measurements of such small dissipation factors. The resolution is much better at high capacitances than at the low end. Equation (5.1) gives, neglecting the correction term,

$$D_H = \frac{\omega R_3 C_2'' \Delta C_3}{\Delta C_2},$$

from which it is seen that as the measured dissipation factor becomes very small, ΔC_3 becomes very small. Since it is very difficult to determine very small differences in relatively large quantities, the method gives rather poor resolution at the lower values of dissipation factor, and this effect is heightened by the fact that the smallest dissipation factors occur when ΔC_2 is smallest. For these reasons, no measurements at ΔC_2 less than 20 pf are included.

Most of the dielectric specimens for which this new holder was designed will have capacitances of 5 to 50 pf. Referring again to figure 8, notice that in this range the dissipation factor does not vary more than about 4×10^{-6}, or in terms of the loss angle,[9] about 4 microradians (μradians).

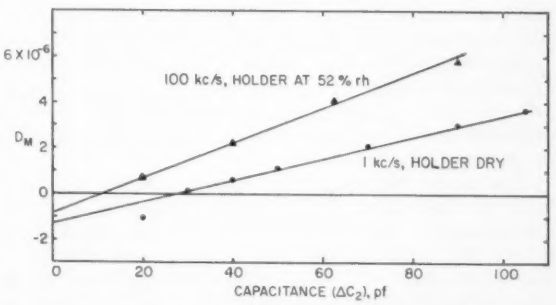

FIGURE 8. *Typical results of actual measurement of dissipation factor of the holder under two widely different conditions, showing that straight-line plots adequately represent the data, and that the dissipation factors are small.*

[9] The dissipation factor, D, is the tangent of the loss angle. $D = \tan \delta$. For small angles $\delta \cong \tan \delta$, and often the term loss angle, expressed in μ radians is used.

The magnitudes of the intercepts of the two sets of measurements are less than 2 μradians. In the light of the preceding analysis, this can be interpreted to show that the sum of the components of loss angle caused by the surface film on the electrodes of the bridge standard capacitor, C_2, and that caused by series resistance in the leads to C_2 is less than 2 μradians at $\Delta C_2=0$. This sets a limit to the slope of the plot of the total dissipation factor of C_2 versus ΔC_2, as is evident from examination of eq (5.3). For convenience this expression is rewritten here:

$$D_H=D_M+2\omega R_{2SL}C_2'+\omega R_{2SL}\Delta C_2+\omega C_2'R_{2SF}'. \quad (5.3)$$

Note that the third term on the right is the same as the second term on the right when $\Delta C_2=2C_2'$. Thus if the loss angle of the bridge standard capacitor is less than 2 μradians at $\Delta C_2=0$, it must be less than 4 μradians at $\Delta C_2=2C_2'=40.000$ pf. Note also that this is true at the highest frequency used, 100 kc/s. Even if the third term on the right were at its maximum, almost 2 μradians, at this frequency, it would be only one-tenth of this or 0.2 μradian at 10 kc/s, and would be no more than 0.02 μradian at 1 kc/s.

To sum up this line of reasoning, we have proven that at frequencies up to 100 kc/s, and at specimen holder capacitances up to 40 pf ($C_H\cong\Delta C_2$), the maximum error in the determination of the loss angle of the empty specimen holder due to neglected series resistance in the leads to the bridge standard capacitor is no greater than 2 μradians. Other tests show that the actual error due to this cause is much smaller than this maximum. Such tests include measurements made at various frequencies, from other initial values of C_2, and on actual specimens of very low loss materials, such as polyethylene.

Our early measurements showed a much greater slope for D_M at 100 kc/s. Examination showed this loss to be attributable to the series resistance of certain leads used at that time. The offending cable was removed and replaced with a type with much lower resistance, and a great improvement was observed. The effect of the residual series resistance in the leads to the specimen holder are still observable in figure 9, where the results of measurements at frequencies of 100 c/s, 1 kc/s, 10 kc/s, and 100 kc/s are shown together. Note that the slope of the 100 kc/s plot is greater than the other slopes. The results shown in figure 9 show that at all measured frequencies except 100 c/s, the intercept is about 1 μradian or less. This confirms and emphasizes that the series resistance in in the leads to C_2 is low.

The data presented in figure 9 were obtained with the specimen holder maintained in a very dry atmosphere. In figure 10 we see the results obtained when this atmosphere had a relative humidity of about 52 percent. Note that in both these cases, the bridge standard capacitor, C_2, was maintained as dry as could be attained with a stream of dry nitrogen flowing through the enclosure containing it. This means that losses in C_2, indicated principally by the intercepts, should remain nearly unchanged for the two sets of data. The higher relative humidity might be expected to increase

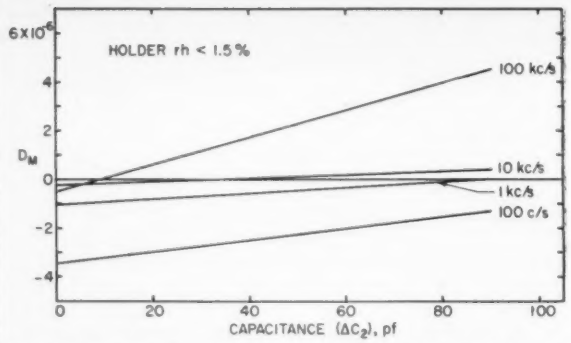

FIGURE 9. *Results obtained at 100 c/s, 1 kc/s, 10 kc/s, and 100kc/s, with the holder maintained in a dry (relative humidity less than 1.5 percent) atmosphere.*

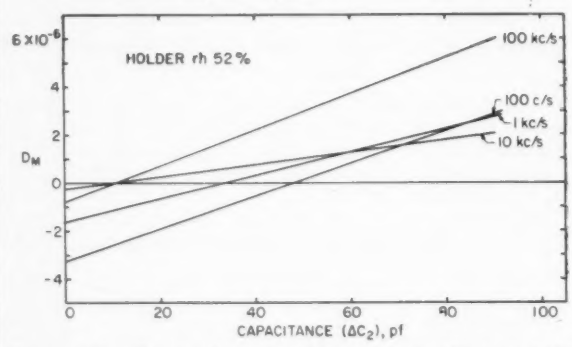

FIGURE 10. *Results obtained at 100 c/s, 1 kc/s, 10kc/s, and 100 kc/s, with the holder maintained in an atmosphere of 52 percent relative humidity.*

the loss in the surface film on the electrodes of the holder. This would be evidenced by an increased slope for D_M plots at the higher relative humidity.

Comparison of figures 9 and 10 shows that actual measurements agree with the behavior anticipated. The intercepts, within experimental error, are the same for both cases, while the slopes are noticeably greater for the higher humidity case.

The agreement of the intercepts is even more evident in figure 11, where values of D_2 obtained under the two different conditions of relative humidity surrounding the holder are plotted together. The agreement is satisfactory, and the curve drawn through the average values shows the variation of D_2 as a function of frequency. The higher dissipation factor at the lower frequencies is evident here, as well as a very slight increase at the high end of the frequency scale. This latter is probably due to the residual series resistance of the leads to the bridge standard capacitor, C_2.

Early in the course of this investigation it was discovered that the apparent loss of the empty specimen holder was profoundly affected by the presence of small amounts of foreign materials on the electrode surfaces. It was necessary to keep the electrodes scrupulously clean, by occasionally cleaning them with distilled water followed by petroleum ether. It was found that electrodes

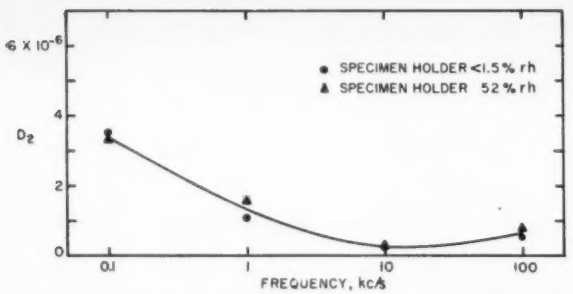

FIGURE 11. *The dissipation factor, D_2, of the bridge standard capacitor, C_2, plotted as a function of frequency.*

Each value is obtained from the intercept of one of the preceding plots, one set from the dry holder plots of figure 9, the other set from the 52 percent relative humidity holder plots of figure 10. Note that C_2 was maintained in an enclosure dried by a stream of dry nitrogen for all measurements (see text).

applied to dielectric specimens must be very clean, to avoid carrying dust particles, etc. to the holder electrodes. The care previously used in the handling of specimens was found to be inadequate, and new precautions were initiated, especially in the case of low loss materials, where a loss contribution due to foreign matter would be a greater percentage of the whole loss.

5.5. Correction for Holder Losses in Dielectric Measurements

After the values of the dissipation factors of the bridge standard capacitor and the empty specimen holder have been determined, the next problem is how to use them properly to correct the measured dissipation factor of a dielectric specimen.

In all cases, it is clear that D_2, the dissipation factor of the bridge standard capacitor, should be added to the measured value of dissipation factor of the specimen, D_M.

If the dielectric specimen has no contact electrodes applied to it, and is larger than the guarded electrode, it is evident that the measured dissipation factor will consist of two components, one due to losses in the dielectric material, the other due to losses in the holder. The latter component, which can be determined by the method described herein, can be subtracted from the measured value to yield the dissipation factor of the dielectric material itself, taking into account the fact that the dielectric constant of the specimen multiplies the effect of D_H. The correct relation to use in this case is:

$$D_x = D_M - \epsilon_x' D_H + D_2, \tag{5.9}$$

where

D_x=dissipation factor of the specimen

and

ϵ_x'=dielectric constant of the specimen.

In the case of a specimen with contact electrodes applied, this question must be answered: does the surface film remain intact, or is electrical contact made directly from the conducting contact electrode to the conducting substrate of the holder electrode material? If the latter is true, then the dielectric film is in effect short-circuited, and does not affect the measured dissipation factor. The problem is then shifted to that of determining what losses occur in the contact electrode material, in the interface of the contact electrode and the dielectric specimen, and in the material serving as adhesive, if any. This is a separate matter, and will not be further treated here.

If the specimen is smaller than the guarded electrode, so that some air capacitance is included in the measurement, the problem can be resolved into two parts, one dealing with the portion involving air capacitance in the space surrounding the specimen, the other dealing with the portion of the volume between the electrodes that is occupied by the dielectric specimen, taking into account its contact electrodes, if any.

Admittedly, some uncertainties arise here with respect to what happens in the case where contact electrodes are used. However, the fact that the surface film contributes (in this case) such a small component of loss, saves one from commiting a grave error, and it is probably best to make reasonable assumptions and proceed, secure in the knowledge that at worst the error will not exceed a few microradians.

5.6. Implications for Further Investigation

A second specimen holder is under construction, quite similar in basic design to the one described herein, except that provision is being made to make the electrodes interchangeable, and several sets of electrodes are in preparation. These electrodes are made of various materials, and will be used to determine which material yields lowest losses in surface layers. In addition to measuring several solid electrodes, it is intended that platings of various kinds will be applied to some of the electrode sets, and the losses in the surfaces measured.

6. Summary and Conclusions

A guard-ring micrometer-electrode specimen holder, especially designed for use for precision measurements of the dielectric properties of dielectric reference standard materials, has been constructed and evaluated. A technique has been devised for determining the spacing between the electrodes to ± 1 μ, using the micrometer.

It was found that resistance in cables often used to connect the components of a bridge can produce losses which are appreciable, and unless a correction is made for such losses, they can produce errors in the values of the dissipation factor of the holder, and also that of the bridge standard capacitor. A preferable method is to keep these resistances as low as possible by proper choice of cable type.

It was found also that minute quantities of foreign matter (such as dust or grease) on the holder electrodes will contribute an appreciable increment to the dissipation factor. It is necessary to be very careful to keep the electrodes scrupulously clean when low-loss materials are being measured.

The dissipation factor of the carefully cleaned holder has been measured, and it has been concluded that at frequencies in the range 100 c/s to 100 kc/s, almost all of the loss is in the surface film on the Type 304 stainless steel electrodes. The value of this dissipation factor was found to be directly proportional to the capacitance of the holder, and therefore inversely proportional to the separation of the electrodes. The relative humidity of the atmosphere surrounding the holder had an effect on the surface losses. The dissipation factor varied from about 1×10^{-8} per picofarad at 1 kc/s in a very dry atmosphere, to about 7×10^{-8} per picofarad at 100 kc/s with an atmosphere of about 52 percent relative humidity.

Knowledge of the values of these empty specimen holder losses is very useful for making corrections to the measured loss of dielectric materials with low losses, where the loss contribution of the electrode surface may be an appreciable fraction of the total loss.

Measurements made by the substitution method with a Schering bridge should also be corrected for the error due to the dissipation factor of the bridge standard capacitor. The method used yielded the value of this correction. The loss in a General Radio Type 722–DS29 variable air capacitor was concluded to be almost entirely in the electrode surfaces, and it was confirmed that the dissipation factor at any single frequency is almost constant over the entire capacitance range. When the capacitor was maintained in an enclosure dried by a stream of dry nitrogen, the dissipation factor was found to range from less than 0.5×10^{-6} at 10 kc/s, to about 3.5×10^{-6} at 100 c/s.

With this new specimen holder, it is possible to measure the spacing of the electrodes with about the same accuracy as that with which the thickness of the specimens can be determined. With the application of corrections determined by the methods described in this paper, the holder can be used to measure the loss angle of low-loss materials to within a few microradians.

7. Appendix

The exact expression for C_H as a function of the Schering bridge parameters is

$$C_H=C_2''\frac{G_3''G_3'+\omega^2C_3'C_3''}{G_3''^2+\omega^2C_3''^2}-C_2'+G_2''\frac{G_3''C_3'-G_3'C_3''}{G_3''^2+\omega^2C_3''^2}. \quad (7.1)$$

The expression for D_H is

$$D_H=\frac{\omega C_2''}{C_3''C_H}\left[C_3''\left(\frac{G_3''G_3'+\omega^2C_3'C_3''}{G_3''^2+\omega^2C_3''^2}\right)-C_3'\right]+\frac{G_2''}{\omega C_H}\left[\frac{G_3'}{G_3''}-\frac{\omega^2C_3''}{G_3''}\left(\frac{G_3'C_3''-G_3''C_3'}{G_3''^2+\omega^2C_3''^2}\right)\right]-\frac{G_2'}{\omega C_H}. \quad (7.2)$$

where

D_H = dissipation factor of the specimen holder and, in general, any specimen contained therein;
C_2' = initial value of C_2, with switch 1, figure 3, in position A;
C_2'' = final value of C_2, with switch 1 in position B;
$\Delta C_2=C_2''-C_2'$;
C_3' = initial value of C_3, with switch 1 in position A;
C_3'' = final value of C_3, with switch 1 in position B;
$\Delta C_3=C_3''-C_3'$;
G_2' = initial value of equivalent parallel conductance associated with C_2;
G_2'' = final value of equivalent parallel conductance associated with C_2;
G_3' = initial value of equivalent parallel conductance associated with C_3; and
G_3'' = final value of equivalent parallel conductance associated with C_3.

Since G_3 is principally the conductance of a fixed precision resistor of not more than 10^5 ohms, it is safe to assume that

$$G_3'=G_3''=G_3.$$

We can now write

$$D_H=\frac{\omega C_2''}{G_3C_H}\left[C_3''\left(\frac{G_3^2+\omega^2C_3'C_3''}{G_3^2+\omega^2C_3''^2}\right)-C_3'\right]+\frac{G_2''}{\omega C_H}\left[1-\frac{\omega^2C_3''(C_3''-C_3')}{G_3^2+\omega^2C_3''^2}\right]-\frac{G_2'}{\omega C_H}. \quad (7.3)$$

For the Schering bridge used, ω/G_3 was held constant at $2\pi\times10^7$, C_3'' never exceeded 1100 pf, and $C_3''-C_3'$ never exceeded 1000 pf. Under these conditions we may write

$$D_H=\frac{\omega C_2''}{G_3C_H}\left[C_3''\left(\frac{G_3^2+\omega^2C_3'C_3''}{G_3^2+\omega^2C_3''^2}\right)-C_3'\right]+\frac{G_2''}{\omega C_H}-\frac{G_2'}{\omega C_H}, \quad (7.4)$$

with no appreciable error in D_H. And

$$D_H=\frac{\omega C_2''}{G_3C_H}(C_3''-C_3')+\frac{G_2''-G_2'}{\omega C_H} \quad (7.5)$$

will give no more than 0.5 percent error in D_H. For less extreme values of C_3'', the error is less. The present work involved very low D_H, and therefore very small $C_3''-C_3'$, resulting in wholly negligible errors due to terms omitted from eq (7.5).

The first term on the right in eq (7.5) may be expressed as

$$\frac{\omega R_3C_2''}{C_H}(C_3''-C_3'),$$

yielding

$$D_H=\frac{\omega R_3C_2''\,\Delta C_3}{C_H}+\frac{G_2''-G_2'}{\omega C_H}. \quad (7.6)$$

In eqs (7.2) through (7.6), the exact expression for C_H given by eq (7.1) may be used. For the present work, however, C_3' was about 100 pf and C_3'' was less than 150 pf, yielding an error in C_H less than 0.003 percent if the correction terms in eq (7.1) are neglected. Therefore, we may with negligible further error write ΔC_2 for C_H in the preceding equations. Thus our expression for D_H becomes

$$D_H=\frac{\omega R_3 C_2''\,\Delta C_3}{\Delta C_2}+\frac{G_2''-G_2'}{\omega\Delta C_2}. \tag{7.7}$$

The last term in eq (7.7) is a correction term necessary if $G_2''\neq G_2'$. If this correction term is ignored, or is negligible, D_H is the term $\omega R_3 C_2''\Delta C_3/\Delta C_2$ which we will call D_M, the measured or uncorrected value of D_H. Then

$$D_H=D_M+\frac{G_2''-G_2'}{\omega\Delta C_2}. \tag{7.8}$$

For present purposes it will be useful to express this in terms of equivalent series resistances.

In parallel notation $D=G_P/\omega C_P$,

where

G_P=equivalent parallel conductance

C_P=equivalent parallel capacitance.

Therefore, let us write

$$\frac{G_2''-G_2'}{\omega\Delta C_2}=\frac{C_2''G_2''}{\Delta C_2\omega C_2''}-\frac{C_2'G_2'}{\Delta C_2\omega C_2'}=\frac{C_2''}{\Delta C_2}\,D_2''-\frac{C_2'}{\Delta C_2}\,D_2'. \tag{7.9}$$

In series notation, $D=\omega R_S C_S$,

where

R_S=equivalent series resistance

C_S=equivalent series capacitance.

Therefore if we let

C_{2S}'=series equivalent of C_2'

C_{2S}''=series equivalent of C_2''

R_{2S}'=equivalent series resistance corresponding to G_2'

R_{2S}''=equivalent series resistance corresponding to G_2''

then

$$\frac{C_2''}{\Delta C_2}\,D_2''-\frac{C_2'}{\Delta C_2}\,D_2'=\frac{C_2''}{\Delta C_2}\,\omega R_{2S}''C_{2S}''-\frac{C_2'}{\Delta C_2}\,\omega R_{2S}'C_{2S}'. \tag{7.10}$$

Because the dissipation factors involved in this work are very small, the series equivalent capacitance is very nearly the same as the parallel capacitance. That is

$$C_{2S}'\cong C_2', \text{ and } C_{2S}''\cong C_2''.$$

Therefore

$$\frac{C_2''}{\Delta C_2}\,\omega R_{2S}''C_{2S}''-\frac{C_2'}{\Delta C_2}\,\omega R_{2S}'C_{2S}'=\frac{C_2''^2\omega R_{2S}''}{\Delta C_2}-\frac{C_2'^2\omega R_{2S}'}{\Delta C_2}. \tag{7.11}$$

Let us now consider the series resistance R_{2S} to be composed of two components: (1) a series resistance term R_{2SL} representing series ohmic resistance in leads, connections etc. and (2) a term R_{2SF} representing the series equivalent resistance of a surface film on the electrodes. That is

$$\begin{aligned}R_{2S}'&=R_{2SL}'+R_{2SF}'\\ R_{2S}''&=R_{2SL}''+R_{2SF}''\end{aligned} \tag{7.12}$$

Because R_{2SL} represents series ohmic resistance, this term is independent of C_2. That is

$$R_{2SL}'=R_{2SL}''=R_{2SL}$$

and

$$D_H=D_M+\frac{C_2''^2\omega(R_{2SL}+R_{2SF}'')}{\Delta C_2}-\frac{C_2'^2\omega(R_{2SL}+R_{2SF}')}{\Delta C_2} \tag{7.13}$$

$$=D_M+\frac{(C_2''^2-C_2'^2)\omega R_{2SL}}{\Delta C_2}+\frac{C_2''^2\omega R_{2SF}''}{\Delta C_2}-\frac{C_2'^2\omega R_{2SF}'}{\Delta C_2}. \tag{7.14}$$

Because $C_2''=C_2'+\Delta C_2$

$$D_H=D_M+\frac{(C_2''^2-C_2'^2)\omega R_{2SL}}{\Delta C_2}+\frac{\omega C_2''R_{2SF}''C_2'}{\Delta C_2}+\frac{\omega C_2''R_{2SF}''\Delta C_2}{\Delta C_2}-\frac{\omega C_2'R_{2SF}'C_2'}{\Delta C_2}. \tag{7.15}$$

The conductance of the surface film, $1/R_{2SF}$, is proportional to the active area of the capacitor plates, which may be expressed

$$1/R_{2SF}=\alpha A.$$

From this $$R_{2SF}=1/\alpha A.$$

The capacitance C_2 is also proportional to the active area of the capacitor plates, or

$$C_2=\beta A.$$

The product $R_{2SF}C_2$ is now seen to be a constant because

$$R_{2SF}C_2=\frac{\beta A}{\alpha A}=\frac{\beta}{\alpha},$$

the ratio of two proportionality constants. From this we see that

$$R_{2SF}''C_2''=R_{2SF}'C_2'.$$

Therefore

$$D_H=D_M+\frac{(C_2''^2-C_2'^2)\omega R_{2SL}}{\Delta C_2}+\frac{\omega C_2'R_{2SF}'C_2'}{\Delta C_2}-\frac{\omega C_2'R_{2SF}'C_2'}{\Delta C_2}+\omega C_2'R_{2SF}'. \tag{7.16}$$

$$D_H=D_M+\frac{(C_2''^2-C_2'^2)\omega R_{2SL}}{\Delta C_2}+\omega C_2'R_{2SF}'. \tag{7.17}$$

Attacking now the second term on the right, we can write

$$D_H = D_M + \frac{(C_2'' - C_2')(C_2'' + C_2')\omega R_{2SL}}{\Delta C_2} + \omega C_2' R_{2SF}' \tag{7.18}$$

Since $C_2'' - C_2' = \Delta C_2$

$$D_H = D_M + (C_2'' + C_2')\omega R_{2SL} + \omega C_2' R_{2SF}', \tag{7.19}$$

and because $C_2'' = \Delta C_2 + C_2'$,

$$D_H = D_M + 2\omega C_2' R_{2SL} + \omega \Delta C_2 R_{2SL} + \omega C_2' R_{2SF}'. \tag{7.20}$$

The authors wish to acknowledge the helpful comments and suggestions of John D. Hoffman and Robert D. Cutkosky, and a contribution to the analysis of the losses by Donald J. Scheiber.

(Paper 65C2–61)

8. References

[1] A. H. Scott and W. P. Harris, A study of materials for their suitability as standard dielectric reference materials, 1959 Annual Report, Conference on Electrical Insulation, Nat. Acad. Sci.—Nat. Research Council, Publ. **756,** 1, (1960).
[2] Methods of test for A–C capacitance, dielectric constant, and loss characteristics of electrical insulating materials, Am. Soc. Testing Materials, Standards, Pt. **9,** 1959 Supplement, D 150—59 T, p. 154 (1959).
[3] J. C. Balsbaugh and P. H. Moon, A bridge for precision power factor measurements on small oil samples, Trans. Am. Inst. Elec. Engrs. **52,** 528 (1933).
[4] J. C. Balsbaugh and A. Herzenberg, Comprehensive theory of a power factor bridge, J. Franklin Inst. **218,** 49 (1934).
[5] W. B. Kouwenhoven and E. L. Lotz, Absolute power factor of air capacitors, Trans. Am. Inst. Elec. Engrs. **57,** (1938).
[6] A. V. Astin, Measurement of relative and true power factors of air capacitors, J. Research NBS, **21,** 425 (1938).
[7] A. V. Astin, Nature of energy losses in air capacitors at low frequencies, J. Research NBS, **22,** 673 (1939).
[8] C. G. Koops, The measurement of very small phase displacements, Philips Tech. Rev., **5,** 300 (1940).
[9] W. Ch. van Geel and B. J. J. Schelen, Some properties of oxide layers produced on aluminum by electrolytic oxidation, Philips Research Reps. **12,** 240 (1957).
[10] P. Winkel and D. G. de Groot, Impedance of dielectric layers, Philips Research Reps. **13,** 489 (1958).
[11] A. M. Thompson, The precise measurement of small capacitances, Inst. Radio Engrs., Trans. on Instrumentation **I–7,** 245 (1958).
[12] Unpublished notes of R. D. Cutkosky, NBS.
[13] M. Kanno and Y. Koizumi, Determination of true loss angle of capacitors, J. Electro-tech. Lab., Japan (June 17, 1956). (In Japanese)

JOURNAL OF RESEARCH of the National Bureau of Standards—C. Engineering and Instrumentation
Vol. 65C, No. 2, April–June 1961

A Bolometer Mount Efficiency Measurement Technique*

G. F. Engen

(December 14, 1960)

In the measurement of microwave power by means of the bolometric technique, the efficiency of the bolometer mount must be measured and applied as a correction in order to meet many of the accuracy requirements of today's technology.

An impedance technique of determining this efficiency was proposed over ten years ago, but has found but little use to date because of the rather severe performance requirements imposed on the attendant instrumentation. This paper describes an improved method of implementing the technique which is based on the reflectometer concept.

A particularly attractive feature of the new method is its substantial independence of connector discontinuity which has been a particularly troublesome source of error in coaxial systems. In further contrast with some of the earlier proposals for implementing this impedance technique, the new method is readily applicable to both matched and unmatched mounts and does not require mathematical approximations (in the first order theory).

A comprehensive error analysis indicates that an accuracy of 0.5 percent is possible in the existing state of the art.

1. Background

The "impedance" method of measuring bolometer mount efficiency devised by Kerns [1] [1] is one of the few basic techniques developed thus far for determining this parameter. As originally outlined, however, the accuracy which could be achieved was rather severely limited by the state of the impedance measuring art, and this led in turn to the development of a number of modifications of the technique with the objective of reducing the overall error. Beatty [2], for example, proposed a modification based on certain mathematical approximations and restrictions in generality which provided improved accuracy, but the associated operating procedures proved to be nonetheless time consuming and exacting, and the accessory instrumentation was never developed or refined to the point where one was, on a routine basis, able to place a great deal of confidence in the results. Additional refinements or modifications of the technique have also been suggested by Weinschel [3], Ginzton [4], Lane [5], and perhaps others, but it is probably safe to say that none of these proposals has, as yet, come into widespread use.

At the Boulder Laboratories of the National Bureau of Standards another variation of the impedance method has been developed which provides improved accuracy and simplified operational procedures but, unlike the earlier modifications, requires neither mathematical approximations (in the first order theory), nor restrictions in the generality of the method. A particularly attractive feature of this new version is its substantial independence of connector discontinuity, which has been an especially troublesome source of error in coaxial systems. This technique constitutes an improved method of making the measurements implicit in the "impedance" method formulated by Kerns, and the subsequent discussion and error analysis will be limited to the procedures to be described. For a discussion of the more basic postulates upon which the procedure is based the reader is referred to the original paper [1]. In particular it should be noted that the technique is, in its present form, applicable to barretter but not to thermistor type bolometers.[2]

2. Introduction

It was shown by Kerns [1] that the efficiency of a bolometer mount may, under suitable conditions, be determined from three impedance measurements at the bolometer mount input terminals corresponding to three different values of bolometer resistance. If one of these resistance values is chosen to coincide with the value of resistance for which the efficiency is desired, this result may be expressed in terms of the input reflection coefficients thus [2]:

$$\eta = K \frac{|(\Gamma_3-\Gamma_2)(\Gamma_1-\Gamma_2)|}{|\Gamma_3-\Gamma_1|(1-|\Gamma_2|^2)} \qquad (1)$$

where the Γ_1, Γ_2, Γ_3 are the reflection coefficients corresponding to bolometer resistances R_1, R_2, R_3, respectively, η is the efficiency when the bolometer

*A preliminary report of this technique was given at a joint meeting of the International Scientific Radio Union and the Institute of Radio Engineers, April 26, 1958, Washington, D.C.

[1] Figures in brackets indicate the literature references at the end of this paper.

[2] In order to apply the technique to a given bolometer mount, it is a *sufficient* (but not necessary) condition that it be possible to determine the microwave impedance of the bolometer element from measurements of its d-c resistance. A somewhat different sufficient condition is that the resistive component of the microwave impedance be related to the d-c value by means of a real proportionality factor (whose magnitude need not be known), and that the reactive component be constant or independent of the d-c resistance. Necessary conditions have not been determined, but it has not been possible, thus far, to relate the microwave impedance to the d-c resistance in an adequate fashion in order to utilize this technique with thermistors.

resistance has the value R_2 (typically 200 ohms), and $K=\left|\frac{2R_2(R_3-R_1)}{(R_2-R_1)(R_3-R_2)}\right|$. For the special case of a "matched" mount ($\Gamma_2=0$) the expression becomes

$$\eta=K\left|\frac{\Gamma_3\Gamma_1}{\Gamma_3-\Gamma_1}\right|. \tag{2}$$

The determination of the factor K, while presenting a number of practical problems, does not pose the difficulties encountered in measuring the factor containing the Γ's. It will be noted that this latter factor is characterized by differences or changes in the reflection coefficient values as the bolometer resistance is varied. Because the resistance variation which can be achieved with the available barretter elements is at best rather limited, the corresponding changes in the reflection coefficient are not large, and if the individual Γ's are measured (by means of a slotted line for example) a rather severe requirement on the accessory instrumentation results. Beatty [2] has shown that an error of ± 1 percent in the VSWR measurements may lead to an error as large as ± 6 percent in the determined efficiency.

More recently, the reflectometer technique has found increased usage in the measurement of reflection coefficient magnitudes. This device, shown in figure 1, ideally yields a response of the form:

$$\left|\frac{b_3}{b_4}\right|=k|\Gamma| \tag{3}$$

where b_3 and b_4 are the wave amplitudes of the signals at the respective detectors, Γ is the reflection coefficient of the bolometer mount or other load terminating arm 2, and k is a (real) constant whose value may be determined by observing the detector outputs with arm 2 terminated by a load of known reflection—a fixed short for example.

While the usual reflectometer fails to produce this type of response because of imperfect directivity and other deviations from ideal behavior of the directional couplers employed, it is possible to compensate for these imperfections at a single frequency by means of auxiliary tuners [6], as shown in figure 2. Procedures for the adjustment of these tuners, such that the response of eq (3) may be realized, were given in the cited reference [6]. In essence the procedure is to adjust the tuning transformer T_x such that the directivity of the associated directional coupler becomes infinite, while T_y is adjusted

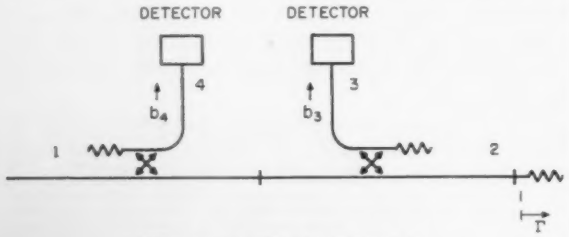

FIGURE 1. *Ideal reflectometer.*

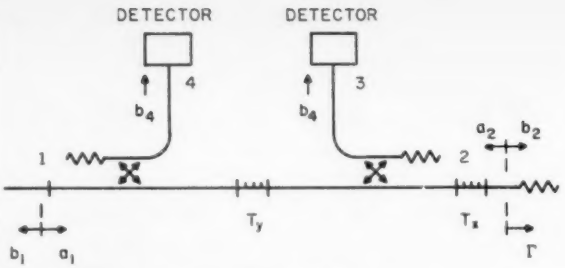

FIGURE 2. *Reflectometer with auxiliary tuners.*

such that the reflection coefficient of the equivalent generator, at the terminals where the bolometer mount is connected, vanishes.

The reflectometer does not, in this form, provide a determination of the argument or phase angle of the reflection coefficient, however Beatty [2] has noted that for matched mounts of high efficiency the reflection coefficient vectors Γ_1 and Γ_3 are nearly colinear so that to a good approximation $|\Gamma_3-\Gamma_1|=|\Gamma_3|\pm|\Gamma_1|$. (The proof of a more general counterpart of this statement will be given later in this paper.) To the extent of the validity of this approximation, the cited reflectometer technique may thus be employed to determine the efficiency of matched bolometer mounts by means of eq (2). The application of the reflectometer method to the more general problem of unmatched mounts is, however, by no means obvious.

Within the limitations discussed, the described method is practical in rectangular waveguide systems. In coaxial systems, however, the procedure leaves a great deal to be desired, and even in rectangular waveguide, as will be subsequently demonstrated, the procedure, as given, is unnecessarily complex for the application.

The problem in coaxial measurements centers around the impedance discontinuity which is part of the coaxial connector. In order to provide a useful result, an overall accuracy in the efficiency determination of 1 percent would appear to be a reasonable goal, and since this figure will include contributions from a number of different sources it is desirable to reduce the individual contributions to the order of 0.1 percent. Applying this criterion to the amount of mismatch permissible in the equivalent generator impedance implies a generator match with a VSWR of 1.002 or less. While this value may be realized in rectangular waveguide systems by means of sufficiently refined techniques, the prospect of achieving such a result in a coaxial system, where connector discontinuities with VSWR's of the order of 1.1 are typical, is certainly far from encouraging.

It may be noted, in passing, that this problem has appeared so regularly in attempts to refine this technique for use with coaxial type bolometer mounts that one is led to wonder if any significant improvement in the technique is possible with the existing coaxial connectors. For example in Beatty's modification, which was based on a variation of the slotted line technique, the measured efficiency included the

losses in that portion of the slotted section between the probe position and bolometer mount, leaving one with the awkward additional problem of measuring and applying as a correction the losses in this portion of the slotted line.

3. General Theory

The contributions of the new method to be described in the following paragraphs include an "exact" procedure for determining the vector difference between two reflection coefficient values, and a tuning procedure which virtually eliminates the potential error from connector discontinuity.

The magnitude of the vector difference between two reflection coefficient values may be determined with the help of the circuit arrangement shown in figure 3. For convenience an ideal reflectometer will be assumed. Terms of the form $|\Gamma_3-\Gamma_1|$ may be determined as follows: The barretter resistance is first adjusted such that the bolometer mount has the input reflection coefficient Γ_1. The signal at the detector 3 is then "nulled" or balanced out by means of the auxiliary signal channel. Under these circumstances the signal provided by the auxiliary channel is proportional to $-\Gamma_1$. If the barretter resistance is now adjusted to produce Γ_3, and if suitable precautions (to be described later) have been taken to isolate the two channels, the detector 3 signal will now be proportional to $|\Gamma_3-\Gamma_1|$ as required.

In order to illustrate the improved tuning procedure it will prove helpful to consider a special case. If a perfectly matched bolometer mount is assumed, the tuning of the reflectometer may be effected as follows. First, with the bolometer mount connected and the bolometer resistance adjusted to the value corresponding to the perfect match, the transformer T_x is adjusted for a null in arm 3, corresponding to infinite directivity for the associated coupler. Next the bolometer mount is replaced by a sliding short and the transformer T_y adjusted such that the ratio $\left|\frac{b_3}{b_4}\right|$ is constant for all positions of the short. As was explained in the reference [6], this adjustment produces an equivalent generator match (provided that the previous adjustment has been correctly made), and having completed these two adjustments, the measurement of the mount efficiency may be carried out using eq (2) as already described. (In practice additional tuning elements, whose use will be described later, are required to isolate the auxiliary channel.)

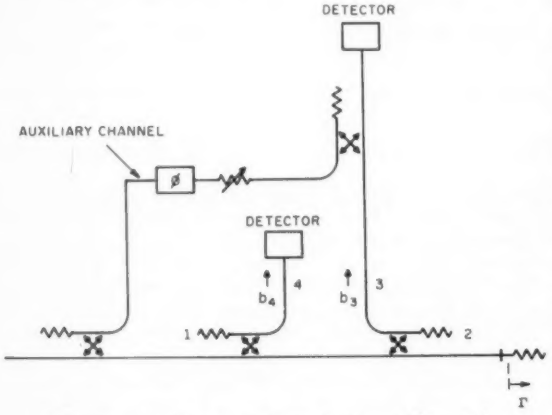

FIGURE 3. *Circuit for determination of* $|\Gamma_3-\Gamma_1|$.

It should be noted that to the extent that the (coaxial) connectors may be considered dissipation free, the attendant impedance discontinuity has no effect upon the sliding short adjustment since an ideal sliding short preceeded by a lossless discontinuity still presents a reflection coefficient of unit magnitude and (except for trivial cases) of variable phase angle. The place where the connector discontinuity is potentially important is in the initially assumed impedance match for the bolometer mount. But, as will be proved, *the assumed impedance match is entirely unnecessary.* To be sure, if the mount is matched, the measurement may be carried out as described; while if the mount is not matched, the identical series of measurements and operations described above will yield the factor

$$\frac{|(\Gamma_3-\Gamma_2)(\Gamma_1-\Gamma_2)|}{|\Gamma_3-\Gamma_1|(1-|\Gamma_2|^2)}$$

as required in the more general expression for mount efficiency.

In other words, the reflectometer adjustment and measurement proceeds on the basis of an assumed perfect impedance match for the bolometer mount (but employing only the specific procedures mentioned). It then develops that the method gives the correct value of efficiency regardless of whether the mount is matched or not! The proof for these assertions will be found in the following paragraphs.

It is a general property of a four-arm junction (of which the reflectometer of figure 2 may be regarded as a special case) that the ratio of the emergent wave amplitudes in arms 3 and 4 may be written in the form:

$$\frac{b_3}{b_4}=\frac{A\Gamma+B}{C\Gamma+D} \tag{4}$$

where the A, B, C, D are functions of the parameters of the four-arm junction and the detectors terminating arms 3 and 4, and Γ is the reflection coefficient of the load terminating arm 2.

If the reflection coefficient of the bolometer mount is designated by Γ_2 when the bolometer is at its nominal operating value R_2 (the value at which the mount efficiency is to be determined) and the junction has been adjusted (by means of T_x) such that the signal b_3 vanishes when arm 2 is terminated by this load (Γ_2), then $B=-A\Gamma_2$. A solution of eq (4), subject to the condition that the ratio $\left|\frac{b_3}{b_4}\right|$ remain constant (as provided by adjustment of T_y) while the phase of Γ varies, yields $\frac{B}{A}=\left(\frac{C}{D}\right)^* |\Gamma|^2$ where the asterisk (*) denotes the complex conjugate.

(A second solution, $A/C=B/D$ is trivial since it gives for $\frac{b_3}{b_4}$ a value which is independent of Γ.) For a sliding short the above result becomes $\frac{B}{A}=\left(\frac{C}{D}\right)^*$. Substituting the first and last of these results in eq (4) gives:

$$\frac{b_3}{b_4}=\frac{A(\Gamma-\Gamma_2)}{D(1-\Gamma\Gamma_2^*)}. \tag{5}$$

Substituting Γ_1 and Γ_3 for Γ and taking the absolute value of the ratio of the product to the difference gives:

$$\frac{\left|\frac{A}{D}\right|^2\left|\frac{\Gamma_3-\Gamma_2}{1-\Gamma_3\Gamma_2^*}\right|\cdot\left|\frac{\Gamma_1-\Gamma_2}{1-\Gamma_1\Gamma_2^*}\right|}{\left|\frac{A}{D}\right|\cdot\left|\frac{\Gamma_3-\Gamma_2}{1-\Gamma_3\Gamma_2^*}-\frac{\Gamma_1-\Gamma_2}{1-\Gamma_1\Gamma_2^*}\right|}=\left|\frac{A}{D}\right|\frac{|\Gamma_3-\Gamma_2||\Gamma_1-\Gamma_2|}{|\Gamma_3-\Gamma_1|(1-|\Gamma_2|^2)} \tag{6}$$

The term on the right is just the one required in the general expression for mount efficiency, while the factor $\left|\frac{A}{D}\right|$ may be determined by observing the system response with the bolometer mount replaced by a short or other termination for which $|\Gamma|=1$. This may be demonstrated by letting $\Gamma=e^{i\theta}$. Then:

$$\left|\frac{b_3}{b_4}\right|=\left|\frac{A}{D}\right|\cdot\left|\frac{e^{i\theta}-\Gamma_2}{1-e^{i\theta}\Gamma_2^*}\right|=\left|\frac{A}{D}\right|\cdot|e^{i\theta}|\cdot\left|\frac{1-\Gamma_2e^{-i\theta}}{1-(\Gamma_2e^{-i\theta})^*}\right|=\left|\frac{A}{D}\right| \tag{7}$$

as required.

Comparison of eqs (5) and (6) with (3) and (2) respectively, indicates that the measurement may be effected as outlined with $\left|\frac{A}{D}\right|$ taking the part of k, and $\frac{\Gamma-\Gamma_2}{1-\Gamma\Gamma_2^*}$ being the more general counterpart of Γ.

4. Circuit Arrangement and Tuning Procedure

A practical waveguide system utilizing these concepts is shown in figure 4. For convenience the directional couplers will be designated by P, Q, R, and S. The auxiliary arm between couplers R and S contains an on-off switch, phase shifter, and attenuator as required to balance out the signals from coupler P. As a matter of operating convenience it is generally helpful (but not essential) to adjust the system in such a way that the signal at detector 4 is nominally constant or independent of Γ. This is achieved by an adjustment of T_z to be described.

In order to obtain the vector difference between two reflection coefficients by the procedure described earlier, it is important to investigate the possible effect of variations in Γ upon the signal delivered to the detector 3 via the auxiliary arm. It is intuitively evident (and proof will be omitted) that the desired operation will be achieved if the following criteria are satisfied.

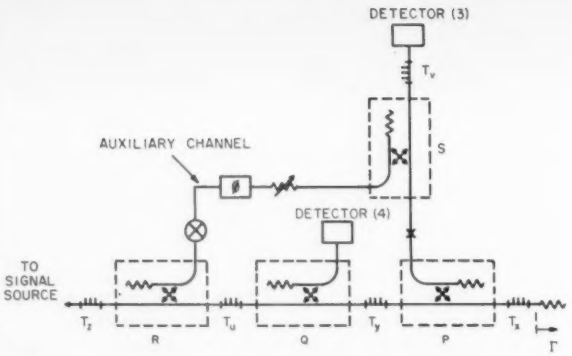

FIGURE 4. *Waveguide system for measuring bolometer mount efficiency.*

1. The signal coupled into the sidearm of coupler R is independent of Γ, or more specifically since it is the ratio of the signal in detector 3 to detector 4 which is observed, this ratio must be independent of Γ.

2. The impedance "looking into" coupler S at its sidearm is independent of Γ.

As a consequence of criterion 2, it will also be true that the impedance looking into this coupler and detector from the main arm will be independent of the operation of the phase shifter, attenuator, or switch in the auxiliary arm.

The adjustment of the tuning transformers to achieve these conditions may be done by the following steps:

(1) Directional coupler P and tuner T_y are temporarily removed from the system. In their place a sliding short is connected to coupler Q, and an auxiliary detector connected at the point X. The microwave signal is then delivered to the detector 3 via the auxiliary arm, and tuner T_z is adjusted for a null in the auxiliary detector connected at point X. This satisfies criterion 2 above.

(2) Tuner T_u is now adjusted such that the ratio $\left|\frac{b_3}{b_4}\right|$ is constant for all positions of the sliding short, and T_z is similarly adjusted such that $|b_4|$ remains constant as the position of the short is varied. If, as is often the case, the type of instrumentation employed to measure $|b_4|$ and $\left|\frac{b_3}{b_4}\right|$ is of such a nature that the measurement of $\left|\frac{b_3}{b_4}\right|$ is awkward in the presence of large variations in $|b_4|$, T_z may be first adjusted such that $|b_3|$ remains constant as the sliding short is varied, and T_u then adjusted for a constant value of $|b_4|$. Ideally, the two procedures will yield identical results, while in practice, depending upon the degree of precision toward which one is working, it may prove desirable to check the result for conformity to the criteria stated earlier.

If attention is centered on the four-arm junction comprised of couplers R, Q, and tuner T_u, it is of interest to note that the adjustment of T_u to make

the ratio $\left|\frac{b_3}{b_4}\right|$ a constant corresponds to the "trivial" solution $A/C=B/D$ rejected in the earlier discussion of a reflectometer. Although a sliding short has been specified, other types of variable loads, for example, a fixed short preceded by a variable attenuator, might also be employed in this particular adjustment. For practical purposes, the method of connecting the directional couplers will determine which of the solutions $A/C=B/D$ or $B/A=(C/D)^*$ is achieved by the sliding short adjustment, but should the question ever arise as to which of the two conditions has been realized by the given procedure it is sufficient to note that the former solution makes $\left|\frac{b_3}{b_4}\right|$ completely independent of Γ while this is not true of the latter one.

(3) The coupler P and tuner T_y are next replaced, the bolometer mount connected and T_x adjusted for a null at detector 3 with the bolometer resistance at its nominal value. The switch in the auxiliary arm is in the "off" position for this and the subsequent adjustments.

(4) The bolometer mount is then replaced by the sliding short and T_y adjusted for a constant ratio $\left|\frac{b_3}{b_4}\right|$ as the position of the short is varied. This completes the alinement procedure.

If the ratios $\left|\frac{b_3}{b_4}\right|$ are designated by subscripts 1, 3, and S, corresponding to values for the bolometer resistance of R_1, R_3, and the response when the bolometer mount is replaced by a short, the desired result may be expressed in terms of the measured values:

$$\frac{\left|\frac{b_3}{b_4}\right|_1 \cdot \left|\frac{b_3}{b_4}\right|_3}{\left|\left(\frac{b_3}{b_4}\right)_3-\left(\frac{b_3}{b_4}\right)_1\right| \cdot \left|\frac{b_3}{b_4}\right|_S}=\frac{|(\Gamma_3-\Gamma_2)(\Gamma_1-\Gamma_2)|}{|\Gamma_3-\Gamma_1|(1-|\Gamma_2|^2)} \qquad (8)$$

where the first factor in the denominator of the left side is determined in the manner described at the beginning of section 3.

5. Practical Considerations

By means of the techniques described in the preceding sections, the microwave impedance measurements required for a determination of mount efficiency have been reduced to a set of tuning adjustments and the measurement or determination of the ratios $\left|\frac{b_3}{b_4}\right|_1$, $\left|\frac{b_3}{b_4}\right|_3$, etc., for which a variety of techniques are available. Depending upon the type of instrumentation employed, the ratio $\left|\frac{b_3}{b_4}\right|$ may be indicated directly, or the terms $|b_3|$ and $|b_4|$ may be obtained individually. If the adjustment of T_x has been made with sufficient care, the signal $|b_4|$ will depend only upon the output level of the signal source; and if the latter is sufficiently stable, $|b_4|$ will be constant and thus may be cancelled out of eq (7), leaving only the values of $|b_3|$ to be determined. Indeed, as discussed in the reference [6], if a sufficiently stable signal source is used the directional coupler Q, detector 4 and tuner T_u may be omitted from the system. Under these conditions, step (2) of the tuning procedure described above consists of adjusting T_x such that $|b_3|$ is constant, while the other steps follow as given with $\left|\frac{b_3}{b_4}\right|$ replaced by $|b_3|$.

The detection techniques which may be employed include audio modulation and detection, heterodyne detection, and bolometric power detection. Although it is not within the scope of this paper to examine each of these methods in detail, it may prove useful to call attention to some of their more prominent features.

Perhaps the most convenient, but one of the least accurate, in the existing state of the art, of the cited methods is that of conventional audio modulation and detection. The detection equipment may take the form of a ratio-meter with barretter detectors such that $\left|\frac{b_3}{b_4}\right|$ is indicated directly. Barretter detectors are specified in order to ensure that the detector impedance will be at least nominally constant as required above. Alternatively, a standing-wave type amplifier may be used, and the signal $|b_4|$ applied to the automatic gain control channel (if available). It should be noted that such an instrument is actually a ratio-meter although the permissible excursion of the input signal applied to the AGC channel is usually quite limited. In practice these excursions may be held to a small value by adjustment of T_x, and once again, if the signal source is sufficiently stable and the adjustment of T_x is made with sufficient care, it is only necessary to measure $|b_3|$, and the AGC channel is not required. The chief problem with conventional audio techniques appears to be in the difficulty of accurately measuring changes in the level of an audio signal. In addition, because the measurements must be made over a nominal 20 db dynamic range, the deviations of the barretter detector from true square law response would be ultimately a source for concern.

Another objection to the conventional audio technique is that the barretter resistance (in the mount to be measured) tends to follow the modulation envelope, in the same manner as occurs in the detectors. In order to avoid this difficulty it is necessary to hold the microwave power dissipated in the barretter to a small fraction, nominally 1 percent or so, of the total bias power. In addition, the resistance excursions which may be realized with the commercially available barretters are such that the reflected signal is down by another nominal 20 db, and thus even if the modification (to be described below) which permits tight coupling to this reflected signal is employed, the signal power available is only of the order of a few microwatts, which taxes the ability of the best audio detection equipment. In spite of these objections, however,

the audio technique does provide a convenient method of developing a familiarity with the overall system behavior, and as this is being written, some of these objections are being overcome [7]. When used in conjunction with some of the additional refinements to be discussed below, the conventional audio technique would probably permit an efficiency determination to an accuracy of a few percent or better.

The IF substitution technique of attenuation measurement is immediately applicable to the measurement of relative levels of $|b_3|$, while a possible scheme for the measurement of $\left|\frac{b_3}{b_4}\right|$ is shown in figure 5. In figure 5, the 30 Mc/s signal derived from b_4 is adjusted by means of the piston attenuator to equal in amplitude that obtained from b_3, while phase balance is obtained from the phase shifter as shown. The changes in $|b_3|$ with respect to $|b_4|$ may thus be read directly from the piston attenuator. The measurement procedure thus consists of a series of nulling adjustments and is independent of fluctuations in the amplitude of the signal source, or the gain of the 30 Mc/s null detector. For these reasons the scheme appears attractive (on paper at least) for the proposed application.

A preliminary investigation of this technique has shown, however, the existence of a number of attendant practical problems. First, the 30 Mc/s circuits are frequency sensitive, requiring high stability of the intermediate frequency. Second, for proper operation the conversion efficiency of the crystal mixer should be independent of the changes in level of the local oscillator signal which inevitably accompany the operation of the phase shifter, but the conversion gain proved to be more sensitive to the local oscillator amplitude than anticipated. Third, the fact that the null is phase sensitive complicates the alignment procedure somewhat, particularly the adjustment of T_y. Undoubtedly, a more careful examination of the technique will uncover additional problems; this technique has not been investigated further because the method described below proved to be more convenient with the auxiliary apparatus on hand.

The method referred to above consists of power detection by the bolometric technique. These techniques have been refined to the point [8] where

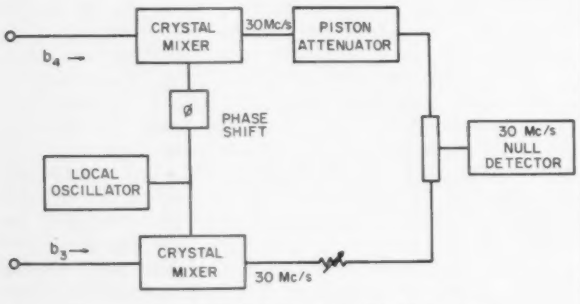

FIGURE 5. *Possible heterodyne detection system.*

accuracies of 0.1 to 0.2 percent may be realized at the required power levels. (It will be noted that questions as to bolometer mount efficiency of the detectors, etc., are unimportant here, since only power *ratios* are required.) It will prove useful to consider certain aspects of this procedure in detail since they are also applicable to the techniques described earlier.

The techniques by which the power is measured were discussed in detail in the cited reference [8] and need not be described here. In order to increase the signal at the detectors to the level where power detection is feasible, the configuration shown in figure 6 is employed. With the exception of the reversal of the connections to the coupler P, the system and tuning procedure are the same as that given for figure 4. A convenient choice of coupling ratio for the couplers P, Q, R, S, is 10 db. Under these conditions, approximately 80 percent of the power reflected from the termination is delivered to the detector 3. A further increase in this figure may be realized by other choices of coupling ratios, for example a figure of 90 percent may be realized by changing R and S to 3 and 20 db respectively, while a value of 98 percent would obtain with the values 20, 20, 3, and 20 db for P, Q, R, and S, respectively. These two alternatives would require an additional 3 and 10 db of power from the generator, however, and thus the first set of values appears to be a reasonable compromise when the available power is a potential problem.

The power delivered to the detector 4 is stabilized or held constant by means of techniques developed in this laboratory, [9] and thus only the values of power at the detector 3 are required.

In order that the detector signal may be as large as possible, it is desirable to operate the barretter, in the mount to be calibrated, over as wide a resistance excursion as possible. The commercially available barretters are not all equally suitable in

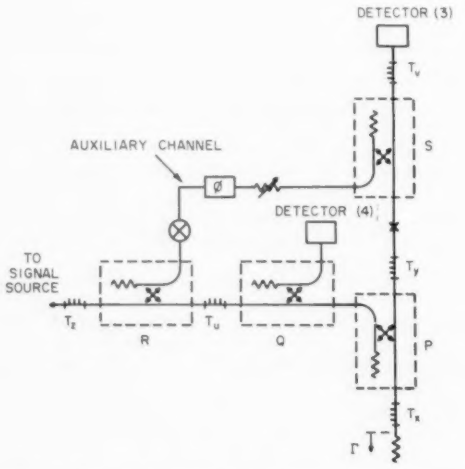

FIGURE 6. *Alternative waveguide system for measuring bolometer mount efficiency.*

this regard, but the type selected for this application may be operated over the range 140 to 260 ohms (nominal operating resistance 200 ohms). In operation the barretter forms one arm of a self-balancing bridge [8], another arm of which is varied to produce the required changes in resistance.

The bolometer mount under measurement is provided with a nominal 10 mw of microwave power, resulting in reflected signals of approximately 310 and 170 μw at the resistance values of 140 and 260 ohms. A practical problem exists with reference to the measurement at 140 ohms, since the 10 mw of microwave power alone, without any additional d-c power, will bias the element at perhaps 180 ohms. This difficulty is avoided by an indirect measurement technique. In order to obtain the measurement corresponding to the 140-ohm resistance value the microwave power is first reduced to such a value that the element may be operated at 140 ohms. The signal in the detector 3 is then nulled or balanced out by means of the auxiliary signal channel. Assuming linearity of the system, this null will be independent of power level. The bolometer resistance is then returned to 200 ohms, and the microwave power increased to its nominal 10 mw value. Under these conditions, the only signal delivered to detector 3 will come from the auxiliary channel and will be equal in amplitude (but opposite in phase) to the signal which would be obtained from the bolometer mount were it possible to reduce its resistance to the 140 ohm value in the presence of the 10 mw signal. This signal is then measured and used in the equations where the 140 ohm value is required.

With the bolometer mount replaced by a short, the reflected signal has, of course, a power level equal to that in the incident wave, nominally 10 mw. The procedure thus requires measurements over the nominal 20 db range between the 10mw and 100 μw power levels. In addition to the measurement of these signal levels, it is also important to be able to recognize the presence of signal levels in the region 60 to 80 db below these values during the course of the tuning operations. For this purpose it has proved convenient to split off a portion of the signal from arm 3 by means of a directional coupler and employ an auxiliary heterodyne detector. A waveguide switch in the secondary arm of this coupler is kept in the nontransmitting position when the adjustment of tuner T_v is made and when the signal amplitudes are being measured by the bolometric detector. In other words, the switch is in the transmitting position only when the high sensitivity for tuning adjustments is required. This isolates the remainder of the system from possible variations in the impedance of this heterodyne detector.

Although little has been said concerning the details of the power measurement, this aspect of the procedure is not without its share of practical problems. In order to make power measurements to an accuracy of a few tenths of a percent at the 100μw level, temperature control of the bolometer mount to about 0.001 ° C is required. A second problem concerns the barretter element itself. In practice it is frequently observed that even though the ambient temperature is held constant, the bias power required to maintain a given operating resistance may still be subject to considerable variation or drift. Certain types of elements have been observed to be much worse than others in this respect, but even among the better ones it is usually necessary to apply the bias power continuously for several days or even a week before stable operation is achieved.

Although the foregoing discussion has been concerned primarily with the barretter element, the measurement also imposes stringent stability requirements on the associated apparatus as well. This will be easily recognized when attention is called to the fact that the bolometric measurement is in reality a differential power measurement. Thus if it is required to measure a one percent change to an accuracy of a part in 10^3, a stability or resolution in the total d-c bias power of a part in 10^5 is implied.

6. Approximate Methods

The foregoing procedure is "exact" in the sense that the only mathematical approximations which have been introduced thus far have been in assuming that eqs (1) and (4) adequately describe the bolometer mount and reflectometer behavior. In a large percentage of the cases of practical interest a considerable simplification in the technique may be effected with little loss in accuracy by the introduction of suitable approximations. As a matter of fact, the accuracy achieved in practice is actually improved in certain instances by one of these approximations which will be described.

The first of these approximations relates to the substitution of $||\Gamma_3|\pm|\Gamma_1||$ for $|\Gamma_3-\Gamma_1|$ in eq (2), or more generally, the substitution of

$$\left|\frac{\Gamma_3-\Gamma_2}{1-\Gamma_3\Gamma_2^*}\right|\pm\left|\frac{\Gamma_1-\Gamma_2}{1-\Gamma_1\Gamma_2^*}\right| \text{ for } \left|\frac{\Gamma_3-\Gamma_2}{1-\Gamma_3\Gamma_2^*}-\frac{\Gamma_1-\Gamma_2}{1-\Gamma_1\Gamma_2^*}\right|$$

in eq (6). (The minus sign is used if both R_1 and R_3 are either greater than or less than R_2, while the positive sign is used when, as in the following example, one resistance value is above and the other below R_2.)

In order to examine the validity of this approximation it is convenient to obtain a general expression for this error in terms of the magnitude and arguments of the complex numbers Γ_1, Γ_3, or their more general counterparts $\frac{\Gamma_1-\Gamma_2}{1-\Gamma_1\Gamma_2^*}$, etc. Let $A=|A|$ and $B=|B|e^{j(\pi-\phi)}$ represent two complex numbers. Then for small values of ϕ, the error in replacing the vector difference by the sum of the magnitudes is given by the expression:

$$\text{Error}=\frac{|AB|}{(|A|+|B|)^2}(1-\cos\phi), \qquad (9)$$

The input reflection coefficient of the bolometer mount is given by the equation [2]:

$$\Gamma = S_{11} + \frac{S_{12}^2 \Gamma_l}{1 - S_{22}\Gamma_l} \tag{10}$$

where Γ_l is the load reflection coefficient, and the $S_{m,n}$ are the scattering coefficients of the bolometer mount (see fig. 7).

A substantial simplification in the analysis results from the fact that it is permissible to choose the impedance normalizing parameters in such a way that $\Gamma_l = 0$ when the bolometer is at its nominal operating value R_2. For any other value of R, Γ_l has the value

$$\Gamma_l = \frac{R - R_2}{R + R_2}.$$

Utilizing these results, the term

$$\frac{\Gamma_1 - \Gamma_2}{1 - \Gamma_1 \Gamma_2^*}$$

becomes:

$$\frac{\Gamma_1 - \Gamma_2}{1 - \Gamma_1 \Gamma_2^*} = \frac{\dfrac{S_{12}^2 \Gamma_{l1}}{1 - |S_{11}|^2}}{1 - \left(S_{22} + \dfrac{S_{11}^* S_{12}^2}{1 - |S_{11}|^2}\right)\Gamma_{l1}}. \tag{11}$$

Let Ψ_{12} denote the argument of S_{12} and let

$$F = \left(S_{22} + \frac{S_{11}^* S_{12}^2}{1 - |S_{11}|^2}\right); \tag{12}$$

then, since the efficiency η of the bolometer mount when terminated in R_2 is given by the expression [2]:

$$\eta = \frac{|S_{12}|^2}{1 - |S_{11}|^2}, \tag{13}$$

eq (11) may be written:

$$\frac{\Gamma_1 - \Gamma_2}{1 - \Gamma_1 \Gamma_2^*} = \frac{\eta \Gamma_{l1} e^{j2\psi_{12}}}{1 - F\Gamma_{l1}}, \tag{14}$$

and

$$\arg \frac{\Gamma_1 - \Gamma_2}{1 - \Gamma_1 \Gamma_2^*} = 2\psi_{12} - \tan^{-1} \frac{-\mathrm{Im}\,(F)\Gamma_{l1}}{1 - \mathrm{Re}\,(F)\Gamma_{l1}}. \tag{15}$$

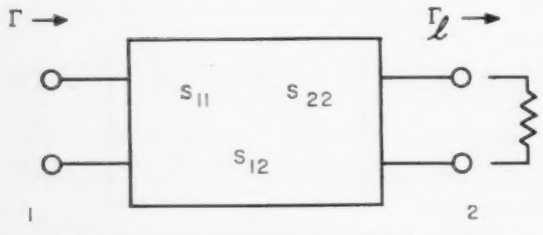

FIGURE 7. *Scattering coefficient representation of bolometer mount.*

It is shown in the appendix that $|F|$ satisfies the inequality

$$|F| \leq 1 - \eta. \tag{16}$$

In a large percentage of the cases of practical interest the efficiency will be in excess of 90 percent, while $|\Gamma_l|$ is ordinarily limited to the range 0.1 to 0.2. Substituting these results in eq (9) yields the approximate result:

$$\mathrm{Error}_{(\max)} \approx \frac{1}{2}|\Gamma_{l1}\Gamma_{l3}|(1-\eta)^2. \tag{17}$$

This is the approximate maximum limit of error which obtains when $\arg F = \pm\frac{\pi}{2}$. For other values of $\arg F$ the error will be smaller, becoming zero for $\arg F = 0$ or π.

In a typical case where the bolometer is operated at the resistance values 140–200–260 ohms and for a mount efficiency of 90 percent the error is approximately ≤ 0.012 percent. The uncertainty introduced by replacing the vector difference by the sum of the magnitudes in this example is thus wholly negligible. Under these conditions it will thus be recognized that the auxiliary waveguide channel, which was introduced to permit a determination of this vector difference, contributes virtually nothing to the accuracy of the final result as far as this aspect of the operation is concerned.

The auxiliary loop is still a practical necessity, however, where power detection is employed because of the problem with the 140-ohm measurement as outlined above. In addition, this auxiliary loop may contribute to the accuracy of the result as follows:

Let the resistance excursion of the bolometer element be chosen in such a way that $\Gamma_{l1} = -\Gamma_{l3}$; then it can be shown that:[3]

$$\frac{1}{4}\left|\frac{\Gamma_3 - \Gamma_2}{1 - \Gamma_3\Gamma_2^*} - \frac{\Gamma_1 - \Gamma_2}{1 - \Gamma_1\Gamma_2^*}\right| \approx \left|\frac{(\Gamma_3 - \Gamma_2)(\Gamma_1 - \Gamma_2)}{(\Gamma_3 - \Gamma_1)(1 - |\Gamma_2|^2)}\right| \tag{18}$$

with an error

$$\mathrm{Error} \leq \Gamma_{l1}^2(1-\eta)^2 \tag{19}$$

which is approximately twice the value obtained in eq (17).

One of the substantial sources of error attending this technique occurs in practice in the measurement of the signal amplitudes (corresponding to the various resistance values) at the detector 3. As outlined above, a total of four measurements are required, while use of the first approximation described reduces this number to three. Use of the approximation (18) however, reduces the number of required measurements to two, the vector difference and the measurement with the bolometer mount replaced by the

[3] The proof may be effected by substituting eq (10), (12), and (16) in (18) and simplifying the resultant expressions.

short. In addition the power level which obtains at detector 3 in measuring this vector difference is four times that obtained from Γ_{l1} alone which reduces the dynamic range and improves the accuracy with which these measurements can be made. In the existing state of the art this latter technique is the most accurate, for mounts of high efficiency, of those described.

7. Measurement of Attenuation

The foregoing presentation has been directed primarily at the problem of measuring bolometer mount efficiencies. The efficiency, however, determines the dissipative component of attenuation, and a modification of the techniques described should also prove useful in other applications, such as measuring the efficiency of waveguide to coax adaptors, short sections of waveguide, etc. A complete discussion of these potential applications and the requisite modifications in the method is not, however, within the scope of this paper.

8. Error Analysis

In any technique or method with potential applications in the field of standards work, a thorough investigation of the attendant sources of error is an important part of the description. The sources of error to be discussed are the following: (1) Error due to misadjustment of tuning transformers, (2) error due to dissipation in reference short, (3) error due to uncertainty in the values of bolometer resistance, and (4) error in the measurement of the signal amplitudes. These will be treated in the order listed.

The error analysis or study which has been made in connection with this technique, is, however, too lengthy to be presented in its entirety. For this reason the discussion to follow will be largely of a summary nature, and devoted primarily to the waveguide system of figure 6. The extension of these results to other variations of the method, however, should prove straightforward. The procedure to be followed in the analysis is that of assuming ideal operation of the system except for the source of error being considered. This technique yields the first order correction terms to the ideal theory for individual sources of error.

8.1. Error Due to Misadjustment of Tuning Transformers

a. Misadjustment of Tuner T_v

The adjustment of T_v and T_u is important in obtaining the vector difference $(\Gamma_1-\Gamma_3)$ etc. As a consequence of the adjustment of tuner T_u the signals delivered to detector 3 via arms 1 and 3 of directional coupler S (see fig. 6) may be considered as originating from two independent sources (of constant amplitude and frequency). If tuner T_v is not properly adjusted, the signal delivered via arm 3 will vary with changes in Γ (as produced by changes in bolometer resistance). If the "null" observed at X in step 1 of the tuning procedure is down from the signal at detector 3 by at least 60 db, then the voltage amplitude of the signal emerging from arm 1 will be down by a factor of 10^3. During the course of the measurement, Γ varies between the approximate limits of $\pm 1/7$, and the maximum anticipated variation in the signal delivered to detector 3 via the auxiliary channel due to this variation is approximately 3 parts in 10^4. Finally, this is approximately one-half the total signal being measured, so the maximum anticipated error is one-half this value and may be neglected.

b. Misadjustment of Tuner T_u

The problem once again is one of attempting to insure that the signal delivered to detector 3 via the auxiliary loop is independent of Γ. This time the possible interaction is through coupler R instead of coupler S. In practice the variation in reflection coefficient observed "looking in" arm 3 of coupler P during the course of the measurement will be approximately ± 0.015. If with the sliding short connected to the output of coupler Q (tuning operation 2), T_u is adjusted so that the maximum variations in $\left|\frac{b_3}{b_4}\right|$ are reduced to 1 percent (0.1 percent may be realized in practice without too much difficulty), the maximum variation in the auxiliary channel signal will be of the order of a part or two in 10^4 and again may be neglected.

c. Misadjustment of Tuner T_x

The function of tuner T_x is to adjust the four arm junction in such a way that it satisfies the condition $B=-A\Gamma_2$. The failure to exactly realize this adjustment may be accounted for by letting $B=-A(\Gamma_2+\delta)$. Substituting this result in the equation for determining the bolometer mount efficiency yields two approximate upper limits for the error due to this source,

$$E\leq\frac{1}{1-|\Gamma_2|^2}\left[\frac{1}{\eta}\frac{|\Gamma_{l1}+\Gamma_{l3}|}{|\Gamma_{l1}\,\Gamma_{l3}|}+2|\Gamma_2|+4\left(\frac{1}{\eta}-1\right)\right]|\delta| \quad (20)$$

and

$$E\leq\frac{1}{1-|\Gamma_2|^2}\left[\frac{1}{\eta}\frac{|\Gamma_{l1}+\Gamma_{l3}|}{|\Gamma_{l1}\,\Gamma_{l3}|}+4|\Gamma_2|+2\left(\frac{1}{\eta}-1\right)\right]|\delta|. \quad (21)$$

The choice of which expression to use obviously depends upon the relative magnitudes of Γ_2 and $\left(\frac{1}{\eta}-1\right)$. It will be noted that the error can be reduced by choosing the resistance variation such that $\Gamma_{l1}=-\Gamma_{l3}$, and if the VSWR (σ) of the mount is less than 1.02, the coefficient of $|\delta|$ has the approximate limit of 0.2 for an efficiency greater than 90 percent. On the other hand, for a resistance excursion of 140 to 200 to 260 ohms and $\sigma=1.5$ as in an earlier example, this coefficient will have the approximate limit 2.8. The desirability of choosing resistance values such that $\Gamma_{l1}=-\Gamma_{l3}$ is readily apparent.

If the approximate method implied by eq (18) is employed, the approximate limit of error is given by the expression

$$E \leq 2\left[\frac{|\Gamma_2|}{1-|\Gamma_2|^2}+\eta(1-\eta)\Gamma_{11}^2\right]\cdot|\delta|. \qquad (22)$$

In this expression the coefficient of $|\delta|$ has the approximate values of 0.06 and 0.5 for VSWR's of 1.02 and 1.5 respectively. The use of this approximation thus reduces the error.

If the tuner T_x has been adjusted such that the signal level at detector 3 is down by 60 db from the level which exists with the shorting plate connected in place of the bolometer element, $|\delta|$ will have the nominal value of 10^{-3}, while an 80 db "null" will yield a value for $|\delta|$ of 10^{-4}. The error due to this source can thus usually be held to 0.1 percent or less.

d. Misadjustment of Tuner T_y

The function of tuner T_y is to adjust the junction such that it satisfies the condition $D/C=(A/B)^*$. The failure to exactly realize this condition may be accounted for by letting $D/C=(A/B)^*+\epsilon$. Substituting this result into the equation for bolometer mount efficiency yields the approximate expression $E\approx|\epsilon|$ for the error due to this source. This error arises primarily in the determination of $|A/D|$ by means of the fixed short.

The failure to realize the proper adjustment of T_y can result from either failure to entirely eliminate the variations in $\left|\frac{b_3}{b_4}\right|$ as the sliding short is moved, or from deviations of the sliding short from the assumed ideal behavior. An analytic treatment of this problem yields for $|\epsilon|$ the approximate limit:

$$|\epsilon| \leq (1+2|\Gamma_2|)\left[\frac{1}{4}\frac{P_{max}-P_{min}}{P_{av}}+(1-|\Gamma_m|^2)|\Gamma_2|+(1-\eta_j)\right] \qquad (23)$$

where P_{max}, P_{min}, and P_{av} represent the maximum, minimum, and average values of the ratio $\left|\frac{b_3}{b_4}\right|^2$ as observed during the course of the sliding short adjustment, Γ_m is the reflection coefficient of the sliding "short", and η_j is the efficiency of the waveguide joint which connects the sliding short to the remainder of the waveguide system. In the above expression the waveguide in which the short slides has been assumed lossless, while in practice, when the correct adjustment has been realized, there will be a gradual and uniform decrease in the ratio $\left|\frac{b_3}{b_4}\right|$ as the sliding short is withdrawn.

The error due to η_j may be eliminated by including a precision waveguide section in arm 2, as shown in figure 8, into which the sliding short may be inserted for this tuning operation. Other implications of this arrangement will be discussed in subsequent paragraphs. It will be noted that the error due to the reflection coefficient of the sliding short (Γ_m) differing from unit magnitude decreases as the impedance match of the bolometer mount is improved. In practice the variations in $\left|\frac{b_3}{b_4}\right|^2$ can usually be reduced to the order of several parts in 10^3 such that the error from these sources can usually be held to 0.1 to 0.2 percent.

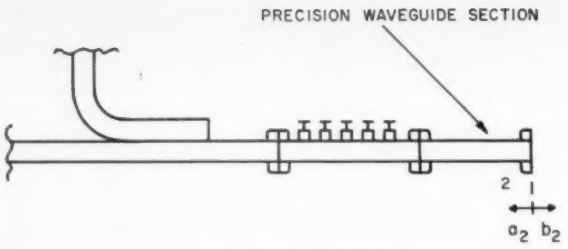

FIGURE 8. *Illustration of use of precision waveguide section.*

e. Error Due to Imperfect Nulling When Using Auxiliary Channel

If this "null" is measured in terms of the signal level which exists in the detector prior to the nulling procedure it will be readily recognized that a 60 db minimum corresponds to a possible difference between the two signals of a part in 10^3, etc. Since this signal is next combined with another one of nominally the same amplitude and phase the error contribution to the final measurement is approximately one-half this value.

8.2. Error Due to Dissipation in Reference Short

The error due to this source is closely connected with section (d) and is given by the approximate expression:

$$E \leq (1+2|\Gamma_2|)(1-|\Gamma_s|) \qquad (24)$$

where Γ_s is the reflection coefficient of the reference or standard short. In the present state of the art the highest reliable reflection coefficients are provided by "quarter wave" shorts, that is, a quarter wavelength section of waveguide terminated by a soldered shorting plate, or the entire structure may be electroformed in a single piece. The advantage of this construction is in the elimination of the longitudinal component of current flow at the plane of connection, thus tending to minimize flange losses. Measurements and calculations of the reflection coefficient magnitudes of such shorts [10] have yielded values in excess of 0.999.

If such a device is used in conjunction with the uniform waveguide section as in figure 8, the measurement will include, as part of the bolometer mount losses, the dissipation occurring at the bolometer mount input flange. If, on the other hand,

the variations in $\left|\frac{b_3}{b_4}\right|$ have not been completely eliminated, there is some advantage in taking the average of the results with a quarter wave and conventional "flat" short. This tends to cancel out the error due to imperfect tuning but introduces other uncertanties if there is an appreciable amount of flange loss [11]. The general features of this problem are discussed in greater detail in the cited reference.

8.3. Error Due to Uncertainty in the Values of Bolometer Resistance

The bolometer resistances enter the expression for bolometer mount efficiency through the factor

$$K=\left|\frac{2R_2(R_3-R_1)}{(R_2-R_1)(R_3-R_2)}\right|.$$

In practice the bolometer is biased by means of a self-balancing d-c bridge [8]. This device is capable of maintaining the bolometer resistance within 0.01 percent of the value called for by the bridge parameters. Use of NBS type resistors makes it possible to maintain the value of the reference arm within 0.01 percent, while an error in the upper or ratio arms cancels out since the R's may be multiplied by an arbitrary factor without changing the value of K. The R's may thus be effectively maintained within the limits ± 0.02 percent. However, because the expression for K involves their differences, the total error due to this source is of the order of 0.1 percent. In addition the measurement will be in error by the ratio of the bolometer lead resistance to R_2.

8.4. Error Due to Measurement of Signal Amplitudes

An approximate limit to the error introduced in the measurement of the signal amplitudes is the sum of the errors in the individual measurements. For the approximation method of eq (18), this error can be kept within 0.15 percent if power detection is employed, while for other variations of the procedure and/or other detection procedures the error will in general be larger.

The error due to instability in the frequency of the signal generator has not been considered explicitly but in general will manifest itself in an inability to realize the tuning conditions to the required degree of precision.

In summary, it will be recognized that the ultimate accuracy attainable will depend primarily upon which of the several alternate procedures is employed and upon the degree of refinement employed in the attendant adjustments and measurements. The foregoing results are somewhat arbitrarily summarized in the following table. The minimum values are intended to represent the approximate best values in the existing state of the art, while the larger values are intended to be typical of what may be achieved if the requirements are relaxed somewhat.

Source of error	Nominal error limits in percent	
	$\sigma<1.02$	$\sigma=1.5$
Adjustment of T_v	0. 00–0. 015	0. 00–0. 015
Adjustment of T_u	. 00– . 02	. 00– . 02
Adjustment of T_x	. 00– . 02	. 05– . 3
Adjustment of T_y	. 05– . 3	. 1 – . 5
Imperfect null in use of auxiliary arm	. 02– . 05	. 02– . 05
Reference short	. 05– . 3	. 05– . 3
Bolometer resistance	. 1 – . 15	. 1 – . 15
Measurement of signal amplitudes	. 15–1. 0	. 15–1. 0
Total	0. 4 –1. 8%	0. 5 –2. 3%

9. Experimental Results

An X-band waveguide setup employing the concepts developed in this paper is shown in figure 9. The efficiency values obtained utilizing this method have consistently shown agreement with microcalorimeteric determinations [12] to within one-half of one percent and usually within a few tenths of a percent. This is of considerable interest since the two methods should, in principle, differ by the amount of the substitution error, and suggests that the substitution error is typically at least an order of magnitude smaller than the previously estimated limits.

10. Appendix

The inequality

$$|F|\leq 1-\eta \tag{16}$$

can be proved in the following manner.

Let the terminals of the 2 arm junction represented in figure 7 be reversed such that the load is connected to arm 1. Then the input reflection coeffi-

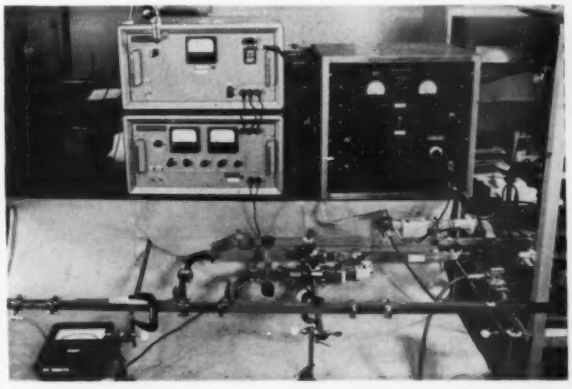

FIGURE 9. *Picture of waveguide system and accessory instrumentation employed in the measurement of bolometer mount efficiency.*

cient at arm 2 will be given by: (cf. eq 10)

$$\Gamma_{in}=S_{22}+\frac{S_{12}^2\Gamma_l}{1-S_{11}\Gamma_l}.$$

This can be written in the form,

$$\Gamma_{in}=\frac{\alpha\Gamma_l+\beta}{\gamma\Gamma_l+\delta} \tag{25}$$

where $\alpha=S_{12}^2-S_{11}S_{22}$

$\beta=S_{21}$

$\gamma=S_{11}$

$\delta=1.$ (26)

Equation (25) indicates that Γ_{in} is related to Γ_l by means of a linear fractional transformation. This transformation has the well known property [4] of mapping circles into circles with straight lines as limiting cases.

Let arm 1 be terminated by a sliding short. Then the locus of Γ_l is the unit circle centered at the origin. From the above property of the transformation it will be recognized that the locus of Γ_{in} is also a circle, and since a reflection coefficient magnitude can never exceed unity it is evident that this circle must lie completely within or on the unit circle as shown in figure 10. The distance to the center of this circle, r_c, and the radius, r, thus satisfy the inequality:

$$r_c\leq 1-r. \tag{27}$$

In terms of the constants of the transformation, r_c and r are given by

$$r_c=\frac{|\beta\delta^*-\alpha\gamma^*|}{|\delta|^2-|\gamma|^2} \tag{28}$$

and

$$r=\frac{|\alpha\delta-\beta\gamma|}{|\delta|^2-|\gamma|^2}. \tag{29}$$

Substituting eqs (26) into (28) and (29) and these in turn into (27) and recalling the definition of F, yields the result:

$$|F|=\left|S_{22}+\frac{S_{11}^*S_{12}^2}{1-|S_{11}|^2}\right|\leq 1-\eta$$

where $\eta=\frac{|S_{12}|^2}{1-|S_{11}|^2}$. See eq (13).

The author thanks R. W. Beatty and D. M. Kerns for their helpful suggestions in reviewing the manuscripts, and W. E. Case, M. E. Harvey, and J. E. Gilbert who provided experimental demonstrations of techniques described.

[4] See a text on complex variable theory.

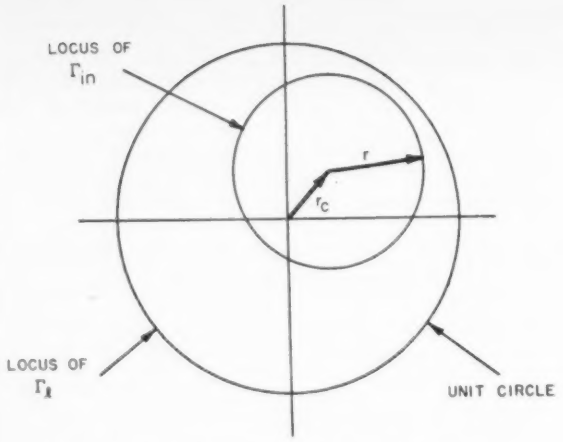

FIGURE 10. *Diagram giving locus of* Γ_l *and* Γ_{in}.

11. References

[1] D. M. Kerns, Determination of efficiency of microwave bolometer mounts from impedance data, J. Research NBS **42,** 579 (1949) RP1995.

[2] R. W. Beatty and F. Reggia, An improved method of measuring efficiencies of ultra-high-frequency and microwave bolometer mounts, J. Research NBS **54,** 321 (1955) RP2594.

[3] B. O. Weinschel, Phase engineering report No. 2 on standard signal generator output power, voltage, and attenuation calibration assembly, Contract AF 33(600)-25238, E.O. No. C-30047 SR-6J3 (May 1956).

[4] E. L. Ginzton, Microwave measurements, p. 185 (McGraw-Hill Book Co., Inc., New York, N.Y., 1957).

[5] J. A. Lane, Measurements of efficiency of bolometer and thermistor mounts by impedance methods, Proc. IEE, pt. D., No. 17, p. 485 (Sept. 1957).

[6] G. F. Engen and R. W. Beatty, Microwave reflectometer techniques, IRE Trans. on microwave theory and techniques **MTT-7,** No. 3, pp. 351-355 (1959).

[7] G. E. Schafer and R. R. Bowman, A modulated subcarrier technique of measuring microwave attenuation, Spring Meeting, International Scientific Radio Union and Institute of Radio Engineers, Washington, D.C., May 3, 1960. (A formal report of this work is in preparation.)

[8] G. F. Engen, A self-balancing DC bridge for accurate bolometric power measurements, J. Research NBS **59,** 101 (1957) RP2776.

[9] G. F. Engen, Amplitude stabilization of a microwave signal source, IRE Trans. on microwave theory and techniques **MTT-6,** No. 2 (1958).

[10] R. W. Beatty and D. M. Kerns, Recently developed microwave impedance standards and methods of measurement, IRE Trans. on Instrumentation, **I-7,** No. 3 and 4 (1958).

[11] R. W. Beatty, G. F. Engen, and W. J. Anson, Measurement of reflections and losses of waveguide joints and connectors using microwave reflectometer techniques, IRE Trans. on Instrumentation, **I-9,** No. 2, 219-226 (Sept. 1960).

[12] G. F. Engen, A refined X-band microwave microcaolrimeter, J. Research NBS, **63C,** No. 1, 77 (1959).

(Paper 65C2-62)

JOURNAL OF RESEARCH of the National Bureau of Standards—C. Engineering and Instrumentation
Vol. 65C, No. 2, April–June 1961

Telescope for Measurement of Optic Angle of Mica*

Stanley Ruthberg

(November 16, 1960)

The described instrument allows rapid measurement of the apparent optic angle to an accuracy of 5′ of arc for samples as large as 2 inches in diameter. This angle is a property pertinent to the quality of mica. Instrumentation is quite simple but dependent upon the complex phenomena of interference figures produced by biaxial crystals in polarized light. Magnification is great, dispersion can be determined, and the uniformity of samples can be observed.

1. Introduction

The optic angle and the uniformity of mica splittings are of interest, for these contribute to the quality of the material, and are properties covered in specifications on visual quality.[1]

The uniformity of the crystals can be determined with parallel, plane polarized light and a polarizing eyepiece of polarization plane at right angles to that of the incident light. The specimen behaves as a wave plate with a resultant pattern dependent upon the variation of thickness and index. The orthoscope arrangement of the petrographic microscope utilizes such procedure.

Direct measurement of the optic angle can be made with a number of instruments. For example, the conoscope arrangement of the petrographic microscope utilizes strongly divergent plane polarized light to produce an interference figure by which the angle can be determined with or without a universal stage, dependent upon the precision desired.[2] The universal stage can be used to a tenth of a degree. A basic spectrometer, i.e., collimator, goniometer, telescope modified with polarizing attachments, and rotary crystal holder can be utilized to greater precision. An instrument employing these components was developed for the precise location of the optic axis of polished quartz plates.[3] Although the instrument and the procedure [4] were for the uniaxial quartz, the instrument itself could be used for biaxial crystals. Such instruments as these are intricate and relatively expensive apparatus, which, further, examine only a very small region of the subject crystal.

Rough measurements, at the other extreme, can be obtained with small apparatus of the type suggested in the ASTM specifications.[5]

The described instrument, which has been used for a detailed study on mica behavior,[6] is relatively simple and readily assembled. It is used to determine both the uniformity of the crystals and the optic angle. In principle it is of the collimator-goniometer-telescope form except that the collimator and telescope are replaced with a primitive lens and the eye; yet, it has greater precision than the conoscope and universal stage. It differs from the previous instruments in that the entire area of a 2 in. diam specimen can be examined simultaneously to give crystal behavior in the large. Magnification of the interference pattern is much greater than that of the conoscope; apparent optic angle can be measured to an accuracy of 5′ of arc, and dispersion can be determined.

2. Theory and Structure

In general the velocity of propagation of light in a crystal is a function of the vibration direction of the wave, or of the direction of propagation and the orientation of the plane of vibration. The optic axis of such a crystal is that direction for which the velocity of propagation is independent of the orientation of the plane of vibration. Then, in any other direction a plane polarized wave may be resolved into two components vibrating at right angles to each other with different indices of refraction. Many crystals, and mica is one, are biaxial. The angle subtended by the axes is the optic angle, labeled $2V$ in figure 1. Waves propagated along the axes, A and B, are refracted upon emergence. The appar-

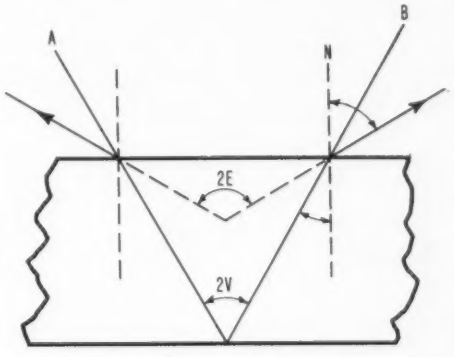

FIGURE 1. *Optic angle of a mica crystal.*

*Work supported by Defense Materials Service, General Services Administration.

[1] American Society for Testing Materials, Tentative specifications for natural muscovite mica based on visual quality, D351–53T.

[2] E.g., Manual of petrographic methods. A. Johannsen, 2nd Ed., 1918 (McGraw-Hill) or Optical crystallography, E. E. Wahlstrom, 2nd Ed., 1957, (John Wiley and Sons).

[3] E. Brodhun and O. Schönrock, Z. Instrumentenk. **22,** 353 (1902).

[4] E. Gumlich, Wiss. Abhand. der Physik.-tech. Reichanstalt **2,** 202 (1895).

[5] Appendix I, ASTM D 351–53T.

[6] Results to be published.

ent optic angle, labeled $2E$, is then that subtended by the refracted rays.

When divergent, plane polarized, monochromatic light of wavelength, λ, passes through a biaxial crystal and then a polarizing plate, or analyzer, an intereference figure is produced which is composed of a family of contour lines of light of equal phase (isochromes) and a superimposed pattern of equal vibration direction (isogyres). When the direction of polarization of the analyzer is at right angles to the plane of polarization, when the optic plane of the crystal is parallel to the direction of polarization of the polarizer or analyzer, and if the angle is symmetrical about the surface normal, the resultant pattern is as in figure 2. Here, the dark maltese cross, A_n–A_n' and P_o'–P_o, is the isogyre, formed by extinction of all light exit from the crystal and vibrating in the plane of polarization of analyzer or polarizer. The bright "circular" patterns are the isochromes, or contours of light of the equal phase difference of $(2n+1)\ \lambda/2$ at the point of emergence between those components whose vibration directions are at right angles. Each integral value of n describes a member of the family. Points A and B represent the intersection of the optic axes with the crystal surface. If the crystal is now rotated 45°, the isogyre breaks off into two hyperbolic brushes as in figure 3, with the optic axes centered in the vertices. The optic angle is then the arc spanning the vertices, A and B, and is the property to be measured.

White light produces a system of isochromes of various colors. In addition, if the optic angle and/or the orientation of the optic plane are frequency dependent, a dispersion pattern results for the 45° orientation. In this, the isogyres are separated into colored bands. In mica, the line of demarcation of the red and blue bands is sharp so that the intersection of this line with the optic plane serves as a fairly precise reference point.

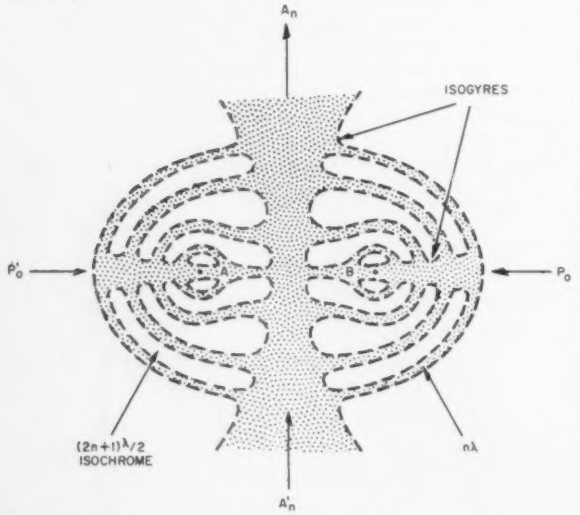

FIGURE 2. *Interference figure for optic plane parallel to one of directions of polarization.*

A_n–A_n' for analyzer. P_o–P_o' for polarizer. A, B for optic axes.

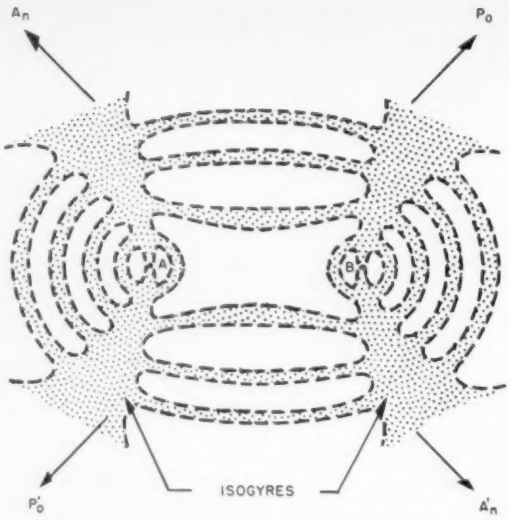

FIGURE 3. *Interference figure for analyzer and polarizer rotated 45°.*

The structure of the "telescope" is as shown in figure 4. A cross hair stretched across a large ground glass screen, illuminated from beyond by an ordinary incandescent light bulb, serves as an object and extended source. The crystal plate is

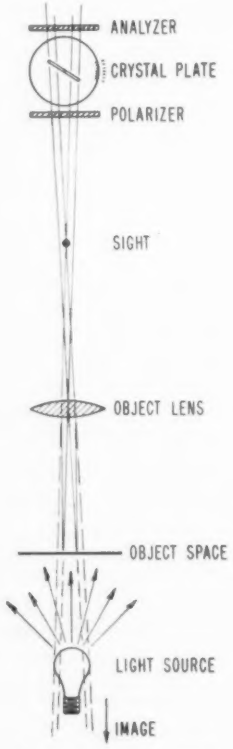

FIGURE 4. *Telescope.*

placed on a rotatable table equipped with protractor and vernier. The polarizer and analyzer are located before and after the table as closely as possible. A simple objective lens of large diameter is positioned approximately at its focal length from the object plane to produce normally a virtual image far beyond the object space. This can be done suitably in the following way. The crystal plate is rotated in its own plane and around a vertical axis in its plane until the 45° position is reached and a vertical trace of an isogyre is centered on the image of the cross hair. For this the eye is positioned above the analyzer in figure 4 and focused on the far off virtual image of the cross hair. The lens is then moved along the telescope axis until the image of the cross hair and the isogyre are parallax free. This procedure achieves a source of small divergence, which in turn produces an optic figure equivalent to great magnification. The line of demarcation of the red and blue fringes of the isogyre can now be fairly accurately centered; however, a vertical blade sight is also incorporated for greater precision. Alinement of the sight, isogyre, and cross hair insures that only axial rays are used and, hence, that the image is precisly centered. This also compensates for distortion by the large, simple lens and by crystal irregularity. The spanning of the specimen with polarizer and analyzer sheets of suitable diameter with close spacing and the use of a lens of large diameter create a large entrance aperture which is necessary to satisfy the demand for a beam of plane polarized light of large cross section needed to determine uniformity of fairly large splittings of mica.

The image secured with the telescope is so large that only a very small portion of the optic figure is seen. That portion about the optic axis fills the view, and the vertex of an isogyre is so extended as to appear as a vertical trace across the entire crystal. This facilitates accurate reading, and in addition shows any variation of the angle of the exit ray across the crystal. which variation does occur in mica. However, to some, the image of the isogyre so found may seem reversed in color sense from that as seen in the petrographic microscope. Actual measurement of the apparent optic angle for the red and blue fringes shows that this is not the case. The appearance of reversal is due to the difference in optics. That is, in the conoscope arrangement of the petrographic microscope the strongly diverging light passes up through the crystal as in figure 5 and is viewed from above. Let A_r and B_r represent the optic axes for red light, with A_b and B_b for blue light, and let the red optic angle be greater than the blue. Thus as one looks toward the surface of the crystal away from the light source, he sees the blue fringe outside the red fringe with respect to that surface normal, for red light propagating along a red optic axis is absorbed in the analyzer to leave a blue excess, and vice versa for the blue light at a blue optic axis. The whole figure may be seen at once. On the other hand, the telescope with its weakly divergent light, extended source, and limited pattern has the behavior of figure 6. Here, as one looks down the light from the axes, B_b and B_r in this

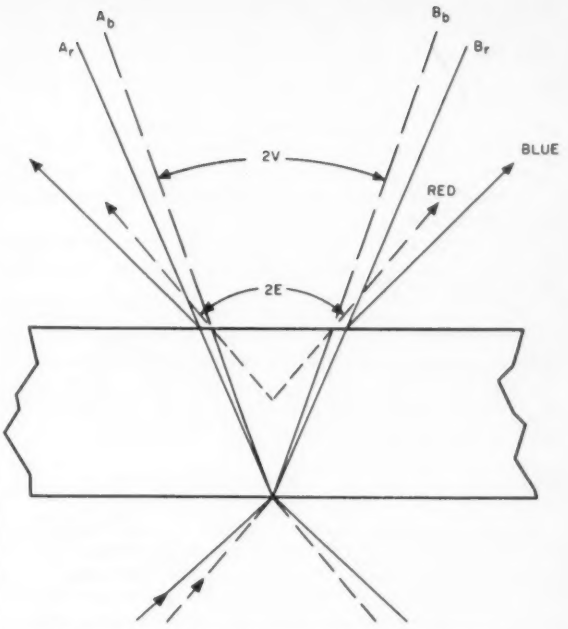

FIGURE 5. *Dispersion of isogyre with conoscope.*
A_r, B_r for red optic axes. A_b, B_b for blue optic axes. $2V$ is optic angle. $2E$ is apparent optic angle. $r>b$

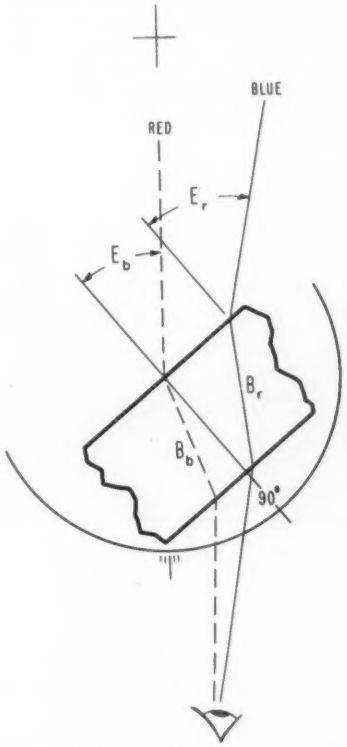

FIGURE 6. *Dispersion of isogyre with telescope.*
B_r is red optic axis. B_b is blue optic axis. $r>b$

example, toward the surface away from the light source, he sees the blue fringe inside the red fringe with respect to that surface normal, and he has only the one isogyre in view. This may seem reversed at first, but as can be seen the effect is due to the extension of the rays from the image plane to the eye through the blue and red optic axes. Thus, as the crystal is rotated in either direction from the position of symmetry, the red fringe, in this example, appears at the cross hair first.

The angle so measured is not the true optic angle but the apparent optic angle because of refraction of emergent rays.

When the crystal plate is normal to the telescope axis and the eye is focused on the specimen, the apparatus serves as a large sample orthoscope utilizing parallel rays. The sample acts as a wave plate to give a color pattern dependent on thickness, birefringence, and uniformity of the surface.

3. Operation

An apparatus is shown in figure 7. The objective lens is an ordinary 4-in. diam reading glass of 25 cm focal length. The analyzer and polarizer are Polaroid sheets of about 4.5 cm diam in rotary holders. The crystal holder and goniometer, which is the only critical part of the apparatus, is pictured in figure 8. Here, the specimen can be rotated in its own plane as well as around a vertical axis.

In use, a crystal is placed in the holder. Analyzer and polarizer are crossed at vertical and horizontal attitude. One's eye is positioned to focus on the crystal itself, which is rotated for maximum and then minimum transmission. This eye position utilizes the instrument for observation of uniformity.

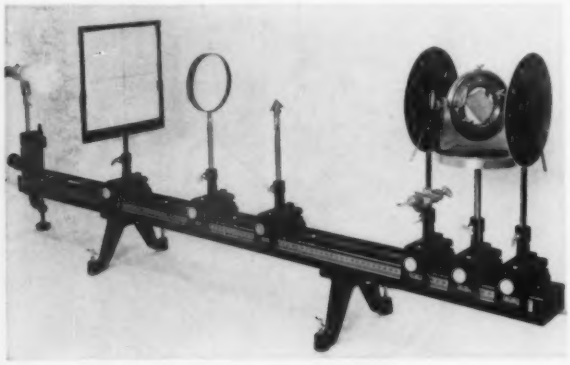

FIGURE 7. *Operational telescope.*

FIGURE 8. *Sample holder and goniometer.*

The eye is then moved in to the analyzer and focused on the image of the cross hair. This converts the instrument for measurement of apparent optic angle. For this the specimen is rotated until the optic plane is horizontal. The horizontal trace of the isogyre may be slightly displaced from the horizontal cross hair for mica. The table is rotated to bring one of the optic axes into view. The Polaroids are then rotated 45°, until the vertices of the isogyres are vertical. The eye is positioned so that the cross hair, sight, and isogyre are centered. The sight also serves to restrict change in vertical position of the eye. The apparent optic angle can so be determined.

Flat specimens allow reproducibility to better than the accuracy of the goniometer itself, which is 5′ of arc. In rippled specimens the measure is affected by local curvature through consequent variation of surface normal and hence refracted angle.

With the components used, the Polaroid sheets limited the field in the examination of uniformity, while the lens limited the field in the determination and inspection of apparent optic angle.

(Paper 65C2–63)

JOURNAL OF RESEARCH of the National Bureau of Standards—C. Engineering and Instrumentation
Vol. 65C, No. 2, April–June 1961

An Automatic Fringe Counting Interferometer for use in the Calibration of Line Scales

Herbert D. Cook and Louis A. Marzetta

(January 31, 1961)

A reversible fringe counting interferometer is described in which mechanical, optical, and electronic adjustments are maintained stable by servomechanism control or by balancing. Mirror parallelism is achieved by detecting the angular error electronically and correcting by means of barium titanate actuators. An electronic interpolator permits recording of the court in digital form to 0.01 fringe without ambiguity. A rate of more than 1,200 fringes per second has been achieved over a range of 14 centimeters. Higher counting rates are possible over shorter ranges. Design factors and details are discussed. A correction factor is derived for the error introduced by finite collimation of the interferometer beam.

1. Introduction

As part of a program to take advantage of the new radiation standard of length, an experimental reversible fringe counting interferometer was developed for use in the calibration of line scales at NBS. At the present time, line scales are calibrated by comparison with a material standard, Meter bar No. 27, the length of which was derived from the International Prototype Meter maintained by the Bureau International des Poids et Mesures at Sevres in France.

Calibration with respect to the wavelength of a suitable radiation such as the lines of Kr 86 or Hg 198 has several advantages over the use of a material standard. The wavelength standard is stable, easily reproducible in any laboratory, and can be accurately compared with the international standard. By means of fringe counting and interpolating techniques, any arbitrary length within the range of interference can be determined with great precision.

Since specially trained personnel are required for calibrating line scales and the work is tedious, the number of lines that can be observed in a working day is limited. As a result, some scales with many graduations can only be partially calibrated. The use of a mechanized instrument incorporating an interferometer and a photoelectric microscope for detecting the position of the lines of the scales is expected to be of help in making more complete calibrations.

In the use of an instrument, the operation of which requires many exacting procedures, the accuracy of measurement depends to some extent on the skill of the operator. Mechanization of such an instrument reduces the dependence on the operator and in some cases permits remotely controlled operation, allowing closer control of the environmental conditions. Carrying the mechanization one step further, automatic control is important if full advantage is to be taken of mechanization of the instrument, and the operator freed from full time attention to the details of the calibration process.

1.1. Problems Encountered in the Design of an Interferometer

The principles of operation of fringe counting interferometers have been extensively described in the literature.[1] However, problems still exist in the application of the principles to a practical instrument.

The basic problem in measuring length with an interferometer is to determine the fringe order accurately as the position of one mirror changes with respect to the other. The number of fringes counted between two positions of the moving mirror is the number of half wavelengths of light in the displacement. If the displacement corresponds to a length to be measured, the value of the integral and fractional fringe count then represents a measurement of the length in half wavelengths. The fringes must be detected and analyzed with sufficient accuracy to allow inference to be made of the lengths represented by them. Any factors that influence the accuracy of measurement must be either under control during operation or be measured and recorded at the time.

Among the more serious problems is that of the mechanical precision required in the mechanism for moving the mirror. In some applications, corner reflectors have been used to eliminate the effect of angular rotation of the moving carriage, but in this application it was considered that their use did not constitute a suitable solution of the problem. If the carriage rotates in an unknown manner, the relationship between the center of reflection and the item being measured is in doubt. It is believed that more confidence can be placed in the accuracy of calibrations if plane mirrors are used and their parallelism maintained by electronic and mechanical means.

Methods must also be provided for overcoming errors which may arise with variations in intensity of the light source and for maintaining necessary adjustments correct throughout the period required for a calibration.

---

[1] See bibliography at the end of this paper.

The method of interpolation must be applicable to operation without manipulation by an operator and yet maintain a precision to the specified tolerance. A sine-cosine method of interpolation requires that the amplitudes and phase angles of the quadrature fringe signals be held always within close limits.

Solutions to these problems have been incorporated in an experimental instrument to be described in this paper. This was built to prove the design for a larger full scale instrument to be used in the length calibration laboratory.

2. Optical Considerations

2.1. Interferometer

A diagram of the optical arrangement is shown in figure 1. The Michelson type of interferometer is especially suited to the fringe counting application because the fringe intensity varies sinusoidally with mirror separation. Also, the range of travel of the moving mirror extends continuously on both sides of the zero-order fringe, allowing a total range double the maximum mirror separation at which fringes can be obtained.

Circular fringes are used in order to obtain the maximum possible light flux through the interferometer and to establish a mechanical symmetry in the system. Efficient use of light is important because of the low source intensity and the small apertures required at large mirror separations, the intensity being a limiting factor on the counting distance and the counting rate.

Two aperture plates are shown; the first at the light source determines the maximum angle, θ_{max}, at which light may pass through the interferometer. The second, placed in the image plane, has larger openings and is used to limit any stray light that might reach the phototubes and also to act in conjunction with a dispersing prism to form a monochromator.

The limit (θ_{max}) of the solid angle of rays passing through the aperture and the interferometer depends on the maximum mirror separation at which reliable counting is required. At greater separations, more than one order of interference occurs in the light reaching the phototube, and the fringe contrast is seriously reduced. The radius of the maximum allowable aperture may be taken as approximately

$$r \simeq f\theta \simeq f\sqrt{\frac{\lambda}{D_{max}}}$$

where D_{max} is twice the maximum mirror separation, f is the focal length of the collimating or objective lens, and λ is the wavelength of the light. This relationship is derived in appendix 2 in addition to a correction factor for an error in the measurement of length due to the use of a finite aperture. Accurate centering of the aperture is also required.

The beam is divided into four parts, each quadrant producing a separate set of fringes which are detected by a separate phototube. This divides the interferometer into essentially four separate interferometers using portions of the same mirrors. The signals from the four phototubes are combined in

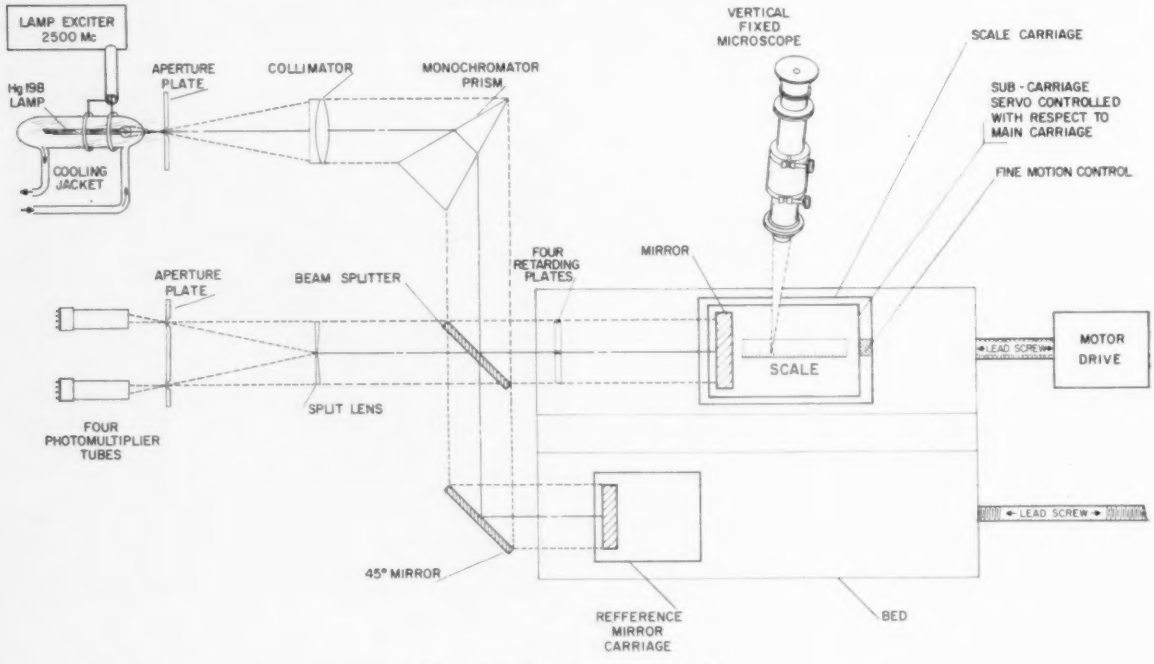

FIGURE 1. *Layout of interferometer.*

different ways for use in parallelism control, stabilization, counting, and interpolation.

In order to take advantage of the 4-phototube arrangement and to obtain the sine and cosine voltages necessary for reversible counting and interpolation, the optical path difference in each quadrant is adjusted so that a displacement of one-quarter fringe exists between adjacent quadrants. Beginning with one quadrant as a reference, the fringe phases are respectively, in rotation, 0°, 90°, 180°, and 270°.

The adjustment of phase is made by means of a retarding plate placed in each quadrant, the effective path length varying with the angle of tilt of the plate. Very close adjustment of the relative phase of the fringes can be made in this manner.

In the form of Michelson interferometer used, the fringe contrast is always less than unity at zero order because of an extra reflecting surface in one beam. The contrast is decreased in proportion to the ratio of the intensities of the two beams and this depends on the square of the coefficient of reflection of the 45-degree mirror. For this reason, the efficiency of this mirror is more important than that of any other single part of the optical system. A coefficient of 0.80 for an aluminized 45-degree mirror gives a maximum contrast of 0.64.

The effect of less-than-unity-fringe contrast on the fringe signal output of the phototubes is to decrease the signal-to-noise ratio by approximately the same factor as the contrast. A dielectric coating on the 45-degree mirror with a coefficient greater than 95 percent is possible and would make the effect negligible.

Although the intensity of one beam is reduced by an extra reflection, that of the other is also reduced by the retarding plates, tending to balance the beam intensities and to increase the contrast and signal to noise ratio slightly.

2.2. Light Source

A suitable light source for measurement by interferometry is one which has high intensity and a spectral line width as narrow as possible, since the length over which interference fringes can be obtained (the coherence length) varies in reciprocal relationship to the width of the spectral line. The light sources available today have a coherence length of somewhat less than a half meter, but improved sources are expected to be available in the near future.

Although the orange line of Kr 86 is the primary standard of length, the Meggers Hg 198 lamp is probably a more suitable source for high-speed fringe counting since the intensity of the lines is higher. Also it is more convenient to operate.

The Hg 198 electrodeless discharge lamp is excited by a high-frequency generator at a frequency which should be higher than 200 Mc/s. A microwave source operating at 2,500 Mc/s has been convenient. The lamp is used end-on and is cooled in order to reduce Doppler broadening and self-reversal of the lines. Immersion in flowing water is a simple method of cooling, but absorption of the exciting energy makes coupling from the source inefficient. Immersion in a jacket with recirculated, cooled oil has been quite satisfactory. For experimental work, selection of the green or blue lines was made by means of pairs of Wratten filters, 58 and 77A for the green, and 47B and 34A for the blue, but considerably more light intensity can be obtained if a prism monochromator is used.

2.3. Phototubes

In order to make use of the interference fringes generated in the interferometer, it is necessary to convert the light flux into an equivalent electrical signal by means of a phototube. Since phototubes are available with operating characteristics covering a wide range, a few words might be said about the factors involved in the selection of a tube for the application.

There are two principal sources of noise within the phototube, noise associated with the presence of light at the photocathode and noise generated by the so-called dark current. A typical photomultiplier tube, in total darkness, can have a dark current flow due to thermionic and other types of electron emission that is equivalent to the current that would result from a radiant flux of about 8×10^{-10} lumens when operated at room temperature. Measurement with the Michelson interferometer used in the described equipment show that the light flux at the phototubes is approximately 1.5×10^{-8} lumens when an aperture is selected for a measurement range of about 15 cm. Since the dark current is at least one order of magnitude below the current due to this value of light flux, it can be neglected, as the signal noise (N_S) and the dark current noise (N_D) add as $\sqrt{N_S^2+N_D^2}$. If the light source were less intense, or the aperture reduced in order to obtain a longer maximum interference path length, the dark current would become important.

The noise associated with the presence of light flux is similar to shot noise in an electron tube and is due to the finite number of electrons per unit time in the current. Although the average phototube current is constant for a given incident light flux, the instantaneous current has a random variation about the average due to the noise. It can be shown that this noise current varies as the square root of the electron current,[2] whereas the electron current varies directly with the light flux. Therefore the signal-to-noise ratio is proportional to the square root of the light flux.

The magnitude of the noise that can be tolerated in the fringe signal must be viewed from a consideration of the statistical behavior of the instantaneous noise pulses. In the length of one meter, the number of fringes to be counted is in the vicinity of 4,000,000, depending on the wavelength. If the noise component amplitude is assumed to have a normal distribution, a calculation will show that the signal-to-noise ratio must be greater than 6:1 if the probability

[2] Schottky's theorem, W. Schottky, Ann Physik Vol. 57, 541, (1918).

of a noise pulse exceeding the signal in amplitude is to be less than one in 5×10^8 fringes when the counter is operating at the maximum rate. The input circuit used with the counter described later reduces the probability of miscount under these conditions.

The quantum efficiency of a photocathode is the ratio of the number of electrons released to the number of photons incident on its surface. The efficiency of selected S11 type cathode materials may be of the order of 10 to 15 percent. Recently a multi-alkali photocathode has been made available with an efficiency near 20 percent at 4200 A. Furthermore, this new material offers a broader response curve over the visual spectrum plus an improvement in efficiency of 3 to 6 times over conventional photocathodes in the red region. Since the orange line of krypton lies in this region, this tube will prove valuable for use with the standard light source.

Measurements with the present equipment have indicated a potential due to the light flux of about 1 v root mean square at the photomultiplier anode. Since a level of about 5 v is needed at the trigger circuits of the counters, it may be necessary to provide a d–c amplifier at the output of each phototube. The 10-stage multiplier tube used in the experimental equipment has a current amplification of about 600,000. A 14-stage photomultiplier operating at a higher supply voltage would have an amplification approaching 9×10^6, eliminating the need for a d–c amplifier, but at a considerable increase in the tube cost.

A small shift in the d–c level at the phototube output due to the fatigue effect can occur under some conditions, with no change of light level.[2a] This can be reduced by operating the tube at reduced anode current. In the described system, the phototube anode load resistor is of the order of 5 megohms, and with the assigned voltage source, the anode current is less than 10 μa. An attempt to further lower the current by increasing the load resistor would result in a reduction of the response bandwidth. It was found to be essential to protect the phototubes from exposure to light levels that are in excess of their normal operating incidence flux. Fatigue effects of this sort usually persist for minutes or hours depending on the level of exposure. Because of the low level of flux present in the fringe pattern, the difference from normal operation to complete darkness that prevails with the equipment off does not result in an appreciable fatigue effect.

3. Electrical Circuits

A block diagram of the electronic circuits is shown in figure 2. The functions of the circuits include combining the outputs of the phototubes to produce stabilized sine and cosine signals, counting, interpolating, and digital readout of the fringe count data. Also, the information necessary for correction of parallelism is derived and applied to actuators which maintain the moving carriage always in correct orientation. Remote controls and monitoring of operations are also required of the electronic system.

[2a] See DuMont in bibliography.

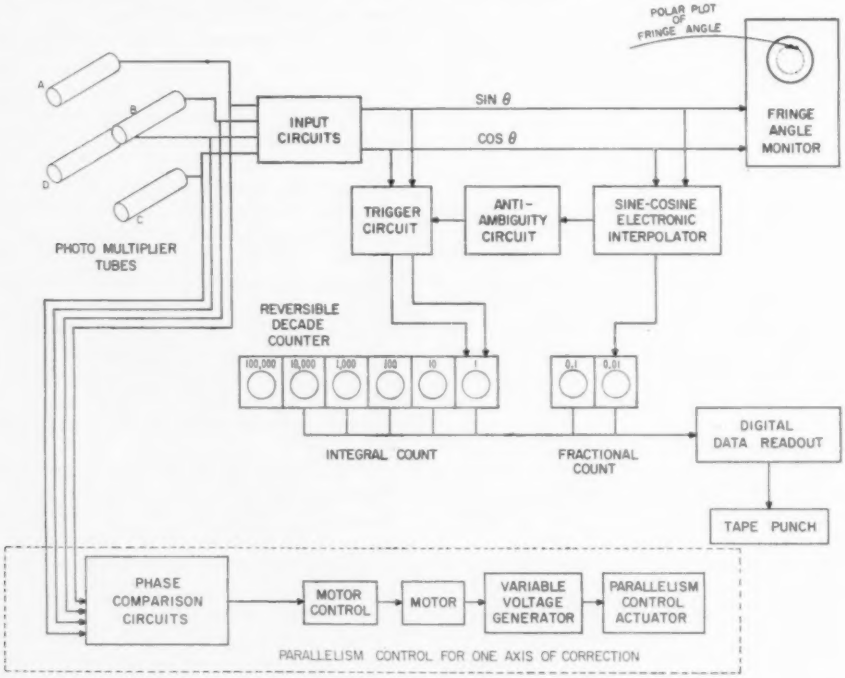

FIGURE 2. *Block diagram of electronic circuits.*

3.1. Stabilization of the Electrical Fringe Signal

The fringes in the interferometer are sensed as fluctuations in the light flux reaching the phototubes. The flux has the form of a fixed value around which the intensity varies as a sine function of the optical path difference. The amplitude of variation depends on optical factors which determine the fringe contrast, such as the flatness of the optical surfaces, reflection ratio of the beam splitter, the optical path difference and the spectral line width of the source. Since the fringe information lies in the variation only, it is necessary to isolate the signal in the form of a sinusoidal function with a baseline of zero. This is done conveniently by making use of the 4-phototube arrangement.

By choice of the effective thickness of the four plates in the interferometer beam, the phase retardation is adjusted so that there is an advance of one-quarter fringe between adjacent quadrants in rotation. Diagonally opposite quadrants are thus in phase opposition. Taking the electrical difference between diagonal phototubes results in a signal which has twice the amplitude of each and a baseline of zero. The baseline remains zero with variations in the intensity of the light source, although the amplitude of the resulting sinusoidal voltage is proportional to the intensity. A further discussion is given in appendix 1. Two outputs are available, one from each pair of diagonal phototubes, one representing the sine function of distance and the other the cosine. These are used to operate the bidirectional counter and the interpolator. The signal-to-noise ratio in the output from each of the diagonal pairs is $\sqrt{2}$ times that for each phototube since the signals are added coherently and the noise noncoherently. Precise adjustments of phasing can be made easily to within 1/400th fringe. The accuracy of the sine and cosine voltages thus obtained is such that interpolation to better than 1/100th fringe is practical by means of sine-cosine methods.

Circuit Details. As shown in figure 3, the fringe signals generated at the four phototubes are directed to individual amplifiers via cathode followers. The combination of anode resistance and circuit capacitance establishes a bandwidth of about 1,200 c/s. The sums and differences are taken for the diagonal pairs AC and BD. A–C represents the sine fringe signal, and B–D represents the cosine fringe signal. The sums A+C and B+D are used for gain level adjustment.

To provide for balancing and adjustment of the photomultiplier gains, the sums and differences of each pair of diagonal phototube outputs are indicated on zero-center meters. The four meters have, associated with each, a variable resistor whose operation influences the supply voltage of the photomultiplier tubes in a manner such that its related meter is nulled. This is done while the interferometer is in operation.

3.2. Reversible Counter

The fringes sensed by the phototubes between two positions of the moving interferometer mirror are counted by an electronic counter and the total indicated as an integral number.

The counter must be reversible in order to insure that the fringe count is true at the end of a measurement, at which point the motion of the interferometer may be reversed to correct an overshoot. This may occur, since in the intended application it is convenient if the interferometer is able to stop at each measurement. Other requirements of a suit-

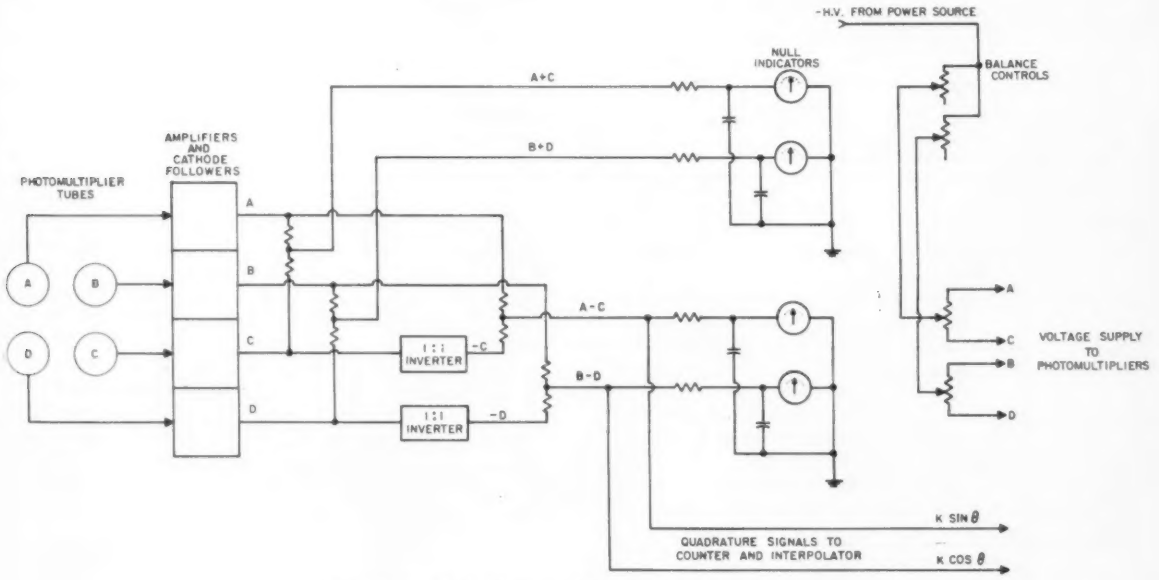

FIGURE 3. *Block diagram of phototube and input circuits.*

able counter include a sufficiently high counting rate, convenient count indicators, and provision for automatically recording the count.

These requirements have been met in a counter using neon glow-transfer tubes. A counter was built for the experimental instrument because a suitable one was not commercially available. The counter has 6 reversible decade stages, allowing a count of 10^6 without repeating. This exceeds the number of fringes in the range of the interferometer.

Counter Circuit Details. Figure 4 shows a block diagram of the counter. The sinusoidal phototube output signals are first transformed into rectangular waves by means of voltage sensitive trigger circuits. The pulses which operate the counter in the forward or reverse direction are generated by differentiating the rectangular waves and are distributed to the ADD or SUBTRACT counter inputs by the use of gating circuits. One of the fringe signals operates a pair of gates which allow transfer of pulses derived from the other fringe signal to the respective counter inputs depending on the polarity of the derivative pulse at the time the gates are open. As shown in figure 3, the upper input becomes the gate signal and the lower one the count signal for the waveforms shown; the positive count pulse occurs during a positive gate signal. This common polarity operates the forward AND gate which in turn provides a pulse to the amplifiers for registering an ADD count at the glow-transfer tubes. The waveforms for reverse operation are such that the positive gate signal coincides with the negative count pulse. A polarity inverter reverses the negative pulse to positive and delivers it to the reverse AND gate. A pulse then goes to the amplifiers to register a SUBTRACT count.

The second stage shown in figure 4 (as well as all subsequent stages), possesses the reversibility feature. In order to provide these stages with the proper signals for reversible counting, 4 of the possible 10-state positions from the previous counter stage are used as input signals. For counting in the forward direction, the sequence of the four states is 8, 9, 0, 1. Proceeding in a forward direction, the activation of state 8 at the first stage counter tube causes an output pulse to operate the lower flip flop into the position that renders the reverse AND gate

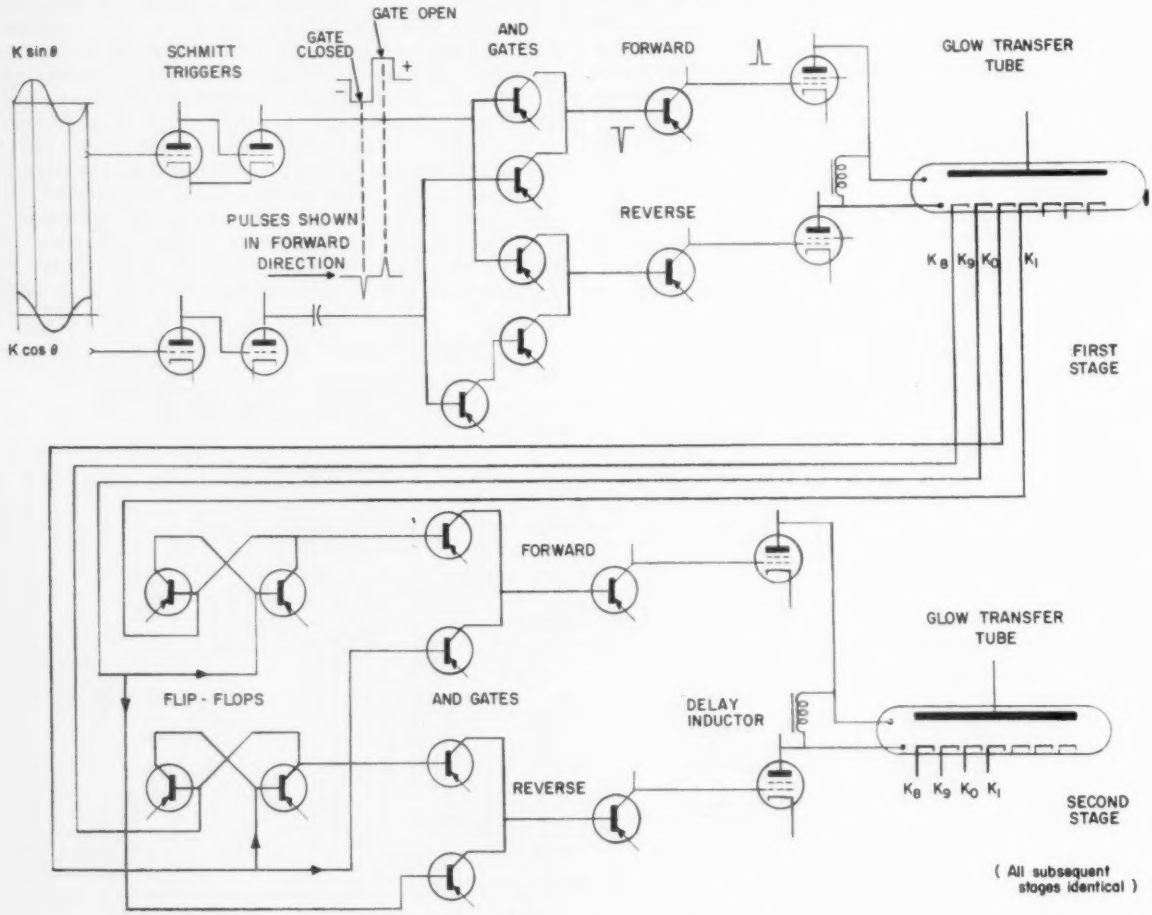

FIGURE 4. *Block diagram of reversible counter.*

inoperative. On the 9th state the upper binary switch functions and places the forward AND gate in a receptive position. The 10th or 0 state pulse passes through the forward AND gate and is registered at the counter tube in the manner previously described. The same 0-state pulse reverses the lower flip flop, placing the reverse gate in its receptive position. If the first counter tube should happen to reverse back to the 9th state, a pulse from this state would pass through the reverse AND gate. The counter would reverse or subtract out one count. The complete arrangement is compatible to the extent that all counters can be made to oscillate in synchronism between 9 and 10 by the application of a single forward or reverse pulse at this unique combination of counter positions.

It may be worth while to say a few words about the glow-transfer counter tube. This electronic device has the ability to count input pulses and also visually indicate the totalized count. Its capacity is 1 decade, and it has provision for bringing out each of the 10 states for data transfer purposes and recording. In order for the tube to count, the input pulse is applied to 1 of 2 transfer electrodes. Connected across the transfer electrodes is an inductance-capacitance delay network whose function is to direct the same input pulse to the second transfer electrode, but with a time delay of several microseconds. It is the application of this time-staggered pair of pulses that causes the ionized-gas glow to be transferred from one state to the next. The transfer electrode requires a fast negative pulse with an amplitude of about 100 v. It is for this reason that a thermionic tube is used in the circuit in lieu of a transistor, with its limited voltage swing.

It was pointed out in the section on phototubes that, from a purely statistical viewpoint, a minimum value of design signal-to-noise ratio is established by the need to avoid miscounts. The probability of a noise pulse exceeding the fringe signal amplitude is one in 5×10^8 counts at the maximum rate for a signal-to-noise ratio of 6:1. With higher signal-to-noise ratios the probability of noise pulses exceeding the signal is negligible. It was further mentioned that the probability can be lowered by the use of a special trigger circuit. The relative noise immunity is achieved by a modification of the Schmitt [3] trigger circuit increasing the hysteresis value. The hysteresis value is the voltage difference between the level at which the trigger circuit changes state in one direction and that for a change in the opposite direction. If the triggering levels are adjusted to be equally positive and negative from zero, and these are also at about half the peak voltage amplitude of the fringe signals, an optimum discrimination against noise results. In this case a rapidly repeated change of state which would be beyond the capability of the reversible counter can not occur unless a noise pulse exceeds the peak amplitude of the signal. If a small value of hysteresis were used, many rapid changes of state would occur with a small value of noise.

[3] Voltage sensitive trigger circuit.

3.3. Interpolation

If the precision of the fringe count is to be greater than $\pm\frac{1}{2}$ fringe, a means is required for determining the fractional fringe beyond the last integral count. In determining the count, some reference point on the sinusoidal function representing the fringe must be chosen. This is usually taken to be one of the points at which the function equals zero. In the past a number of methods of interpolation have been used, including a means of changing the effective path length of the interferometer until the fringe fiducial point is reached. The fraction is then read on a scale which is calibrated by changing the path by one whole fringe. In another method, sine and cosine voltages from the interferometer are displayed on a cathode ray tube, the two voltages being put on separate deflection axes. The display spot then follows a circle with the advance of the fringe, and the fringe fraction is equal to the polar angle measured around this circle, since there is one revolution per fringe. In order that the fraction may be accurately determined by this method, the voltages must accurately represent the sine and cosine values, the quadrature being accurate to a few degrees. Both of these methods are difficult to apply to automatic operation.

Since automatic data recording is a requirement for the application, development of an electronic means for determining the fringe angle was undertaken. The result is a relatively simple analog computer which indicates the angle in digital form to 1/100th fringe in 1 millisecond. The decimal fraction is indicated on counters of the same type as are used for the integral count, so that the method of data recording is the same for both.

The electronic operations in the conversion process may be described as taking place in three steps. Let ϕ represent the fringe angle; $\phi=360°$ for a displacement of one fringe. First, the two input voltages $A\sin\phi$ and $A\cos\phi$ from the phototube circuits are used to determine the amplitude of quadrature components of an alternating voltage with an arbitrary angular frequency ω_1. The result is $A\sin\phi\sin\omega_1 t$ and $A\cos\phi\cos\omega_1 t$. Second, the difference between these voltages is taken. The result can be expressed by a trigonometrical identity:

$$A\sin\phi\sin\omega_1 t - A\cos\phi\cos\omega_1 t \equiv A\cos(\omega_1 t+\phi).$$

The third step is to measure the phase shift between this sum and $\sin\omega_1 t$, since the phase difference is equal to the fringe angle ϕ.

Interpolator Circuits. A block diagram of the interpolator is shown in figure 5.

Electronic balanced modulation or multiplication is generally difficult and subject to errors in linearity. A technique which is believed to be new greatly simplifies the generation of the products required in the first step. The method makes use of linear gates in the resonance paths of LC networks. The principle of generation is shown in figure 6.

Two resonant LC circuits, one for each of the quadrature signals, are excited to oscillation simul-

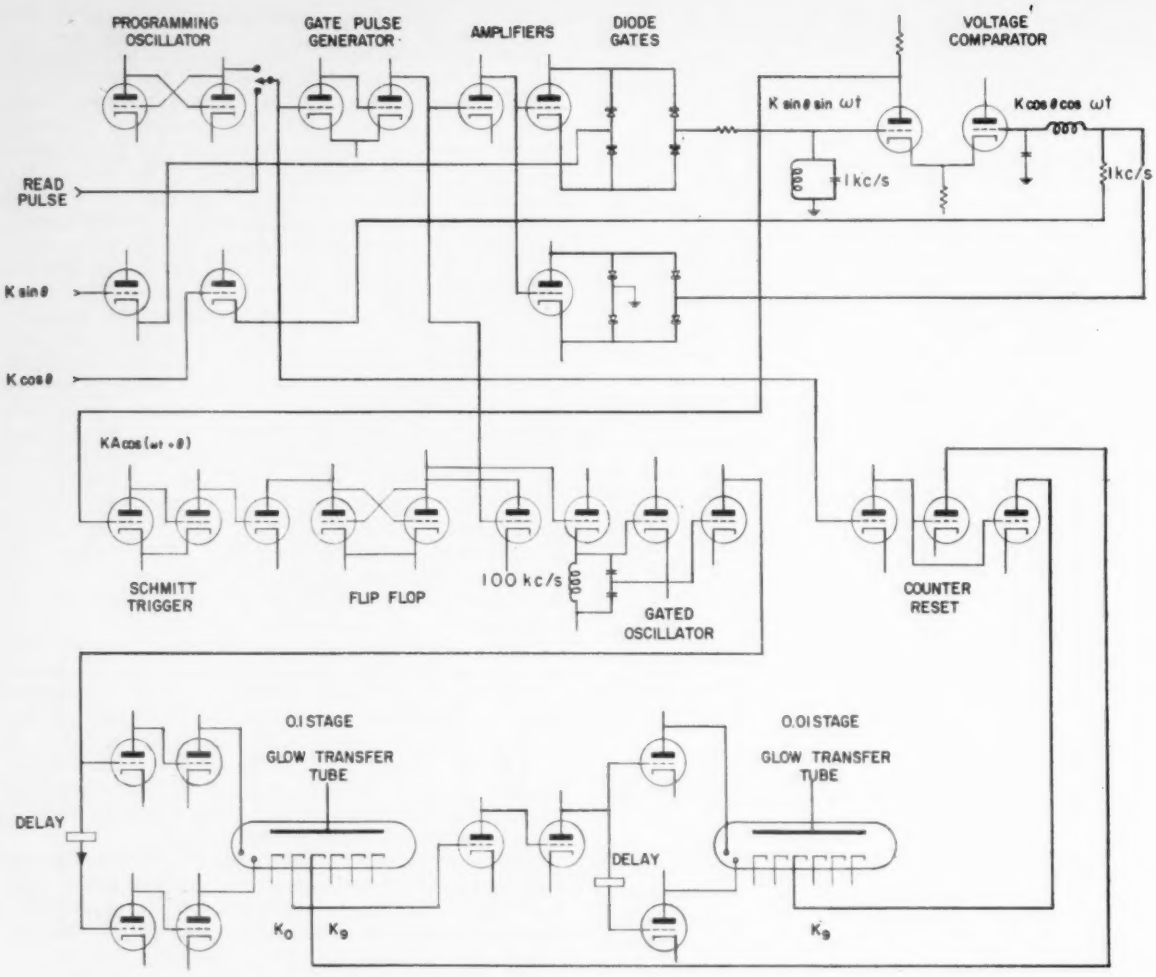

FIGURE 5. *Block diagram of digital interpolator.*

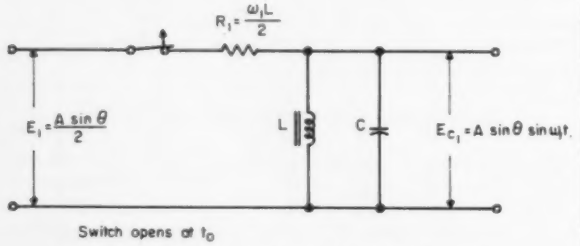

FIGURE 6a. *Generator for A sin θ sin $\omega_1 t$.*

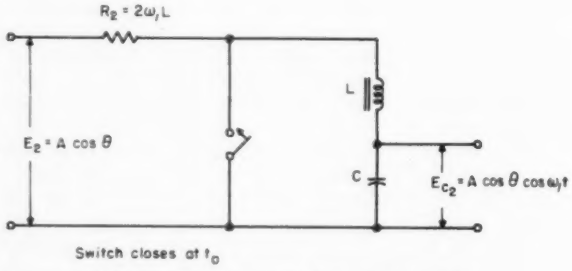

FIGURE 6b. *Generator for A cos θ cos $\omega_1 t$.*

taneously, the amplitudes being proportional to the values of sin ϕ and cos ϕ. The arrangement of gating is such that one LC circuit generates a cosine wave at angular frequency ω_1 and the other a sine wave at the same frequency. The energy by which the resonant circuits are excited is introduced by a current proportional to sin ϕ in the inductor of one, and a voltage proportional to cos ϕ on the capacitor of the other. At a time t_0, an initiating pulse is generated either manually or automatically, causing operation of the gating circuits and allowing the LC circuits to oscillate at their resonance frequency for a period of at least 1 cycle. The voltage on the respective capacitors then becomes sin ϕ sin $\omega_1 t$ and cos ϕ cos $\omega_1 t$. The difference between these is com-

pared with zero by means of a voltage sensitive trigger circuit, and the time interval to the first positive zero crossing measured. The time intervals measured by the use of an alternating voltage of angular frequency 100 ω_1 and 2 decade cycle counters which indicate the fringe angle in decimal form.

Operation of the interpolator is not necessary during the process of counting, but is needed only to determine the fractional fringe at either end of a measurement. One initiating pulse at each position is sufficient to read the fraction, although it is convenient to apply repeated pulses at perhaps 15 or 20/sec when watching the count visually. The appearance is that of a continuous reversible fringe count reading to 0.01 fringe.

3.4. Ambiguity in the Fringe Count

Since there is hysteresis in the trigger circuits of the integral counter, the purpose of which is to eliminate multiple triggering at zero crossings of the fringe signals, the indicated count does not change exactly at the fringe fiducial point used as a reference for the interpolator. This results in an ambiguity of a unit count in the region near the zero point of each fringe.

In order to insure that the same fringe zero reference point is used for both the integral counter and interpolator, it is necessary to make use of information developed by the interpolator. In forward counting, if the interpolator indicates that the zero point is passed, the integral counter must be forced to indicate the next higher count. In reverse counting, the reverse must be true when the interpolator indicates less than zero. This is necessary only when an interpolation is made, since only the final count is recorded.

The antiambiguity circuit consists of a set of pulse generators responding to the 0.8, 0.9, 0.0, and 0.1 states of the second glow-transfer tube of the interpolator counter. At the end of the processing time of the interpolator, a pulse is generated which is negative if the interpolation indicates 0.8 or 0.9, and positive if the indication is 0.0 or 0.1 One such pulse is applied to the counter trigger circuit and superimposed on the fringe signal. The pulse forces the signal voltage to exceed the triggering threshold in the direction of the count, eliminating the ambiguity.

3.5. Interpolation Bandwidth

The signal-to-noise ratio allowable in the input of the interpolator depends on the desired accuracy of interpolation. The value of the sine or cosine input voltage may not vary by more than ± 6 percent of the maximum amplitude if the reading is to be accurate to $\pm 1/100$th fringe. Allowing for the statistical character of the noise and the characteristics of the counter and interpolator, a ratio of approximately 1000:1 is required between the bandwidth for counting reliably and the bandwidth for interpolating to 1/100th fringe. The maximum fringe rate when counting or interpolating has this same ratio.

3.6. Parallelism

Measurement of length with a Michelson interferometer is accomplished by moving one of the plane mirrors which is mounted on a carriage, along a set of precise ways. Angular errors of motion of the carriage affect the geometry of the interferometer, and these may amount to as much as a micron per centimeter. If the error is greater than one-half wavelength across the mirror, the fringes are entirely lost and counting is impossible.

Cube corners used as reflectors maintain the fringe pattern in spite of angular errors, but for the application it was considered more desirable to maintain parallelism by correcting the error. If this is done, plane mirrors can be used. Also it is made certain that the position of a reference point on the moving carriage on which the mirror is mounted always maintains a fixed relationship to the effective plane of reflection so that length measurements may be made accurately.

In the instrument described here the angular errors are eliminated by means of a servomechanism which includes first, a means for detecting the error, and second, a set of actuators to provide the necessary correction. A voltage indicating the error is obtained from a comparison of the phase of the fringes detected at diagonally opposite corners of the mirror. For this purpose the interferometer beam is divided into 4 quadrants with a separate phototube for each, thus dividing the instrument into essentially 4 separate interferometers working simultaneously. If the mirror is in perfect alinement, there is no phase error detected, but if there is an angular error and one mirror quadrant leads its diagonally opposite quadrant, a phase difference occurs between the respective phototube signals. An error of 1/100th fringe is easily detected.

The actuators alter the relationship between the mirror and the carriage by an amount nearly equal to the angular error of the carriage so that the mirror does not depart from parallelism by more than is necessary to produce an error signal. Barium titanate is used for the actuators in the experimental equipment, but is limited to a few microns in its range of motion. Small hydraulic acutators have also been used successfully for this purpose. In addition to their simplicity, both types of actuators have an advantage in that there is a minimum of energy dissipated in their operation, and none is required to hold a fixed position.

Since in this equipment the phase is determined from the relative timing of the axis crossings of the phototube signals, the mirror must be moving at the time of correction. It is necessary, therefore, to incorporate some means of maintaining the correction voltage or pressure if the parallelism is to be held for long periods at rest. A suitable voltage memory is a motor-driven potentiometer controlled by the error signal. In the case of the hydraulic actuators, flexible tubes containing a fluid are raised or lowered to provide the required pressure.

Circuit Description. In figure 7, A and C represent one diagonal pair of phototube outputs, and B and D the other. The discussion for one pair will hold equally well for the other. Each of the amplified phototube outputs is applied to a voltage sensitive trigger tube in order to generate square waves, the transitions occurring very close to the zero crossings of the sinusoidal fringe signal. The networks following the amplifiers form the sum of the square waves, A' and C', to their opposite derivatives, $dC'dt$ and $dA'dt$. In figure 7, the waveforms shown are for the condition in which the mirrors are out of parallelism in a direction such that signal C lags signal A by slightly more than the normal 180 deg. Note that for this condition, the $C'+(dA'dt)$ output has a sharp positive pulse on top of the pedestal. If the mirror were to be tilted out of parallelism in a direction opposite to the previously assumed direction, the upper waveform, $A'+(dC'dt)$, would have the positive pulse on its pedestal.

For a mirror travel restricted to one direction only, the circuits described would be sufficient to provide a signal for correction purposes. However, for bidirectional travel, the correction sense must be reversed if the direction is reversed. This is done by means of a circuit in which gates are actuated by signals from the B and D signal channels. As shown in figure 7, the gate outputs are combined by diodes to form two separate output lines. Signals appearing at each line are further amplified (in addition to a polarity inverter in one line), and are recombined at the grid of a cathode follower. The positive or negative output of the latter (depending upon mirror tilt and travel direction) is used as the error control signal in the servo loop for maintaining the mirror position.

As mentioned previously, the servo loop includes a motor-driven voltage control for the purpose of providing position memory of mirror parallelism while the interferometer is at rest. The d–c output of the control in turn is amplified to a potential of several hundred volts in order to drive the barium titanate transducer.

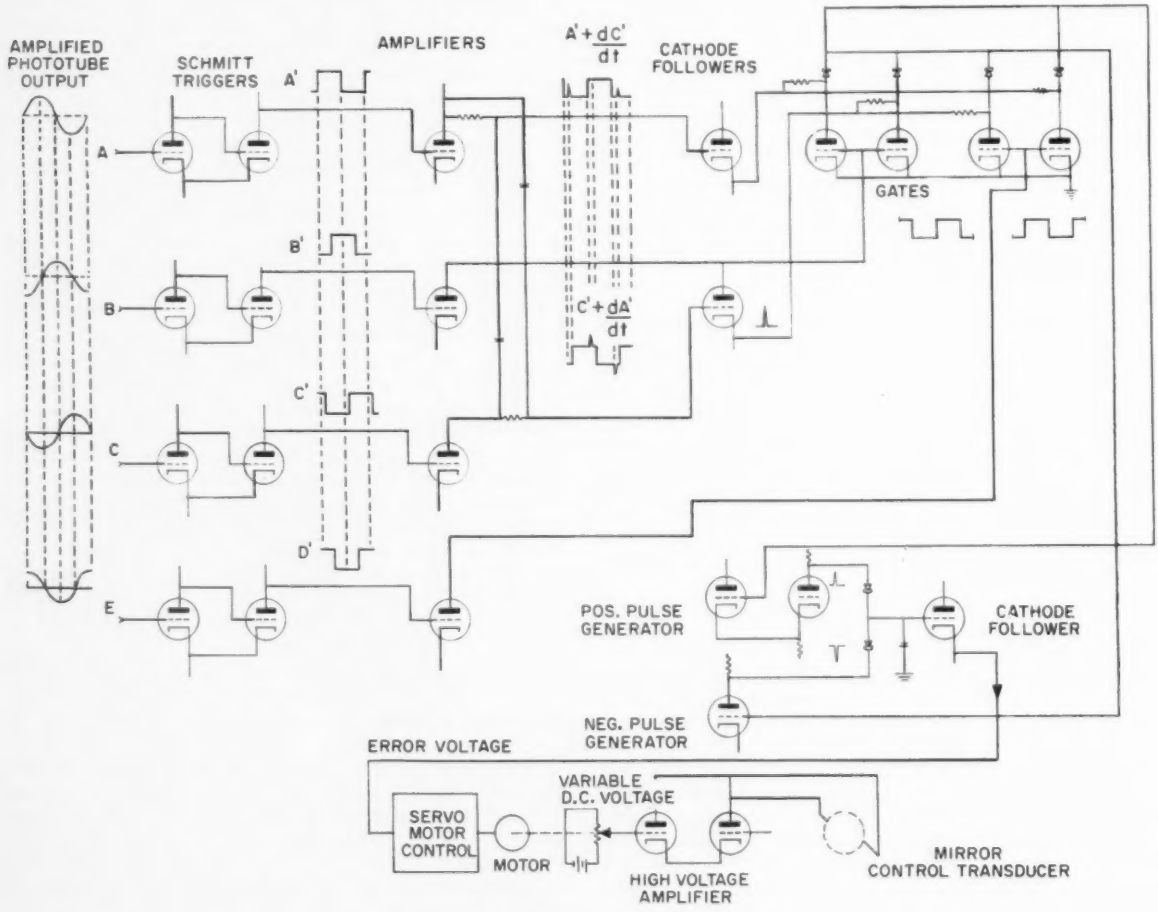

FIGURE 7. *Mirror parallelism control circuit.*

The phase detector circuit is capable of resolving a phase difference of 0.01 fringe. With a mirror 3-cm square and with green light, this is equivalent to 10^{-7} radians, or about 0.02 sec of arc.

4. Accuracy of Measurements

Since a length measured by the interferometer is a comparison with respect to the wavelength of the light source, any variation in the wavelength in the interferometer affects the accuracy of measurement. The stability of the wavelength of the krypton lamp may be 1 part in 10^9, whereas the mercury 198 lamp is affected by the presence of a carrier gas by a few parts in 10^7. The Hg 198 lamp is calibrated, however, and may be relied on to the extent that the argon pressure is known. The wavelength is given to one part in 10^8.

A greater variation in the wavelength in the interferometer is due to the refractive index of the ambient air. The refractive index error is proportional to the density of the medium and is therefore affected by the temperature, the pressure, and the proportion of other constituents such as CO_2 and water vapor. If the wavelength is to be known to one part in 10^8, the atmospheric pressure must be known to approximately 0.0025 cm of Hg, the air temperature to 0.01 °C, water vapor content to 0.25 mm partial pressure, and CO_2 to 1/100.[4]

5. Aperture Error Correction

Another factor influencing the accuracy of measurement is characteristic of the interferometer. In an interferometer in which a phototube is used to detect the fringes, the number of fringes counted is not exactly equal to the distance of mirror travel divided by one-half the wavelength of light, since the phototube receives light from more than the central fringe. The ratio of the count obtained to the true count is a constant factor which depends on the degree of collimation of the light in the interferometer. The difference is significant since the numerical value of the necessary correction is generally greater than one part in 10^6 and may total more than one fringe in a given measurement. A correction factor for the error can be applied which is fortunately a constant for a given angular aperture and applies equally throughout the range of measurement. It is also the same for a fixed aperture for any wavelength of light.

If the source were a point on the axis of the collimator, the fringes would truly represent the separation of the interferometer plates, but since the brightness of the source is finite, the light flux obtained from a point on the axis would be zero. In order that the light flux through the interferometer be finite, the source must be broad, and as a result, essentially all of the rays that are used are nonparallel to the axis. The average path of rays that are seen by the phototube is thus at an angle to the axis and the average optical path difference is not equal to that normal to the axis.

[4] W. F. Meggers, C. G. Peters, Bull. BS **14**, 697 (1918); B. Edelen, J. Opt. Soc. Am. **43**, 339 (1953).

Integration of the light flux received by a phototube in an interferometer has been described in a number of published papers.[5] An expression for the fringe contrast versus optical path difference and aperture is derived in appendix 2. The magnitude of the length correction is given.

6. Conclusion

The interferometer described here is applicable to uses in which the fringe count and interpolation is required to be continuously available, as in systems where fully automated control is desired.

Further improvement in the measuring ability of the instrument will be in the direction of extended range and in the speed of counting. Such improvement depends primarily on the light source, the important factors being the monochromaticity of the radiation and the flux per Angstrom of spectrum per unit solid angle from a source of unit area. Both of these factors are characteristic of the coherent sources now being developed elsewhere and which should be available in the not too distant future.

With present light sources, there is an approximately reciprocal relationship between the maximum range of fringe counting and the speed of counting, the acceptance angle of the collimator aperture being the variable parameter. This is true within the limitations of (1), the length over which interference can be obtained, and (2), the maximum rate of the counter.

In the application of the interferometer to scale calibration, it is used in conjunction with a photoelectric microscope which has comparable precision. Measurement of a scale which is longer than the maximum range of the interferometer is done by measuring sections of the scale, allowing the measurements to overlap with several lines in common. The error in adding the sections to derive the total is thereby minimized by the redundancy in reading the lines.

7. Appendix 1. Relation of Phototube Signals

If the source intensity is I and the fringe contrast m, the currents in the phototubes A, B, C, D are respectively:

$$k_A I(1+m_A \sin \phi)$$
$$k_B I(1+m_B \cos \phi)$$
$$k_C I(1-m_C \sin \phi)$$
$$k_D I(1-m_D \cos \phi)$$

When balance adjustments are made, k_A, k_B, k_C, k_D become equal.

The difference between A and C is then:

$$A-C=kI(m_A+m_C) \sin \phi$$

[5] M. Francon, Rev. D'Opt. **26**, 434 (1947). E. R. Peck, S. W. Obetz, J. Opt. Soc. Am. **43**, 505 (1953). Joseph H. Jaffe, J. Opt. Soc. Am. **43**, 1170 (1953). R. D. Huntoon, A. Weiss, J. Opt. Soc. Am. **44**, 4 (1954). G. R. Harrison, G. W. Stroke, J. Opt. Soc. Am. **45**, 112 (1955). E. R. Peck, J. Opt. Soc. Am. **45**, 931 (1955). Bruce, Opt. Acta **4**, 127 (1957). M. V. R. K. Murty, J. Opt. Soc. Am. **50**, 7 (1960).

Also

$$B-D=kI(m_B+m_D)\cos\phi$$

The result is a sine function and a cosine function of ϕ with baselines equal to zero and amplitudes proportional to I.

8. Appendix 2. Calculation of the Correction Factor

A ray from a point within the aperture leaving the collimating lens at an angle θ with respect to the axis of the system passes through the interferometer at this same angle. Since the optical path difference in the interferometer varies as the cosine of this angle, the average optical path difference for the complete set of rays is less than that for a ray which is parallel to the axis. The total light flux reaching the phototube through the aperture and interferometer is found by integrating the interference function over the angular aperture.

The point intensity of a ray parallel to the axis is proportional to

$$1+m\cos\frac{2\pi D}{\lambda} \tag{1}$$

where D is twice the mirror separation, λ is the wavelength, and m is a factor representing the fringe contrast for a perfectly collimated beam at an optical path difference equal to D. For any ray the expression becomes:

$$1+m\cos\left(\frac{2\pi D}{\lambda}\cos\theta\right) \tag{2}$$

Integrating over a sphere from zero to θ_1, the limit of the angular aperture,

$$\text{Flux}=\int_0^{\theta_1}\left[1+m\cos\left(\frac{2\pi D}{\lambda}\cos\theta\right)\right]\sin\theta\,d\theta$$

$$=1-\cos\theta_1+m\,\frac{\sin\frac{2\pi D}{\lambda}-\sin\left(\frac{2\pi D}{\lambda}\cos\theta_1\right)}{\frac{2\pi D}{\lambda}} \tag{3}$$

By trigonometric identity this is equal to

$$1-\cos\theta_1+2m\,\frac{\sin\left(\frac{2\pi D}{\lambda}\cdot\frac{1-\cos\theta_1}{2}\right)}{\frac{2\pi D}{\lambda}}\cos\left(\frac{2\pi D}{\lambda}\cdot\frac{1+\cos\theta_1}{2}\right) \tag{4}$$

This is a cosine function of D the optical path difference in which the argument is similar to that of the intensity function for an axial ray except for the factor $(1+\cos\theta_1)/2$. This is the correction factor by which the fringe count must be multiplied in order to obtain a true measurement of length in half wavelengths of light. It is approximately equal to

$$1-\frac{\theta_1^2}{4}+\frac{\theta_1^4}{48}. \tag{5}$$

The expression also shows the variation of the amplitude of the cosine function with respect to D, assuming no reduction in contrast for other reasons. The amplitude becomes zero when $D=\lambda/(1-\cos\theta_1)\cong 2\lambda/\theta_1^2$. The maximum useful counting distance D_{max} is considerably less than this, perhaps λ/θ_1^2 where the amplitude is about half the maximum.

9. Bibliography

1951. Wood, R. N., A photoelectric recording interferometer of measurement of dimensional changes, NBS J. Research **47,** 2.

1951. Harrison, G. R., J. E. Archer, Interferometric calibration of precision screws and control of ruling engines, J. Opt. Soc. Am. **41,** 8.

1952. Root, Elihu III, Measuring device employing light interference fringes, U.S. Patent No. 2,604,004.

1953. Peck, E. R., S. Wendell Obetz, Wavelength or length measurement by reversible fringe counting, J. Opt. Soc. Am. **43,** 6.

1953. Branin, F. H. Jr., A bidirectional electronic counter for use in optical interferometry, J. Opt. Soc. Am. **43,** 10.

1954. Huntoon, R. D., A. Weiss, J. Wray Smith, Electronic fringe interpolator for an optical interferometer, J. Opt. Soc. Am. **44,** 4.

1957. Harrison, G. R., et al., Ruling of large diffraction gratings with interferometric control, J. Opt. Soc. Am. **47,** 1.

1958. Eisner, R. L., Reversible photoelectric fringe counter, Rev. of Sci. Inst. **29,** 6.

1959. Hara, Ko, D. S. Smith, Length measurement by fringe counting, Rev. Sci. Inst. **30,** 8.

1959. DuMont Multiplier Photo Tubes, Allen B. DuMont Laboratories, Inc., Clinton, N. J.

(Paper 65C2–64)

JOURNAL OF RESEARCH of the National Bureau of Standards—C. Engineering and Instrumentation
Vol. 65C, No. 2, April–June 1961

Publications of the National Bureau of Standards*

Selected Abstracts

Heat treatment and properties of iron and steel, T. G. Digges and S. J. Rosenberg. *NBS Mono.* **18** *(1960) 35 cents. (Supersedes C495).*

This Monograph has been prepared to give an understanding of heat treatment principally to those unacquainted with this subject. To this end, the basic theoretical and practical principles involved in the heat treatment of iron and steel are presented in simplified form.

Household weights and measure, *NBS Misc. Publ. 234 (1960) 5 cents. (Supersedes M39)*

The purpose of this card is to present in convenient form the weights and measures tables most useful for household purposes, together with associated weights and measures information of general interest.

Transistorized building blocks for data instrumentation, J. A. Cunningham and R. L. Hill, *NBS TN68 (PB161569) (1960) $2.00.*

The National Bureau of Standards has developed a number of modular transistorized digital circuits that have been used in automatizing many data recording and preliminary processing tasks encountered in its scientific operations. These versatile building blocks can be connected together systematically to form digital circuits that accept raw data from experimental equipment and transpose these data into a form suitable for input to a high-speed electronic computer. These blocks can be used where: (1) data are produced in large volumes; (2) data taking is extremely fast, extremely slow, or extremely precise; (3) a need exists to minimize human error, tedium, and eyestrain; or (4) computation is extensive. This report describes 5 major packages and 8 special purpose packages.

Thermal voltage converters for accurate voltage measurements to 30 megacycles per second, F. L. Hermach and E. S. Williams, *Commun. Electron.* **AIEE,** *No. 49, 200-206 (July 1960).*

Thermal voltage converters, each consisting of a resistor in series with a thermoelement in a coaxial line, have been developed for measurements of rms voltages of 1 to 200 volts at frequencies from 3 cps (cycles per second) to 30 mc (megacycles). An accuracy of 0.1 percent or better may be obtained by a.c.-d.c. transfer techniques up to at least 10 mc and 0.2 percent at 30 mc.

The strength of ten structural adhesives at temperatures down to minus 424 °F., W. M. Frost, *Proc. 1959 Cryogenic Engr. Conf.* **5,** *375-384 (Sept. 2-4, 1959).*

The shear strengths of lap-joints bonded with commercially manufactured structural adhesives were determined at −107 °F, −323 °F, and −424 °F. The effect of rapid cooling on bond strength was studied at −323 °F. Epoxy-phenolic adhesives on glass cloth generally showed the highest strengths over the range of test temperatures.

Maser frequency stability, R. C. Mockler and J. A. Barnes, *Proc. 13 Annual Frequency Control Symp., 583-595 (May 12-14, 1959).*

The effort of the Bureau of Standards in maser work has been directed toward the attainment of high frequency stability for extended periods of time. A maser stabilized frequency multiplier chain has been controlled to 1×10^{-11} for periods of 6 hours. These preliminary measurements and tests indicate that the maser can be held within narrow frequency limits for periods of weeks with simple modifications. The masers have been employed to study frequency multiplier and crystal oscillator stability. The data have enabed us to make some predictions of the behavior of extremely long atomic beam machines.

Some mechanical properties of magnesium alloys at low temperatures, R. F. Reed, R P. Mikesell, and R. L. Greeson, *Proc. 1959, Cryogenic Eng. Conf.* **5,** *397–405 (Sept. 2–4, 1959).*

Unnotched tensile tests and Charpy V-notch impact tests were conducted on six magnesium alloys at four temperatures: 300 °K, 195 °K, 76 °K and 20 °K. The magnesium alloys tested were wrought AZ31B–0, ZE10A–H11, HM21A–T6 and HK31A–0; extruded HM31A–F and sand cast HK31A–T6.

It was found that the magnesium alloys generally increase in tensile strength, decrease in tensile elongation and decrease in impact strength with a decrease in temperature. Photomicrographs which illustrate the principal modes of fracture were taken of the fracture surfaces.

The behavior in tension and impact of magnesium alloys at low temperatures is compared with that of other common cryogenic fabricating materials, considering weight as an important criterion.

Report on the standardization of pH and related terminology, R. G. Bates and E. A. Guggenheim, *Intern. Union Pure and Appl. Chem.* **1,** *No. 1, 163–168 (1950).*

The standardization of pH has been achieved in Great Britain, in the United States, and recently also in Japan. In their essential elements, the three standards are in agreement; only differences of detail exist. It is the object of this report to summarize, for the information of all national groups interested in pH, the extent of standardization already achieved and to indicate how this area of agreement could perhaps be extended to other conceptions related to pH.

Regulated power supply for instruments, W. V. Loenbenstein, *Electronics* **33,** *No. 48, 132 (Nov. 1960).*

This paper describes a simple, low-cost device which will maintain output current constant to within $\pm\frac{1}{10}$ percent when the input is subject to normal fluctuations in line voltage. The device was used to supply d.c. heater current for a thermocouple-type vacuum gauge.

Experimental investigation of creep deflection of extruded and riveted I-beams, L. Mordfin and N. Halsey, *NASA Tech. Note D–662 (Dec. 1960).*

Five beams of 2024–T4 aluminum alloy were tested in creep bending at 450 °F. These were extruded **I**-beams, two of which were reinforced with riveted flanges. The beams were simply supported at the ends and loaded with weights at the third-points.

The creep deflections were compared with theoretical values calculated by the methods presented in another report. Agreement is found to be very good, thereby providing a measure of substantiation to the theory.

Examples are used to demonstrate various aspects of the creep bending problem, such as the effect of rivet creep on stress distribution and deflection.

The measurement of thermal conductivity, D. G. Ginnings, *Book, Thermoelectric Materials and Devices, edited by I. B. Cadoff and E. Miller, Chapter 8, 113–132 (Reinhold Publ. Corp., New York, N.Y., 1960).*

This chapter covers material given in a talk in a Thermoelectric Materials and Devices course at New York University in June 1959. The talk was intended for novices in the field of heat measurements, with emphasis on measurements at high temperatures. This paper is one of twenty presented.

Analytical study of creep deflection of structural beams, L. Mordfin, *NASA Tech. Note D–661 (Dec. 1960).*

A study was made of existing methods of analyzing the creep deflections of beams. It was found that none of these methods are directly applicable to structural beams of the types used in airframe construction.

Using Popov's elastic followup technique, which is based on the hypothesis that plane sections before bending remain plane after bending, the stress and strain distributions are determined for the creep bending of beams of nonrectangular cross section having unequal creep properties in tension and compression. It is shown how the deflections are obtained, both for pure bending and for nonuniform bending. The corrections required by transverse shear and by creep in the riveted connections are then developed. It is shown that the analyses are adaptable to beams fabricated from two or more materials. Finally, the effects of shear lag on creep deflections are discussed.

Evaluation of ball bearing separator materials operating submerged in liquid nitrogen, W. A. Wilson, K. B. Martin, J. A. Brennan, and B. W. Birmingham, *ASLE. ASME Lubrication Conf., October 17–19, 1960 (Boston, Mass.), Am. Soc. Lubrication Engrs. Preprint No. 60 LC–4 (1960).*

The demand for the reliable operation of rotating machinery in cryogenic applications has resulted in a continuing program directed toward determining the life and durability of ball bearings operating at cryogenic temperatures. On the basis of past work in this field, it was determined that the ball separator, when made from conventional materials, usually was the cause of failure. A program of screening separator materials with bearings subjected to actual operating conditions was undertaken. A number of different separator materials and arrangements were tested to determine their relative durability. The apparatus used provided a method of loading the bearing axially and included a means of measuring bearing torque, wear and load during operation. All of the tests of this screening program were conducted using liquid nitrogen. The results are presented in the form of bearing life, progressive bearing torque and progressive bearing wear for the various configurations and types of separator materials tested. Photographs showing the test apparatus and some test bearings are included in addition to a graphic presentation of the test results. This test program proved that a ball separator made from filled PTFE material is far superior to the other separator materials tested in liquid nitrogen.

Aircraft storage batteries, W. J. Hamer, *AIEE Trans.* **79,** *Pt. II, 1–11 (Sept. 1960).*

The characteristics and performance of lead-acid, nickel-cadmium, and silver-zinc storage batteries of aircraft design are discussed. A standard test program is outlined. In this program the batteries are subjected to a cycle of tests with constant-potential charging interspersed at intervals; part of the program is conducted manually, another part automatically. Performance data obtained at 80 °F and 0 °F are given for the various types of batteries. Discharge characteristics of the three types of batteries at various rates and temperatures are presented. Charge characteristics of the three types of batteries on constant-potential charging at 120 °F, 80 °F, 0 °F, and −20 °F are considered. Finally an outline of physical tests and areas for future research are presented.

Stress-strain relationships in yarns subjected to rapid impact loading. *Part VI:* **Velocities of strain waves resulting from impact,** J. C. Smith, J. M. Blanford, and H. F. Schiefer, *Textile Research J.* **30,** *No. 10, 752–760 (Oct. 1960).*

When a textile yarn is impacted transversely, strain waves and transverse waves are initiated, which travel outwards away from the point of impact. Each strain-wave front travels at constant velocity. A transverse-wave front, however, changes its velocity each time it meets a reflected strain-wave front. This effect forms the basis of a new method used to measure strain-wave propagation velocities in a selection of textile yarns. Velocities obtained in this way are in good agreement with velocities obtained by two other methods. These velocites range in values from 1400 m/sec for undrawn nylon to 5000 m/sec for high tenacity rayon and glass fiber.

A comparison of atomic beam frequency standards, R. E. Beehler, R. C. Mockler, and C. S. Snider, *Nature* **187,** *No. 4738, 681–682 (Aug. 20, 1960).*

A general qualitative description of atomic beam devices is given with particular emphasis on cesium atomic frequency standards.

The various uncertainties in frequency measurements are discussed including the effects of the uniform C field, the effect of a phase difference between the two oscillating fields that excite the atomic transition, and the effect of exciting an atomic transition with signals that are not monochromatic. The two cesium beam devices constructed at the National Bureau of Standards are described in some detail. The various tests are described for determining the uncertainties in the frequency measurements. The results of these tests are given.

The accuracy of these two quite dissimilar machines is considered to be $\pm 1.5\times10^{-11}$ and the precision of measurement is 2×10^{-12}. The latter figure represents the standard deviation of the mean for measurement times of a few hours or about 100 separate measurements.

Other NBS Publications

Journal of Research 65A (Phys. and Chem.) No. 2 (March 1961) 70 cents.

Mass spectra of some deuteroethanes, E. I. Quinn and F. L. Mohler.

Heats of hydrolysis and formation of potassium borohydride, W. H. Johnson, R. H. Schumm, I. H. Wilson, and E. J. Prosen.

Heat of combustion of borazine $B_3N_3H_6$, M. V. Kilday, W. H. Johnson, and E. J. Prosen.

Thermodynamic properties of thorium dioxide from 298 to 1,200 °K, A. C. Victor and T. B. Douglas.

Calculated energy dissipation distribution in air by fast electrons from a gun source, J. E. Crew.

Vitrons as flow units in alkali silicate binary glasses, L. W. Tilton.

Tetragermanates of strontium, lead, and barium of formula type AB_4O_9, C. R. Robbins and E.M. Levin.

Journal of Research 65B (Math. and Math. Phys.) No. 1 (January 1961) 75 cents.

On transient solutions of the "baffled piston" problem, F. Oberhettinger.

Special types of partitioned matrices, E. V. Haynsworth.

Bound for the p-condition number of matrices with positive roots, P. J. Davis, E. V. Haynsworth, and M. Marcus.

Some computational problems involving integral matrices, O. Taussky.

Computational problems concerning the Hilbert matrix, J. Todd.

Index to the distributions of mathematical statistics, F. A. Haight.

Selected bibliography of statistical literature, 1930 to 1957: IV. Markov chains and stochastic processes, L. S. Deming and D. Gupta.

Journal of Research 65D (Radio Prop.) No. 2 (March 1961) 70 cents.

Ionospheric motions observed with high-frequency backscatter sounders, L. H. Tveten.

Relationship between red auroral arcs and ionospheric recombination, G. A. M. King and F. E. Roach.

Fresnel region fields of circular aperture antennas, Ming-Kuei Hu.

Free-balloon borne meteorological refractometer, J. F. Theisen and E. E. Gossard.

Weather and reception level on a troposphere link—annual and short-term correlations, L. G. Abraham, Jr., and J. A. Bradshaw.

Initial results of a new technique for investigating sferic activity, G. Hefley, R. H. Doherty, and R. F. Linfield.

Effect of antenna radiation angles upon HF radio signals propagated over long distances, W. F. Utlaut.

Graphic determination of radio ray bending in an exponential atmosphere, C. F. Pappas, L. E. Vogler, and P. L. Rice.
A formula for radio ray refraction in an exponential atmosphere, G. D. Thayer.
The impedance of a monopole antenna with a circular conducting-disk ground system on the surface of a lossy half-space, S. W. Maley and R. J. King.
Radio-wave propagation in the earth's crust, H. A. Wheeler.

Journal of Research 65D (Radio Prop.) No. 3 (May 1961) 70 cents.

Propagation studies using direction-finding techniques, E. C. Hayden.
Diversity effects in long distance high frequency radio pulse propagation, S. A. Bowhill.
Influence of ionospheric conditions on the accuracy of high frequency direction finding, P. J. D. Gething.
Phase difference observations at spaced aerials and their application to direction finding, W. C. Bain.
Research at the National Bureau of Standards applicable to long-distance location and direction-finding problems, R. Silberstein.
Design for spinning goniometer automatic direction finding, W. J. Lindsay and D. S. Heim.
Resolution characteristics of correlation arrays, I. W. Linder.
Instrumentation for propagation and direction-finding measurements, E. C. Hayden.
Brooke variance classification system for DF bearings, E. M. L. Beale.
Estimation of variances of position lines from fixes with unknown target positions, E. M. L. Beale.
Statistics of a radio wave diffracted by a random ionosphere, S. A. Bowhill.
Space analysis of radio signals, John B. Smyth.
Effect of receiver bandwidth on the amplitude distribution of VLF atmospheric noise, F. F. Fulton, Jr.
Excitation of VLF and ELF radio waves by a horizontal magnetic dipole, J. Galejs.

Specific heats and enthalpies of technical solids at low temperatures. A compilation from the literature, R. J. Corruccini and J. J. Gniewek, NBS Mono. 21 (1960) 20 cents.
Amplitude-probability distributions for atmospheric radio noise, W. Q. Crichlow, A. D. Spaulding, C. J. Roubique, and R. T. Disney, NBS Mono. 23 (1960) 20 cents.
Screw-thread standards for federal services, 1957. Amends in part H28 (1944) (and in parts its 1950 Supplement). NBS Handb. H28 (1957)—Part III (1960) 60 cents.
Standard frequencies and time signals from NBS stations WWV and WWVH, NBS Misc. Pub. 236 (1960) 10 cents.
Research highlights of the National Bureau of Standards, Annual Report, fiscal year 1960, NBS Misc. Pub. 237 (1960) 65 cents.
Supplementary world maps of F2 critical frequencies and maximum usable frequency factors, D. H. Zacharisen, NBS TN2–2 (PB151361–2) (1960) $3.50.
Quarterly radio noise data—June, July, August 1959, W. Q. Crichlow, R. D. Disney, and M. A. Jenkins, NBS TN18–3 (PB151377–3) (1960) $1.00.
Quarterly radio noise data—September, October, November 1959, W. Q. Crichlow, R. D. Disney, and M. A. Jenkins, NBS TN18–4 (PB151377–4) (1960) $1.50.
Quarterly radio noise data—December, January, February 1959–60, W. Q. Crichlow, R. D. Disney, and M. A. Jenkins, NBS TN18–5 (PB151377–5) (1960) $1.75.
Quarterly radio noise data—March, April, May 1960, W. Q. Crichlow, R. D. Disney, and M. A. Jenkins, NBS TN18–6 (PB151377–6) (1960) $1.75.
On the nature of the crystal field approximation, H. Goldberg and C. Herzfeld, NBS TN67 (PB161568) (1960) $2.50.
Vapor pressures of organic compounds in the range below one millimeter of mercury, E. E. Hughes and S. G. Lias, NBS TN70 (PB161571) (1960) 75 cents.
Calibration of five gamma-emitting nuclides for emission rate, J. M. R. Hutchinson, NBS TN71 (PB161572) (1960) 75 cents.
Table of magnitude of reflection coefficient versus return loss $\left(L_R = 20 \log_{10} \frac{1}{|\Gamma|}\right)$, R. W. Beatty and W. J. Anson, NBS TN72 (PB161573) (1960) $1.25.
Some experiments on the deposition of gases at 4.2 °K, T. Baurer, NBS TN73 (PB161574) (1960) $1.00.
Scattering of cobalt-60 gamma radiation in air ducts, C. Eisenhauer, NBS TN74 (PB161575) (1960) 75 cents.
Soviet research in field electron and ion emission, 1955–1959; an annotated bibliography, T. W. Marton and R. Klein, NBS TN75 (PB161576) (1960) $1.25.
VHF and UHF power generators for RF instrumentation, A. H. Morgan and P. A. Hudson, NBS TN77 (PB161578) (1960) 75 cents.
Oblique incidence receiving antenna array for a relative ionospheric opacity meter, A. C. Wilson, NBS TN78 (PB161579) (1960) 50 cents.
Our measurement system and national needs, A. V. Astin, Sperryscope **15,** No. 6, 16–19 (1960).
Standards of heat capacity and thermal conductivity, D. C. Ginnings, Book Thermoelectricity (including Proc. Conf. Thermoelectricity, sponsored by the Naval Research Lab., Sept. 1958), p. 320–341 (1960).
Neutron-insensitive proportional counter for gamma-ray dosimetry, R. S. Caswell, Rev. Sci. Instr. **31,** No. 8, 869–871 (Aug. 1960).
A study of 2-Mc/s ionospheric absorption measurements at high altitudes, K. Davies, J. Geophys. Research **65,** 2285–2294 (Aug. 1960).
Carrier-frequency dependence of the basic transmission loss in tropospheric forward scatter propagation, K. A. Norton, J. Geophys. Research **65,** 2029–2045 (July 1960).
The ionization constants of 2-chloro-4-nitrophenol and 2-nitro-4-chlorophenol, V. E. Bower and R. A. Robinson, J. Phys. Chem. **64,** 1078 (1960).
Closed circuit liquid hydrogen refrigeration system, D. B. Chelton, J. W. Dean, and B. W. Birmingham, Rev. Sci. Instr. **31,** 712–716 (July 1960).
A quantitative formulation of Sylvester's law of inertia, A. M. Ostrowski, Natl. Acad. Sci. Proc. **45,** No. 5, 740–744 (May 1959).
Infrared transmission of clouds, D. M. Gates and C. C. Shaw, J. Opt. Soc. Am. **50,** 876–882 (Sept. 1960).
Comparative fixation of calcium and strontium by synthetic hydroxyapatite, R. C. Likins, H. G. McCann, A. S. Posner, and D. B. Scott, J. Biolog. Chem. **235,** No. 7, 2152–2156 (July 1960).
VI. Microscopic and macroscopic energy loss distributions. 1. Theoretical reviews: A summary, U. Fano, Natl. Acad. Sci., Natl. Research Council Publ. **752,** Report 29, p. 24 (Aug. 1960).
The mechanical properties of ceramics and their measurement at elevated temperatures, S. J. Schneider, Book, Thermoelectricity, Chap. 21, p. 342–357 (1960).
A rating method for refrigerated trailer bodies hauling perishable foods, C. W. Phillips, W. F. Goddard, Jr., and P. R. Achenbach, ASHRAE J. **2,** No. 5, 45–50 (May 1960).
Reply to, On the structure of trimethylamine-trimethylboron, D. R. Lide, Jr., J. Chem. Phys. **32,** No. 5, 1570 (May 1960).
Dimensional changes occurring in dentures during processing, J. B. Woelfel, G. C. Paffenbarger, and W. T. Sweeney, J. Am. Dental Assoc. **61,** No. 4, 413–430 (Oct. 1960).
Teeth, artificial, G. C. Paffenbarger and G. B. Denton, Encyclopaedia Britannica **21,** 878 (Jan. 1960).
A method of improving isolation in multi-channel waveguide systems, G. F. Engen, IRE Trans. Microwave Theory and Tech. Letter **MTT–8,** 460–461 (July 1960).
Influence of earth curvature and the terrestrial magnetic field on VLF propagation, J. R. Wait and K. Spies, J. Geophys. Research **65,** 2325–2331 (Aug. 1960).
Charge transfer and electron production in $H^- + H$ collisions, D. G. Hummer, R. F. Stebbings, W. L. Fite, and L. M. Branscomb, Phys. Rev. **2,** 668–670 (July 1960).
The characteristic energy losses of electrons in carbon, L. B. Leder and J. A. Suddeth, J. Appl. Phys. **8,** 1422–1426 (Aug. 1960).
Note historique sur les premières années de la microscopie électronique, L. Marton, Extrait Bull. acad. roy. Belg. (Classe des Sciences) **5,** 119–121 (Mar. 1959).

An optical study of the boundary layer transition processes in a supersonic air system, W. Spangenberg and W. R. Rowland, Phys. of Fluids **3,** No. 5, 667–684 (Sept.–Oct. 1960).

Thermodynamic structure of the outer solar atmosphere. VI. Effect of departures from the Saha equation on inferred properties of low chromosphere, S. R. Pottasch and R. N. Thomas, Astrophys. J. **132,** 195–201 (July 1960).

Polymer decomposition: Thermodynamics, mechanisms, and energetics, L. A. Wall, Soc. Plastic Engrs. Pt. I, 810–814 (Aug. 1960); Pt. II, 1031–1035 (Sept. 1960).

The role of surface tension in determining certain clay-water properties, W. C. Ormsby, Bull. Am. Ceramic Soc. **39,** No. 8, 408–432 (Aug. 1960).

The dynamic compressibility of a rubber-sulfur vulcanizate and its relation to free volume, J. E. McKinney, H. V. Belcher, and R. S. Marvin, Trans. Soc. Rheology **IV,** 347–362 (1960).

Procedure for the determination of the noble metal content of dental gold alloys, H. J. Caul, W. S. Clabaugh and M. E. Susa, J. Am. Dental Assoc. **61,** No. 4, 339–443 (Oct. 1960).

Theory of anisotropic fluids, J. L. Ericksen, Trans. Soc. Rheology **IV,** 29–39 (1960).

Rapid frequency analysis of fading radio signals, J. M. Watts and K. Davies, J. Geophys. Research **65,** No. 8, 2295–2301 (Aug. 1960).

On Stokes flow about a torus, W. H. Pell and L. E. Payne, Mathematika **7,** 78–92 (1960).

Reply to criticisms concerning Ireland contained in article "Basic research in Europe," D. M. Gates, Science **128,** No. 3318, 1–9 (Aug. 1, 1958).

Modern theories of materials, C. Truesdell, Trans. Soc. Rheology **IV,** 9–22 (1960).

Use of the incoherent scatter technique to obtain ionospheric temperatures, T. E. VanZandt and K. L. Bowles, J. Geophys. Research **65,** 2627–2628 (Sept. 1960).

Highlights of the consultative committee on international radio (CCIR) activities in the field of radio propagation, J. W. Herbstreit, 9th Plenary Assembly of CCIR Proc. IRE **48,** No. 1, 45–53 (Jan. 1960).

Graphs for bivariate normal probabilities, M. Zelen and N. C. Severo, Ann. Math. Stat. **31,** No. 3, 619–624 (Sept. 1960).

Temperature stratification in a non-venting liquid helium dewar, L. E. Scott, R. F. Robbins, and B. W. Birmingham, Proc. 1959 Cryogenic Engr. Conf. **5,** (Sept. 2–4, 1959).

A microwave impedance meter capable of high accuracy, R. W. Beatty, IRE Trans. Microwave Theory and Tech. **MTT-8,** No. 4 (July 1960).

Variational treatment of electron-hydrogen atom elastic scattering, S. Geltman, Phys. Rev. **119,** No. 4, 1283–1290 (Aug. 1960).

Relaxation processes in multistate systems, K. E. Shuler, Phys. Fluids **2,** No. 4, 442–448 (July–Aug. 1959).

Comment on models of the ionosphere above $h_{max}F2$, J. W. Wright, J. Geophys. Research **65,** 2595–2596 (Sept. 1960).

Some magnetoionic phenomena of the Arctic E-region, J. W. Wright, J. Atmospheric and Terrest. Phys. **18,** 276–289 (Aug. 1960).

Tables of thermodynamic and transport properties of air, argon, carbon dioxide, carbon monoxide, hydrogen, nitrogen, oxygen and steam, J. Hilsenrath, C. W. Beckett, W. S. Benedict, L. Fano, H. J. Hoge, J. F. Masi, R. L. Nuttall, Y. S. Touloukian, and H. W. Woolley, 478 pages (Pergamon Press, Oxford, London, New York, and Paris, 1960).

Methods of nuclear orientation, E. Ambler, Progress in Cryogenics **2,** 235–280 (Heywood & Co., Ltd., London, England, 1960).

A conference on the propagation of ELF electromagnetic waves, J. R. Wait, Proc. IRE **48,** 1648–1649 (Sept. 1960).

The Stokes flow about a spindle, W. H. Pell and L. E. Payne, Quart. Appl. Math. **18,** 257–262 (1960).

Possibility of detecting ionospheric drifts from the occurrence of spread F echoes at low latitudes, R. W. Knecht, Nature Letter **187,** 927 (Sept. 1960).

A compilation and correlation of the PVT data of normal hydrogen from saturated liquid to 80 degree K., R. B. Steward and V. J. Johnson, Proc. 1959 Cryogenic Engr. Conf. **5,** 548–556 (Sept. 2–4, 1959).

Pressure dependence of rotationally perturbed lines in the ultraviolet band spectrum of CN, H. P. Broida and S. Golden, Can. J. Chem. **38,** 1666–1677 (1960).

Neighbor interactions and internal rotations in polymer molecules. IV. Solvent effect on internal rotations, S. Lifson and I. Openheim, J. Chem. Phys. **33,** No. 1, 109–115 (July 1960).

Improvements in radio propagation prediction service, W. B. Chadwick, Elec. Engr. 1–4 (Sept. 1960).

Carbon resistance thermometry with mixed dc and rf currents, J. J. Gniewek and R. J. Corruccini, Rev. Sci. Inst. **31,** No. 8, 899–900 (Aug. 1960).

Some SEAC computations of subsonic flows, P. Davis and P. Rabinowitz. Book, Bergman's Linear Integral Operator Method in the Theory of Compressible Fluid Flow, by M. Z. Krzywoblocki, p. 148–172 (Wien, Springer-Verlag, Berlin, Germany, 1960).

Spatial distribution of energy dissipated by fallout beta rays, A. E. Boyd and E. E. Morris, Health Phys. **2,** 321–325 (1960).

Comment on a paper of Mori on time-correlation expressions for transport properties, M. S. Green, Phys. Rev. **119,** No. 3, 829–830 (Aug. 1960).

Acid-base equilibria in benzene at three temperatures. The comparative reactivities of a phenolic acid and a carboxylic acid with triethylamine with 1, 3-diphenyl-guanidine, M. M. Davis and M. Paabo, J. Am. Chem. Soc. **82,** 5081–5084 (1960).

Absolute isotopic abundance ratio and the atomic weight of silver, W. R. Shields, D. N. Craig, and V. H. Dibeler, J. Am. Chem. Soc. **82,** 5033–5036 (1960).

Electron spin resonance studies of free radicals in irradiated materials, L. A. Wall, Symp. on Materials in Nuclear Application, Am. Soc. Testing Materials Spec. Tech. Publ. No. 276, p. 208–223 (1959).

Flexural strength of specimens prepared from several uranium dioxide powders; its dependency on porosity and grain size and the influence of additions of titania, F. P. Knudsen, H. S. Parker, and M. D. Burdick, J. Am. Ceram. Soc. **43,** No. 12, 641–647 (Dec. 1960).

Green and purple sulfur: Electron-spin resonance studies, H. E. Radford and F. O. Rice, J. Chem. Phys. **33,** No. 3, 774–776 (Sept. 1960).

Correlation of an auroral arc with a subvisible monochromatic 6300 A arc with outer-zone radiation on November 28, 1959, B. J. O'Brien, J. A. Van Allen, F. E. Roach, and C. W. Gartlein, J. Geophys. Research **65,** No. 9, 2759–2766 (Sept. 1960).

Spectrum of ReF_6, J. C. Eisenstein, J. Chem. Phys. **33,** No. 5, 1530–1531 (Nov. 1960).

Effect of structure on the spectra emitted by solid nitrogen during electron bombardment, L. J. Schoen and H. P. Broida, J. Mol. Spectroscopy **5,** No. 5, 416–419 (Nov. 1960).

Chemical reactions of free radicals at low temperatures, R. A. Ruehrwein, J. S. Hashman and J. W. Edwards, J. Phys. Chem. **64,** 1317–1322 (1960).

Spatial distribution of energy dissipated by fallout-rays, A. E. Boyd and E. E. Morris, Health Phys. **2,** 321–325 (1959).

Megaroentgen dosimetry employing photographic film without processing, W. L. McLaughlin, Radiation Research **13,** No. 4, 594–609 (Oct. 1960).

The reaction of hydrogen atoms with solid propene at low temperatures, R. Klein, M. D. Scheer and J. G. Waller, J. Phys. Chem. **64,** 1247–1250 (1960).

Programming for a closed-loop, manned-machine combined system, D. C. Friedman, Proc. Combined Analog-Digital Computer Systems Symp., December 16 and 17, 1960, Philadelphia, Pa., 12th Article (Dec. 1960).

Irrational power series, M. Newman, Proc. Am. Math. Soc. **11,** 699–702 (Oct. 1960).

Microwave spectrum, structure, and dipole moment of propane, D. R. Lide, Jr., J. Chem. Phys. **33,** No. 5, 1514–1518 (Nov. 1960).

Topological derivation of the Mayer density series for the pressure of an imperfect gas, M. S. Green, J. Math. Phys. **1,** No. 5, 391–394 (Sept.–Oct. 1960).

Surface area determination of kaolinite using glycerol adsorption, K. H. Woodside and W. C. Ormsby, J. Am. Ceram. Soc. **43,** No. 12, 671–672 (Dec. 1960).

Magnetic resonance determination of the nuclear moment of tantalum-181 in $KTaO_3$, L. H. Bennett and J. I. Budnick, Phys. Rev. **120,** No. 5, 1812–1815 (Dec. 1, 1960).

Electrodeless passage of direct current through an electrolyte, A. Brenner, J. Electrochem. Soc. **107,** No. 12, 968–973 (Dec. 1960).

Preparation and thermal stability of tetrakis-(pentafluorophenyl)-silane and tris-(pentafluorophenyl)-phosphine, L. A. Wall, R. E. Donadio, and W. J. Pummer, J. Am. Chem. Soc. **82,** No. 18, 4846–4852 (Sept. 1960).

The centennial of spectrochemistry, W. F. Meggers, J. L. Tech, J. Opt. Soc. Am. **50,** No. 11, 1035–1038 (Nov. 1960).

Rate of reaction of nitrogen atoms with ethylene, J. T. Herron, J. Chem. Phys. **33,** No. 4, 1273–1274 (Oct. 1960).

Structure of the isobutane molecule; change of dipole moment on isotopic substitution, D. R. Lide, Jr., J. Chem. Phys. **33,** No. 5, 1519–1522 (Nov. 1960).

Condensation coefficient of arsenic trioxide glass, A. B. Bestul and D. H. Blackburn, J. Chem. Phys. **33,** No. 4, 1274–1275 (Oct. 1960).

The compound $BaTiGe_2O_9$, C. R. Robbins, J. Am. Ceram. Soc. **43,** No. 11, 610 (Nov. 1960).

**Publications for which a price is indicated (except for NBS Technical Notes) are available only from the Superintendent of Documents, U.S. Government Printing Office, Washington 25, D.C. (foreign postage, one-fourth additional). Technical Notes are available only from the Office of Technical Services, U.S. Department of Commerce, Washington 25, D.C. (Order by PB number). Reprints from outside journals and the NBS Journal of Research may often be obtained directly from the authors.*

UNIVERSITY OF MICHIGAN
GENERAL LIBRARY
DOCUMENTS SECTION
ANN ARBOR MICH
SJR-C DEC D-18 [illegible]

UNITED STATES
GOVERNMENT PRINTING OFFICE
DIVISION OF PUBLIC DOCUMENTS
WASHINGTON 25, D.C.

OFFICIAL BUSINESS

PENALTY FOR PRIVATE USE TO AVOID PAYMENT OF POSTAGE, $300 (GPO)

JOURNAL OF RESEARCH of the National Bureau of Standards — Vol. 65C, No. 2 — April–June 1961
C. Engineering and Instrumentation

Contents

Page

An experimental study concerning the pressurization and stratification of liquid hydrogen. A. F. Schmidt, J. R. Purcell, W. A. Wilson, and R. V. Smith. 81

Temperature dependence of elastic constants of some cermet specimens. Sam Spinner. 89

Analog simulation of zone melting. H. L. Mason. 97

Residual losses in a guard-ring micrometer-electrode holder for solid-disk dielectric specimens. Arnold H. Scott and William P. Harris. 101

A bolometer mount efficiency measurement technique. G. F. Engen. 113

Telescope for measurement of optic angle of mica. Stanley Ruthberg. 125

An automatic fringe counting interferometer for use in the calibration of line scales. Herbert D. Cook and Louis A Marzetta. 129

Publications of the National Bureau of Standards. 141

For sale by the Superintendent of Documents, U.S. Government Printing Office, Washington 25, D.C. Price 75 cents (single copy)
Subscription price: $2.25 a year; 50 cents additional for foreign mailing.

UNITED STATES GOVERNMENT PRINTING OFFICE, WASHINGTON : 1961